DEVELOPMENT OF ANISOTROPY DURING THE COLD ROLLING OF ALUMINIUM SHEET

by

Mostafa Benferrah

A Thesis Submitted to the
Faculty of Graduate Studies and Research
in Partial Fulfillment of the Requirements for the
Degree of Master of Engineering

Department of Mining and Metallurgical Engineering
McGill University
Montreal, Canadå

ISBN 0-315-34446-6

To My Parents

ABSTRACT

Sheets of annealed commercial purity aluminium were rolled repeatedly in order to produce ten different strain states ranging from $\bar{\varepsilon} = 0$ to about 2.6. The R-values at 0°, 45° and 90° from the rolling direction were measured during tensile tests for the annealed sheet and the first two reductions. A back-extrapolation technique was used to determine the R-value at zero tensile strain.

Uniaxial tension and compression and plane strain tension tests were performed on each sheet in order to establish the corresponding yield stresses. From there, sections of the respective yield surfaces were constructed; these are compared to the Hill ellipsoid derived from the measured R_0 and R_{90} values. It is shown that the behaviour of the sheet is better described by a generalized yield criterion with m = 1.7 than the conventional quadratic yield surface. A modified version of this criterion is proposed in order to take into account the planar anisotropy which has generally been overlooked in the past when dealing with non-quadratic criteria.

The R-value at 45° is shown to be larger than both R_0 and R_{90} for all sheets; thus $\Delta R < 0$, so that 45° earing is expected. This is in general agreement with the predictions of the CMTP analysis based on experimental pole figures, although the CMTP values for R_{45} are always higher than those calculated from the generalized anisotropic yield criterion.

It is concluded that better CMTP predictions require more detailed information regarding the texture components, in particular the volume fraction of each ideal orientation.

RESUME

Une tôle d'aluminium recuit de pureté commerciale a été laminée à plusieurs reprises afin d'obtenir dix états différents de déformation allant de $\bar{\varepsilon} = 0$ à 2.6 environ. Les coefficients de Lankford $R(\alpha)$ correspondant à des angles $\alpha =$ 0°, 45° et 90° par rapport à la direction de laminage, ont été mesurés par des essais de traction simple sur la tôle initiale et après les deux premières réductions. Une méthode d'extrapolation a été utilisée pour déterminer la valeur de R correspondant à une déformation nulle en traction.

Des essais de traction et compression uniaxiales ainsi que de traction plane ont été effectués pour chaque tôle afin de déterminer les contraintes d'écoulement. Les surfaces d'écoulement correspondantes ont alors été construites et comparées avec l'ellipse de Hill obtenue à partir des valeurs R_0 et R_{90} mesurées auparavant. On voit que la caractérisation du comportement de la tôle est meilleure lorsqu'un critère généralisé est utilisé, pour lequel l'exposant m est égal à 1.7. Une version modifiée de ce critère est proposée afin de tenir compte de l'anisotropie plane qui est généralement négligée quand il s'agit d'un critère non-quadratique.

On trouve que R_{45} est supérieur à R_0 et R_{90} pour toutes les tôles, donc $\Delta R < 0$ et des cornes d'emboutissage à 45° sont prévisibles. Ceci est en accord global avec les résultats de la méthode CMTP basée sur des figures de pôles expérimentales, bien que les valeurs R_{45} obtenues par le CMTP

soient toujours supérieures à celles calculées par le critère généralisé. On conclut que pour obtenir de meilleures prévisions par la méthode CMTP, il faudrait disposer de plus de détails sur les composantes de textures présentes dans la tôle, en particulier les fractions volumiques de chaque orientation idéale représentant la texture.

ACKNOWLEDGEMENTS

I wish to express my sincere appreciation to my thesis supervisor Professor John J. Jonas for his guidance, constant encouragement and understanding during the course of this research. I am also indebted to Professor F. Montheillet, who first introduced me to this research topic. My gratitude is further extended to my fellow graduate students for their stimulating comments and suggestions.

I would like to thank Dr. D.J. Lloyd of Alcan International Ltd., Kingston Laboratories, Kingston, Ontario, for supplying the aluminium sheet, and the Ministry of Education, Province of Quebec (FCAR program) for providing financial support. I would also like to acknowledge the assistance I have received from Martin Knoepfel in the preparation of test specimens, Carol Mercure for typing the thesis, and Lorraine Mello and Carol Rousseau in completing the various administrative formalities during my stay at McGill.

Finally, I am most grateful to my father, brothers and sisters who have been waiting patiently for me to return home.

TABLE OF CONTENTS

Page

LIST OF FIGURES

LIST OF TABLES

INTRODUCTION

The production of commercial purity aluminium sheet for deep drawing applications has been aimed at meeting two main requirements: (i) good drawability and (ii) minimum earing tendencies [1,2]. The relation between these characteristics and texture has been known for a long time, and the investigations dealing with this subject have evolved through the following stages: in the earliest period it was confirmed that plastic anisotropy plays an important role in determining the press formability of sheet metals; in the next stage, it was clarified that both the R-value and therefore the deep drawability can be estimated from knowledge of the preferred orientations present; the last stage, known as "texture tailoring", consists of attempting to produce, by means of fabricating processes, for example, a suitable balance of annealing and rolling textures in order to assure the minimum possible earing tendency [3-5].

From a macroscopic point of view, Whiteley [6] has shown in his original analysis that when a cylindrical cup is drawn, the limiting drawing ratio (LDR) depends on the relative resistance to deformation (β) of two regions, the cup flange in which most of the deformation occurs, and the wall which must transmit sufficient force to cause deformation in the flange. He then used Hill's quadratic theory of anisotropic plasticity to relate β to the more easily measured R-value. However, small deviations of the yield locus from

the elliptical shape assumed in Hill's theory can cause substantial errors in the calculation of LDR [7]. This is why, when the mathematical theory of plasticity is applied to sheet metal forming, it should be based on an experimental yield locus for the material concerned [8].

The aim of the present work was to characterize the anisotropy of an annealed commercial purity aluminium sheet and to study its development during cold rolling. After a brief review of the literature, given in chapter one, the continuum theory of anisotropy is presented in chapter two, together with Hill's generalized criterion and the more recent 'continuum mechanics for textured polycrystals' (CMTP) method.

The experimental procedure is described in chapter three, and in chapter four it is shown that the aluminium sheet investigated has an 'anomalous' behaviour and is therefore better described by a non-quadratic criterion. In order to take into account the planar anisotropy observed, a new criterion is proposed. R (α) values based on experimental pole figures and the CMTP analysis are also calculated. The latter are compared to the results obtained by mechanical testing in Chapter five, where comments on the direct measurement of R-value are given and a comparison between two non-quadratic yield criteria is also made.

CHAPTER 1

LITERATURE REVIEW

1.1) Deep Drawing:

When cups are drawn from anisotropic sheet, the rims develop undulations at positions which are usually symmetric with respect to the rolling direction. These undulations are termed "ears", and their presence on a drawn cup is disadvantageous because of the additional cost entailed in removing them and because of the extra material required. Because of this, any form of anisotropy was originally considered undesirable in deep drawing applications. Then in 1950, Lankford et al. [9] reported a good correlation between press performance and the drawing of an automotive fender and the product R times n, where R is defined as the ratio of width to thickness strain measured in a strip tensile test ($R = \varepsilon_w/\varepsilon_t$; see paragraph 1.2 below), and n is the index in the Ludwik empirical stress-strain relation ($\sigma = K\,\varepsilon^n$). Whiteley [6] later showed both experimentally and analytically that for the drawing of cylindrical flat bottom cups, the drawability depends on R alone. Thus anisotropy can be desirable, as long as it is the thickness direction which is resistant to flow (low ε_t), and not a set of directions in the plane of the sheet.

Although there are several types of drawability test [10], the most common and simplest is the Swift test with a

flat punch [11]. In this test, the drawability is expressed as a limiting drawing ratio (LDR), which is the largest ratio of blank-to-cup diameter that may be drawn successfully.

1.2) The Plastic Strain Ratio (R):

The plastic anisotropy of sheet metal is generally expressed in terms of the $R(\alpha)$ coefficient defined as the ratio of the width to thickness strain in a uniaxial tensile test specimen oriented at α degrees to the sheet rolling direction. It has been proposed that the R coefficient be measured at the deformation corresponding to the limit of uniform elongation [9], or at 15% elongation [12]. However, the strain ratio determined in this way does not characterize the behaviour of the sheet, since its value changes during the test due to the formation of fiber texture [13-17]. In order to obtain the value of strain ratio fully characterizing the anisotropy of the examined sheet, it is necessary to measure strain ratio values at different degrees of straining, and to extrapolate the function $R = f(\varepsilon)$ back to the initial state [18,19]. At zero strain, the ratio of plastic strains $\varepsilon_w/\varepsilon_t$ is equivalent to that of the incremental strains $d\varepsilon_w/d\varepsilon_t$. The advantage of working with the latter is that it can be derived from the theoretical yield function.

1.3) Limiting Drawing Ratio (LDR):

Whiteley's original correlation between limiting drawing ratio and R has been confirmed by other workers [20-22].

The basis for Whiteley's analysis is the relative resistance to deformation of two regions, the cup flange in which most of the deformation occurs, and the wall which must transmit sufficient force to cause deformation in the flange (see Figure 1.1). If the blank diameter is too large, the force that must be transmitted by the wall will be excessive, thereby causing it to yield and fail. A high R-value indicates a high resistance of the sheet to thinning. Since drawing failures occur by necking of the wall by thinning, high R-values indicate a high wall strength. On the other hand, deformation in the flange is primarily by circumferential contraction and a high R-value suggests a low resistance to width (circumferential) strain. The combined effect of stronger wall and weaker flange allows larger blanks to be drawn without failure.

In his analysis [6], Whiteley assumed no work hardening, no thickness change in the flange, radially symmetric properties in the sheet (i.e. no variation in R-value with direction in the plane of the sheet) and the validity of the Hill quadratic criterion in order to express LDR as a function of R alone. The analysis is summarized below:

Consider the surface area of the sheet to remain unchanged, (see Figure 1.2), then

$$\pi\rho^2 + 2\pi r_1 h = \pi\rho_0^2 \qquad (1.1)$$

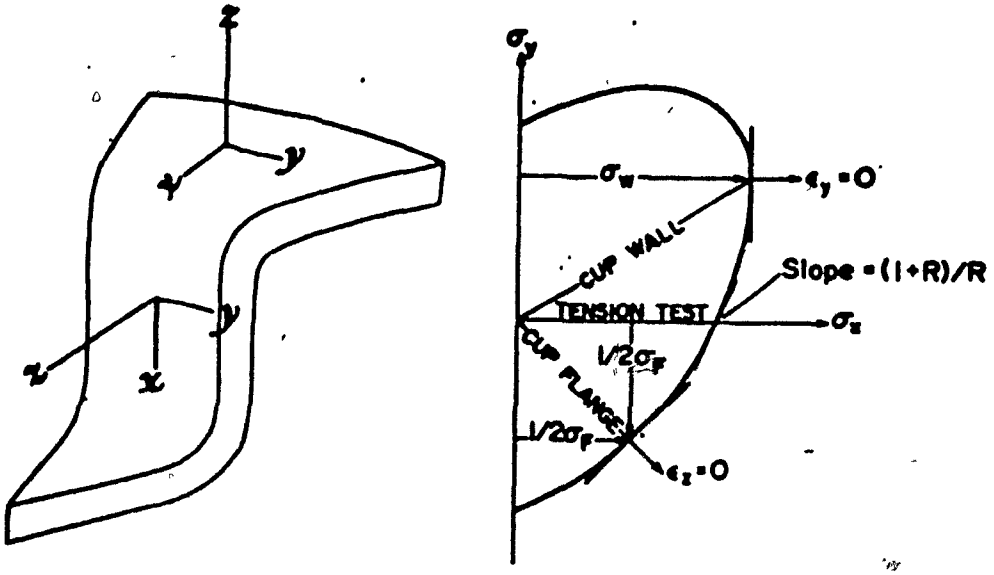

Figure 1.1 Schematic yield locus indicating loading paths important to deep drawing. The theory assumes plane strain ($\epsilon_z = 0$) in the flange. Yielding of the wall corresponds to plane strain, $\epsilon_y = 0$. Because the strain ratio, R, is measured on a third loading path (x-direction tension), predictions of drawability based on R are very sensitive to the yield locus shape.

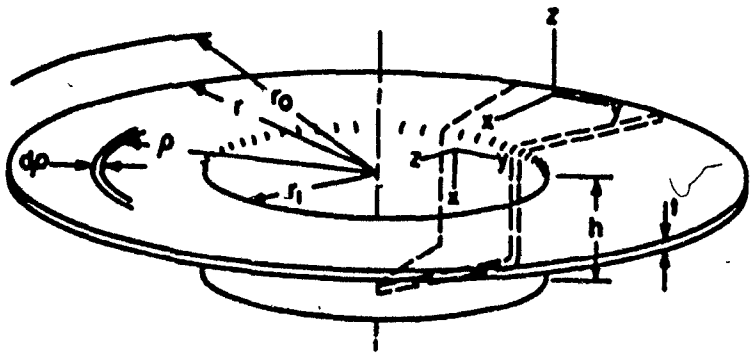

Figure 1.2 Schematic illustration of partially drawn cup showing the coordinate system and dimensional notation.

and, since $d\varepsilon_z = 0$,

$$d\varepsilon_x = -d\varepsilon_y = r_1 dh/\rho^2 \qquad (1.2)$$

The incremental work done on an element at a distance ρ from the centre is equal to its volume ($2\pi t \rho d\rho$) times the incremental work per unit volume ($\sigma_x d\varepsilon_x + \sigma_y d\varepsilon_y + \sigma_z d\varepsilon_z$). The work done on the element is therefore

$$dw = 2\pi t \rho d\rho \, (\sigma_x - \sigma_y) \, r_1 dh/\rho^2 \qquad (1.3)$$

The term ($\sigma_x - \sigma_y$) is now designated as σ_f (the flow strength of the flange). With $d\varepsilon_z = 0$ and $\sigma_z = 0$, $\sigma_y = -\sigma_x$, so $\sigma_f = 2\sigma_x$.

Then the total work per increment of punch travel is:

$$\frac{dw}{dh} = \int_{r_1}^{r} \frac{2\pi r_1 t \sigma_f d\rho}{\rho} = 2\pi r_1 t \sigma_f \ln(r/r_1) \qquad (1.4)$$

The drawing force Fd (= dW/dh) therefore has its largest value at the beginning of the draw, where $r = r_0$, so:

$$Fd(max) = 2\pi r_1 t \sigma_f \ln(r_0/r_1), \text{ or}$$

$$Fd(max) = \pi d_1 t \sigma_f \ln(d_0/d_1) \qquad (1.5)$$

where d_0 and d_1 are the blank and punch diameters respectively.

In the cup wall which must carry the force Fd(max), the axial stress σ_x is $Fd(max)/2\pi r_1 t$, so that

$$\sigma_x = \sigma_f \ln(d_0/d_1) \qquad (1.6)$$

Assuming n = 0 (no work hardening), the wall starts to neck as soon as it yields. The drawing limit is thus reached when the stress reaches the flow strength of the wall, σ_w, i.e. when $\sigma_w = \sigma_f \ln d_0/d_1$, or

$$\ln (LDR) = \ln(d_0/d_1) = \sigma_w/\sigma_f \qquad (1.7)$$

where d_0 is the largest blank diameter which can be drawn into a cup of diameter d_1 without the bottom being torn out.

Note that the flow strength of the wall is characterized in terms of plane strain because the wall circumference itself is prevented from shrinking by the punch. Thus the LDR is governed by the ratio of two plane strain strengths:

$$\beta = \frac{\sigma_w(\varepsilon_y = 0)}{\sigma_f(\varepsilon_z = 0)} \qquad (1.8)$$

For an isotropic material, $\beta = 1$, so the LDR is equal to e =

2.72, but in practice it is lower because the theory neglects friction and the work of bending or redundant work. This can be taken into account by a deformation efficiency η, leading to:

$$\ln (LDR) = \eta\beta \qquad (1.9)$$

where $\eta \approx .7$ to $.8$.

At this point, Whiteley used Hill's anisotropic plasticity theory to relate β to the more easily measured R. From the Hill quadratic criterion [23], it can easily be shown that

$$\sigma_f = (\sigma_x - \sigma_y)_{(\varepsilon_z = 0)} = X \sqrt{\frac{1 + R}{R + \frac{1}{2}}} \qquad (1.10)$$

and

$$\sigma_w = \sigma_{x(\varepsilon_y = 0,\ \sigma_z = 0)} = \left(\frac{1 + R}{\sqrt{2R + 1}}\right) \qquad (1.11)$$

where X is the uniaxial tensile yield stress. Substitution of the above two relations into the definition of β (Equation 1.8) leads to the prediction that

$$\beta = \sqrt{(R + 1)/2} \qquad (1.12)$$

so that

$$\ln(LDR) = \eta\beta = \eta \sqrt{(R + 1)/2} \qquad (1.13)$$

Note that, in real sheets, the R-value actually varies with direction; as a result it is better to use the average strain ratio $\bar{R}$ in equations 1.12 and 1.13. $\bar{R}$ is defined here as $\bar{R} = (R_0 + 2R_{45} + R_{90})/4$, where R_0, R_{45} and R_{90} are the strain ratios at $\alpha = 0°$, $45°$ and $90°$, respectively. The theoretical curves for equation 1.13 are shown in Figure 1.3 and it can be seen that the experimental data cannot be fitted by a unique curve for which η is constant.

There have been more rigorous analyses of cupping which allow for both work hardening and thinning or thickening of the flange [10,22]. These, however, also rely on Hill's quadratic theory to characterize the flow behaviour, and predict a greater dependence of LDR on $\bar{R}$ than is observed experimentally.

Probably the largest source of error is the use of Hill's quadratic criterion to characterize the anisotropy. In fact, small deviations of the actual yield locus from the elliptical shape assumed in the Hill theory can cause substantial errors in equation (1.12). This is because measurement of the strain ratio R is equivalent to establishing the slope of the yield locus for a loading path in uniaxial tension, whereas β is the ratio of the flow stresses along two other loading paths [7].

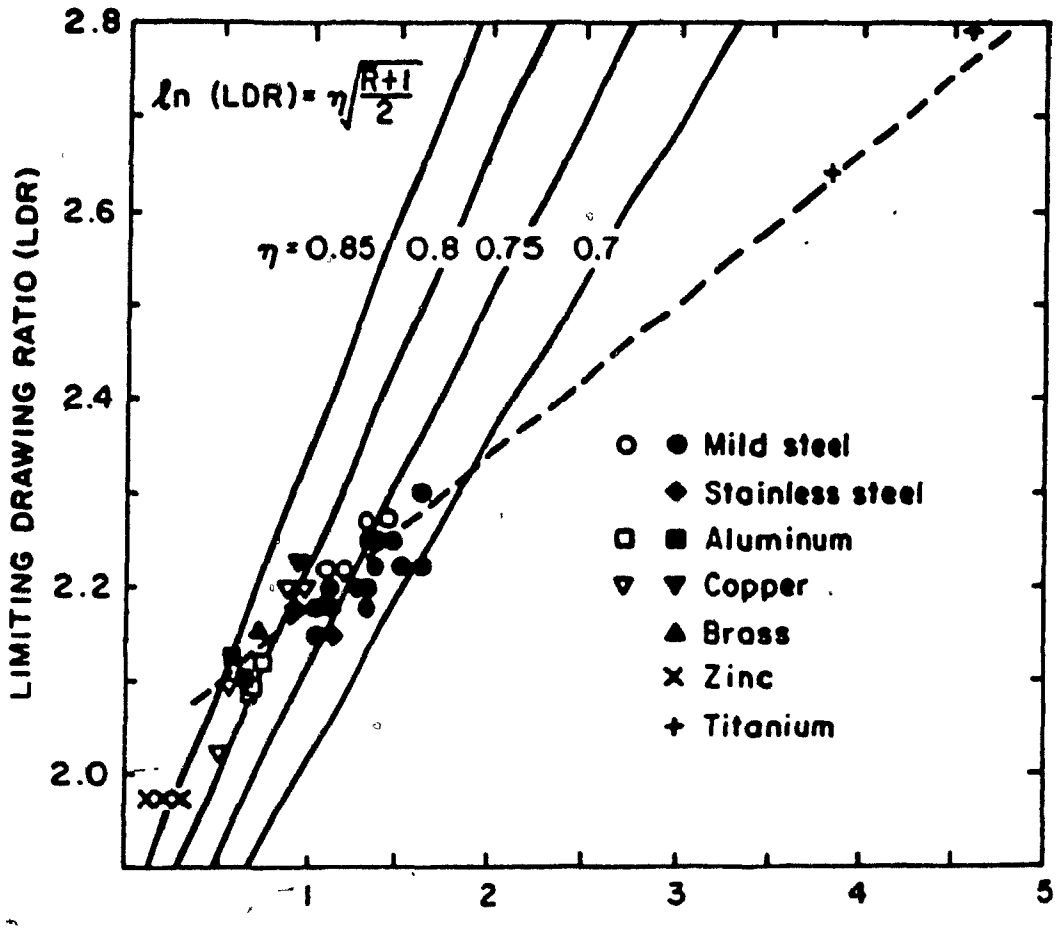

Figure 1.3 Correlation between limiting drawing ratio for cylindrical flat bottom cups and average strain ratio. Solid points are from Whiteley [6], open points from Lloyd [20], and crosses from Wilson and Butler [21]. The theoretical curves for Equation (1.13) do not fit the data.

1.4) Crystallographic Basis of the Dependence of Deep-Drawability on Normal Anisotropy:

The validity of equation 1.12 depends sensitively on the exact shape of the yield locus for the reasons mentioned in the previous section. The Hill quadratic theory must, therefore, be regarded only as a simple and very useful engineering approximation for describing anisotropic behaviour [7]. In fact, the experimentally determined yield loci are often not elliptical, even for cubic metals. Yield loci can also be calculated on the basis of a crystallographic analysis [24-27]. Some of these, which lead to correlations between LDR and R in much better agreement with experimental results, will now be described.

The early analysis of Taylor [28] of the deformation of polycrystals, together with the later developments by Bishop and Hill [29], have provided a basis for predicting plastic anisotropy from texture in FCC and BCC metals. Figures 1.4 and 1.5 are the result of computer calculations based on the Bishop and Hill analysis for FCC metals. The basic method of calculation is described by Piehler and Backofen [24]. Textures with rotational symmetry about an [hkℓ] direction normal to the sheet were approximated by averaging M vs. r curves for individual orientations differing by 1 or 2 degree rotations about [hkℓ]. Here M is the Taylor factor defined as

$$M = \frac{dw}{\tau d\varepsilon_x} = \frac{1}{\tau}\left[\sigma_x - r\sigma_y + (r-1)\sigma_z\right] \qquad (1.14)$$

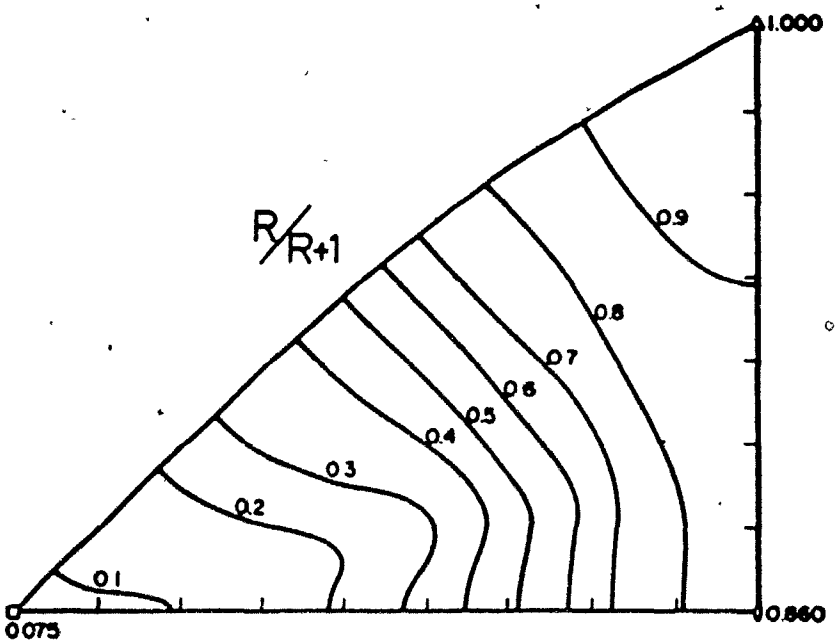

Figure 1.4 Orientation dependence of the calculated strain ratio R/R + 1 for rotationally symmetric textures in cubic metals with [hkℓ] normal to the sheet [7].

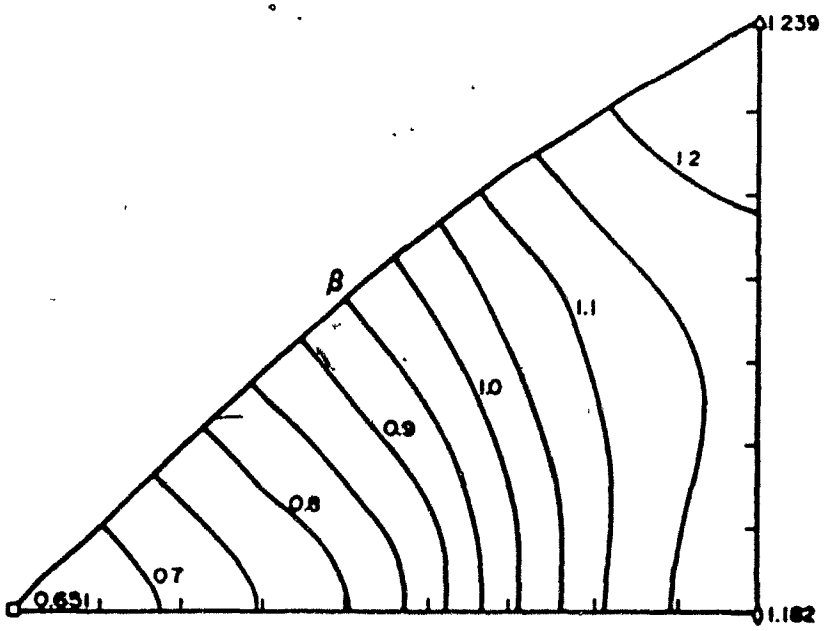

Figure 1.5 Calculated variation of the anisotropy parameter β with orientation for rotationally symmetric textures in cubic metals with [hkℓ] normal to the sheet [7].

and

$$r = \frac{R}{R + 1} = - \frac{d\varepsilon_y}{d\varepsilon_x} \qquad (1.15)$$

where x, y and z are the length, width and thickness directions in a tensile specimen cut from the sheet. The β values are taken as equal to the ratios $\bar{M}(r=1)/\bar{M}(r=0)$, and the r values expected experimentally are assumed to correspond to the minimum in $\bar{M}$ vs. r curves, such as the ones shown in Figures 1.6 and 1.7 [30], where $\bar{M}$ represents the average M defined above.

The β values calculated in this way are plotted in Figure 1.8 vs. the calculated R-values for 47 orientations over the basic orientation triangle. The relation between β and R according to Hill's quadratic criterion (equation 1.12) is also shown. It is clear that, for R > 1, equation 1.12 predicts too much dependence of β on R. The crystallographic calculations can be used instead of the continuum theory to predict the dependence of β (and therefore LDR) on R. This does not lead to an analytical relationship but is defined by the trend line of Figure 1.8. It should be noted that the theoretical curves are for FCC metals assuming {111} < 110 > slip (or {110} < 111 > slip for BCC metals), and the fact that the points for HCP zinc and titanium lie some distance from the curves should not be considered problematic in view of their entirely different slip systems [31,32]. A practical implication of these crystallographic calculations is

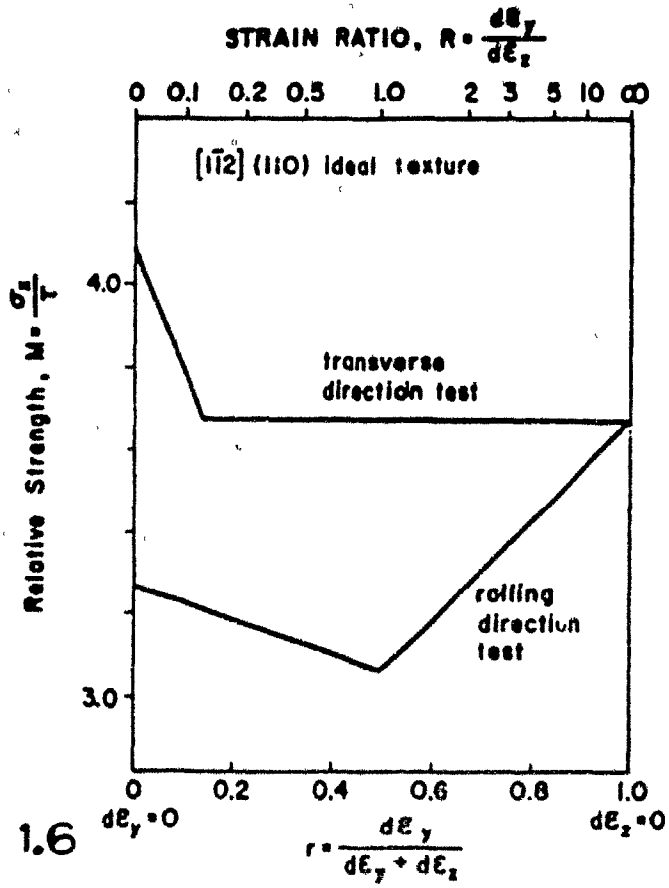

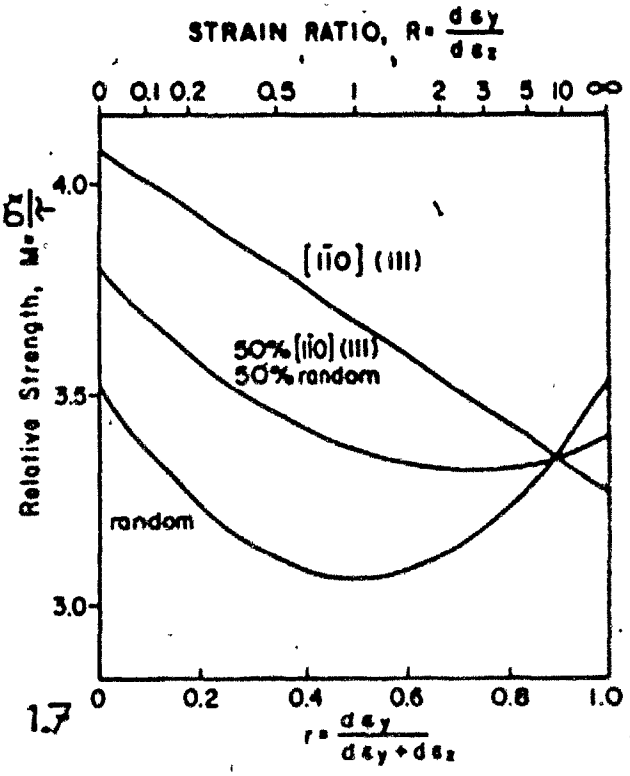

Figure 1.6 Dependence of M on r for rolling and transverse direction tension tests in a sheet of ideal [112] (110) texture. Expected behaviour corresponds to lowest M values [30].

Figure 1.7 Dependence of M on r for rolling direction tension tests of sheets with ideal [110] (111) texture, with randomly oriented grains, and with equal mixture of ideal [110] (111) and random components. The presence of 50% randomly oriented grains shifts the minimum M from r = 1, (R = ∞) to r = 0.7 (R = 2.33) [30].

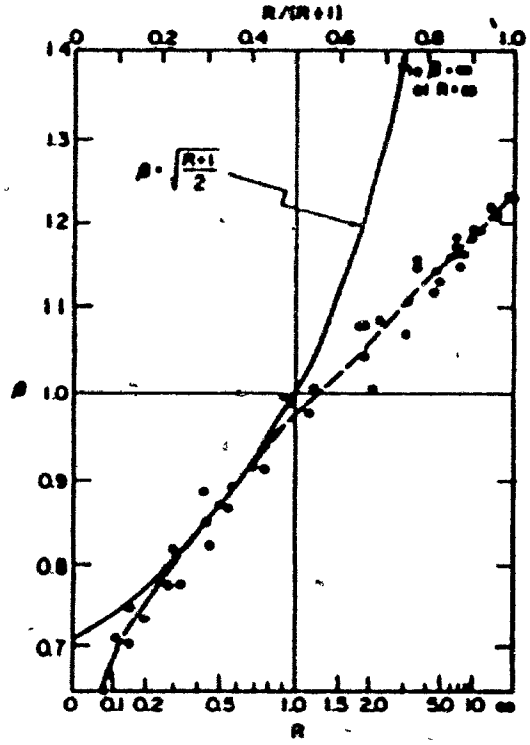

1.8

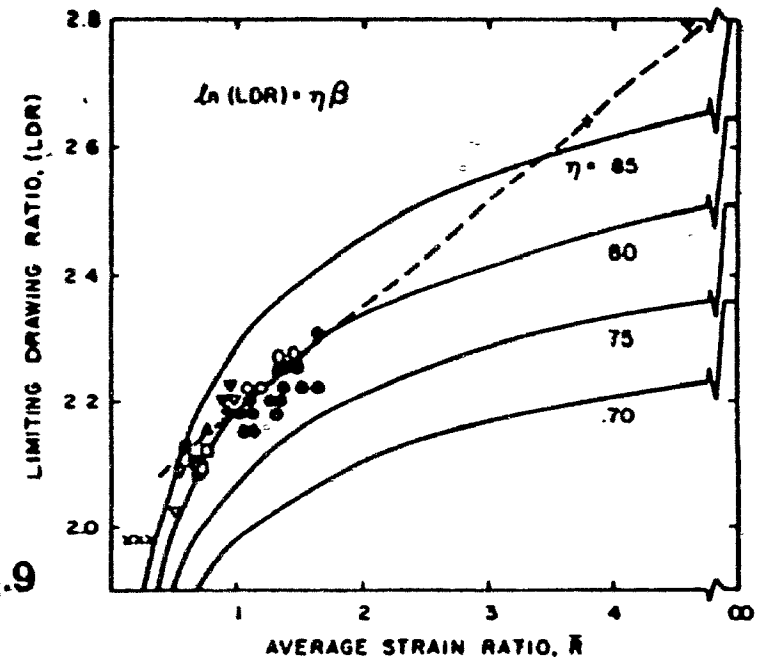

1.9

Figure 1.8 Relation between R and β for radially symmetric sheets. Points are calculated R and β values for 47 orientations over the basic orientation triangle for cubic metals with rotationally symmetric textures. The solid line is Equation 1.12, based on Hill's theory. Clearly this overestimates the dependence of β on R for R > 1 [31].

Figure 1.9 Correlation between limiting drawing ratio and average strain ratio. Experimental points are the same as in Figure 1.3. The theoretical curves were developed by substituting the R-β relationship for cubic metals from Figure 1.5 into Equation 1.13. Note the improved fit, except for hcp Ti and Zn [31].

that the further improvement of R-value through texture control can be expected to lead to only modest improvements in drawability, i.e. to improvements considerably below those expected from the Hill theory. Even when $R = \infty$ (pure {111} texture, see Figure 1.4) the LDR should only reach about 2.48 when $\eta = 0.75$ (see Figure 1.9).

CHAPTER 2

ANALYTICAL YIELD SURFACES

2.1) Hill's Quadratic Theory:

Hill [23] formulated a quantitative treatment of plastic anisotropy without direct regard to its crystallographic basis. He assumed a homogeneous material characterized by three mutually orthogonal planes of symmetry, the intersections of which are known as the principal axes of anisotropy. In a rolled sheet, these principal axes are the rolling (1), transverse (2) and through-thickness or normal (3) directions. The theory assumes that there is no Bauschinger effect (hence linear terms must not be included), and that the superposition of a hydrostatic stress does not influence yielding (hence only differences of the normal components can appear).

The proposed quadratic yield criterion has then the form:

$$2f(\sigma_{ij}) = F(\sigma_{22}-\sigma_{33})^2 + G(\sigma_{33}-\sigma_{11})^2 + H(\sigma_{11}-\sigma_{22})^2 + 2L\sigma_{23}^2 + 2M\sigma_{31}^2 + 2N\sigma_{12}^2 = 1 \qquad (2.1)$$

where F,G,H,L,M and N are constants which characterize the anisotropy.

2.2) Relation Between Stress and Strain-increments:

If attention is restricted to cases involving only the normal stresses, σ_1, σ_2 and σ_3, the yield surface may be represented as a cylinder whose axis is equally inclined to the σ_1, σ_2 and σ_3 axes (Figure 2.1.a). No loss of generality is incurred in a two-dimensional section on the $\sigma_3 = 0$ plane (Figure 2.1.b). Any stress state for which $\sigma_3 \neq 0$ is represented on such a locus by an equivalent stress state, $(\sigma_1', \sigma_2', \sigma_3') = (\sigma_1 - \sigma_3, \sigma_2 - \sigma_3, 0)$, which differs from the $(\sigma_1, \sigma_2, \sigma_3)$ state only by the hydrostatic components [33,34].

The strain which occurs during yielding must obey the flow rule,

$$d\varepsilon_{ij} = d\lambda \frac{\partial f(\sigma_{ij})}{\partial \sigma_{ij}} \qquad (2.2)$$

which means that the strain vector must be normal to the yield locus (Fig. 2.1.b).

Applying this flow rule, the strain increments are then:

$$d\varepsilon_{11} = d\lambda[G(\sigma_{11} - \sigma_{33}) + H(\sigma_{11} - \sigma_{22})] \qquad (2.3.a)$$

$$d\varepsilon_{22} = d\lambda[F(\sigma_{22} - \sigma_{33}) + H(\sigma_{22} - \sigma_{11})] \qquad (2.3.b)$$

$$d\varepsilon_{33} = d\lambda[F(\sigma_{33} - \sigma_{22}) + G(\sigma_{33} - \sigma_{11})] \qquad (2.3.c)$$

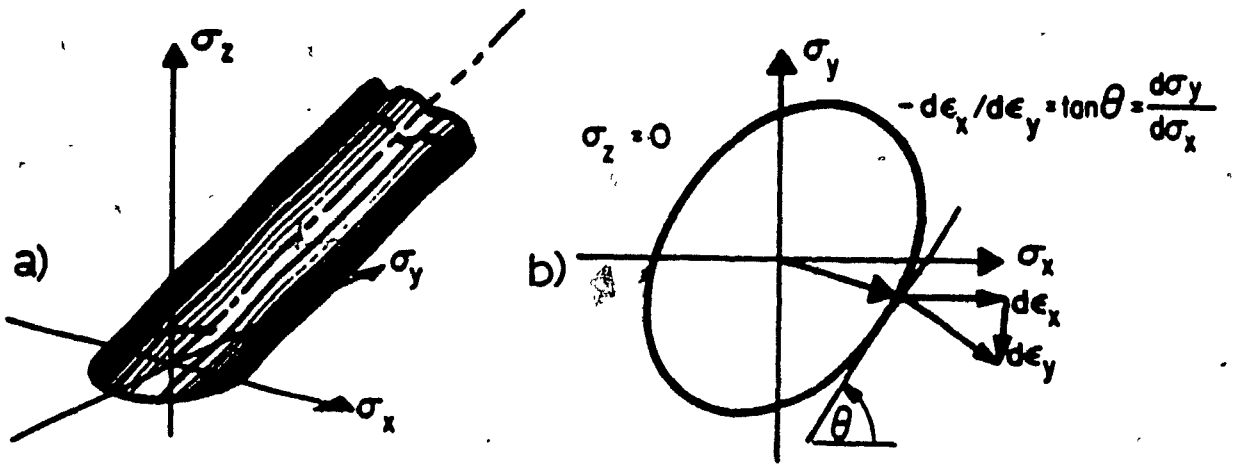

Figure 2.1 a) The yield surface of a material in which yielding is not sensitive to hydrostatic stress. The locus is a cylinder with an axis equally inclined to the three normal stress directions.

b) The $\sigma_3 = 0$ section of the above locus. The vectors representing the plastic strains on yielding are normal to the yield locus at the point of yielding.

If, however, there is a shear stress component σ_{12}, there must automatically be a shear strain increment as well:

$$d\varepsilon_{12} = d\varepsilon_{21} = d\lambda\ N\ \sigma_{12} \qquad (2.3.d)$$

2.3) Determination of Strain Ratio R from the Hill Parameters:

The R value is defined as the ratio of incremental strains in the width and thickness directions in a tensile specimen pulled at an angle α from the rolling direction in the plane of the sheet (see Figure 2.2). If $d\varepsilon_{yy}$ and $d\varepsilon_{zz}$ are the strain increments in the width and thickness directions, respectively, then:

$$R = \frac{d\varepsilon_{yy}}{d\varepsilon_{zz}} \qquad (2.4)$$

The stress tensor during idealized uniaxial testing, expressed in the specimen axes, is:

$$[\sigma]_{xyz} = \begin{bmatrix} \sigma_{xx} & 0 & 0 \\ 0 & 0 & 0 \\ 0 & 0 & 0 \end{bmatrix}$$

and in the principal axes of anisotropy, it becomes:

$$[\sigma]_{123} = T \cdot [\sigma]_{xyz} \cdot T^{-1},$$

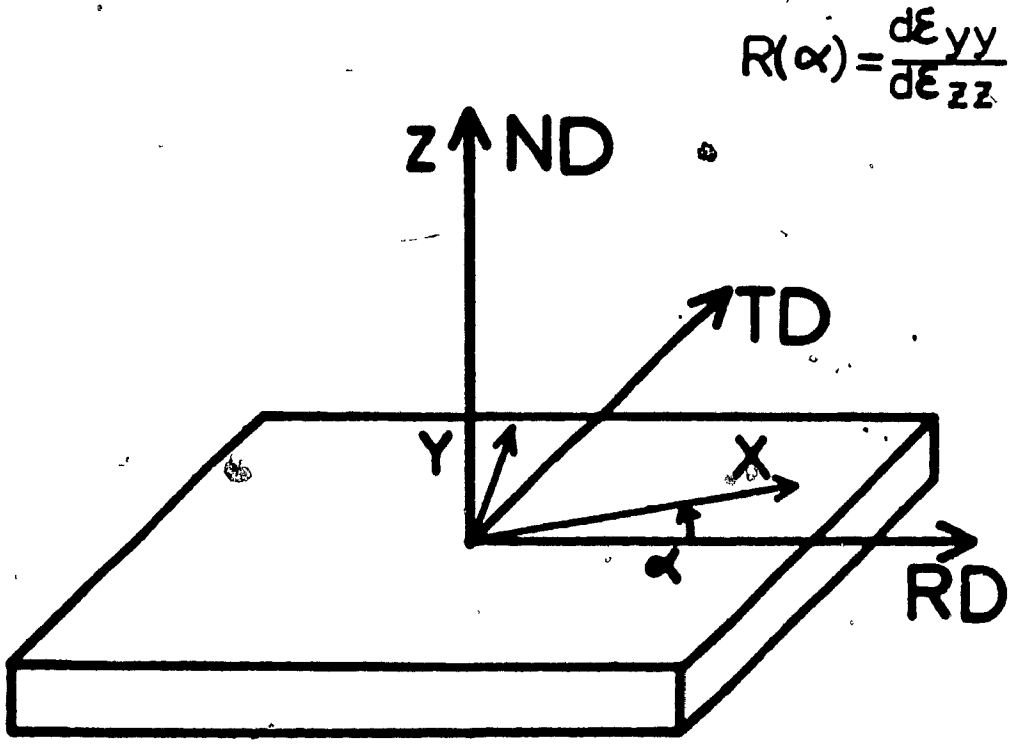

Figure 2.2 System of coordinate axes for rolled sheet and tensile specimen inclined at an angle α to the rolling direction.

where T is the transformation matrix, and T^{-1} its inverse:

$$T = \begin{bmatrix} \cos\alpha & -\sin\alpha & 0 \\ \sin\alpha & \cos\alpha & 0 \\ 0 & 0 & 0 \end{bmatrix}, \text{ and } T^{-1} = \begin{bmatrix} \cos\alpha & \sin\alpha & 0 \\ -\sin\alpha & \cos\alpha & 0 \\ 0 & 0 & 0 \end{bmatrix},$$

then,

$$[\sigma]_{123} = \begin{bmatrix} \sigma_{xx}\cos^2\alpha & \sigma_{xx}\cos\alpha\sin\alpha & 0 \\ \sigma_{xx}\cos\alpha\sin\alpha & \sigma_{xx}\sin^2\alpha & 0 \\ 0 & 0 & 0 \end{bmatrix} = \begin{bmatrix} \sigma_{11} & \sigma_{21} & \sigma_{31} \\ \sigma_{12} & \sigma_{22} & \sigma_{32} \\ \sigma_{13} & \sigma_{23} & \sigma_{33} \end{bmatrix}$$

Now Equations 2.3.a to 2.3.d become:

$$d\varepsilon_{11} = d\lambda\ \sigma_{xx}\ [H(\cos^2\alpha - \sin^2\alpha) + G\cos^2\alpha] \qquad (2.5.a)$$

$$d\varepsilon_{22} = d\lambda\ \sigma_{xx}\ [F\sin^2\alpha + H(\sin^2\alpha - \cos^2\alpha)] \qquad (2.5.b)$$

$$d\varepsilon_{33} = d\lambda\ \sigma_{xx}\ [-G\cos^2\alpha - F\sin^2\alpha] \qquad (2.5.c)$$

$$d\varepsilon_{12} = d\lambda\ \sigma_{xx}\ N\cos\alpha\sin\alpha \qquad (2.5.d)$$

$$d\varepsilon_{23} = d\varepsilon_{31} = 0 \qquad (2.5.e)$$

Again transforming back to the xyz system,

$$[d\varepsilon]_{xyz} = T^{-1}[d\varepsilon]_{123}\ T,$$

hence,

$$d\varepsilon_{xx} = \cos^2\alpha\, d\varepsilon_{11} + \sin^2\alpha\, d\varepsilon_{22} + 2\cos\alpha \sin\alpha\, d\varepsilon_{12} \qquad (2.6.a)$$

$$d\varepsilon_{yy} = \sin^2\alpha\, d\varepsilon_{11} + \cos^2\alpha\, d\varepsilon_{22} - 2\cos\alpha \sin\alpha\, d\varepsilon_{12} \qquad (2.6.b)$$

$$d\varepsilon_{zz} = d\varepsilon_{33} \qquad (2.6.c)$$

$$d\varepsilon_{xy} = -\sin\alpha \cos\alpha\, d\varepsilon_{11} + \sin\alpha \cos\alpha\, d\varepsilon_{22} + (\cos^2\alpha - \sin^2\alpha)\, d\varepsilon_{12} \qquad (2.6.d)$$

$$d\varepsilon_{xz} = d\varepsilon_{yz} = 0 \qquad (2.6.e)$$

Then, substituting 2.5.a,b,c and d into 2.6.b and c, we get:

$$R(\alpha) = \frac{d\varepsilon_{yy}}{d\varepsilon_{zz}} = \frac{H + (2N - G - F - 4H)\sin^2\alpha \cos^2\alpha}{G\cos^2\alpha + F\sin^2\alpha} \qquad (2.7)$$

Thus, the $R(\alpha)$ values can be written, for $\alpha = 0°$, $45°$ and $90°$, as follows:

$$R_0 = H/G \qquad (2.8)$$

$$R_{90} = H/F \qquad (2.9)$$

$$R_{45} = \frac{N}{F+G} - \frac{1}{2} \qquad (2.10)$$

2.4) Determination of Hill Parameters:

In order to calculate the values R_0, R_{90} and R_{45} expressed in equations 2.8 to 2.10 above, it is necessary to determine the four Hill parameters F, G, H and N. This requires at least four experimental tests.

i) Uniaxial tension:

When loading is restricted to plane stress, the Hill's criterion becomes:

$$F\sigma_{22}^2 + G\sigma_{11}^2 + H(\sigma_{11} - \sigma_{22})^2 + 2N\sigma_{12}^2 = 1 \qquad (2.11)$$

The yield stress along an x-axis inclined at an angle α from the rolling direction in the plane of the sheet can be expressed as a function of F, G, H and N by writing:

$$\sigma_{11} = \sigma_{xx} \cos^2\alpha$$

$$\sigma_{22} = \sigma_{xx} \sin^2\alpha \qquad (2.12)$$

$$\sigma_{12} = \sigma_{xx} \sin\alpha \cos\alpha$$

If x, y and x_{45} are the yield stress along the directions α = 0, 90° and 45° respectively, it can easily be shown, by substituting equations 2.12 into equation 2.11, that:

$$G + H = 1/x^2$$

$$F + H = 1/y^2 \qquad (2.13)$$

$$F + G + 2N = 4/x_{45}^2$$

ii) Uniaxial compression:

In this test, the only applied stress is σ_{33} along the through-thickness direction. Here Hill's criterion reduces to:

$$F\sigma_{33}^2 + G\sigma_{33}^2 = 1 \qquad (2.14)$$

If z is the yield stress in this test, then:

$$F + G = 1/z^2 \qquad (2.15)$$

iii) Plane strain tension:

In plane strain tension along a principal direction in the plane of the sheet, all the shear stresses (σ_{12}, σ_{23}, σ_{13}) and the normal stress (σ_{33}) are zero, and Hill's criterion reduces to:

$$F\sigma_{22}^2 + G\sigma_{11}^2 + H(\sigma_{11} - \sigma_{22})^2 = 1 \qquad (2.16)$$

For the test along the transverse direction, $d\varepsilon_{11} = 0$ by definition and thus, $\frac{\partial f}{\partial \sigma_{11}} = 0$. Therefore, differentiation with respect to σ_{11} yields:

$$2G\sigma_{11} + 2H\sigma_{11} - 2H\sigma_{22} = 0$$

or $$\sigma_{11} = \frac{H}{H+G}\ \sigma_{22} \qquad (2.17)$$

Substituting equation 2.17 into equation 2.16 finally gives:

$$\frac{H + G}{FH + FG + GH} = \sigma_{22}^2 = P'^2 \qquad (2.18)$$

where P' is the plane strain yield stress in the 2-direction. Similarly if P is the plane strain yield stress in the 1 direction, it can be shown that:

$$\frac{H + F}{FH + FG + GH} = \sigma_{11}^2 = P^2 \qquad (2.19)$$

Finally, the 6 equations developed from the tests described above are summarized as follows:

$$F + G = 1/z^2 \qquad (2.20.a)$$

$$G + H = 1/x^2 \qquad (2.20.b)$$

$$F + H = 1/y^2 \qquad (2.20.c)$$

$$F + G + 2N = 4/x_{45}^2 \qquad (2.20.d)$$

$$\frac{H + F}{FH + FG + GH} = p^{2} \qquad (2.20.e)$$

$$\frac{H + G}{FH + FG + GH} = p'^{2} \qquad (2.20.f)$$

It is now possible to solve for F, G, H, and N by using the above 6 equations. Leaving out equation (2.20.d), which is the only one where N appears, there remain 5 equations (2.20.a, b, c, e, f) and 3 unknowns (F, G, H). This suggests that ten different systems of equations may be solved, but since some tests are more reliable than others, only 3 systems should be solved (see Results chapter).

The final values of F, G and H will be an average of the values determined from the three systems, and using these values, the parameter N can then be found from equation 2.20 d. The values so determined can in turn be substituted into equations 2.8 to 2.10 to find R_0, R_{90} and R_{45}.

2.5) Special Case of Rotational Symmetry:

When rotational symmetry is assumed in the plane of the sheet, with $\sigma_3 = 0$, the Hill yield criterion reduces to:

$$(\sigma_1 + \sigma_2)^2 + (1 + 2R)(\sigma_1 - \sigma_2)^2 = 2(1 + R)\sigma_u^2 \qquad (2.21)$$

where σ_u is the yield stress in a uniaxial tensile test in

any direction in the plane of the sheet, and R is the ratio of the width plastic strain increment to the thickness plastic strain increment.

An important consequence of equation (2.21) is the relation between the yield stress in an equal biaxial tension test ($\sigma_1 = \sigma_2 = \sigma_b$), σ_u and R, that is:

$$\sigma_b = \left(\frac{1 + R}{2}\right)^{\frac{1}{2}} \sigma_u \qquad (2.22)$$

Many authors [35-39] have investigated the relationship between σ_b, σ_u and R in order to check the validity of Hill's criterion. Since σ_u and R vary with direction, the average values $\bar{\sigma}_u$ and $\bar{R}$ are generally taken from the values obtained in several uniaxial tests performed at various angles with respect to the rolling direction. As can be seen from equation (2.22), the σ_b/σ_u ratio is expected to lie on the same side of unity as R. This gives rise to what Woodthorpe and Pearce [37] have named "the anomalous behaviour of aluminum". They measured $\bar{R}$ values to be less than one while they found $\bar{\sigma}_b/\bar{\sigma}_u$ to be greater than one. Figure 2.3 shows results of uniaxial tension and balanced biaxial tension carried out by Pearce [38] on annealed rimmed steel having an average R-value of 0.38. It is seen that the experimental curve is above the uniaxial curves, whereas the predicted curve falls well below the uniaxial curves. Mellor and Parmar [39] have stated that the theory of orthotropic plasticity does

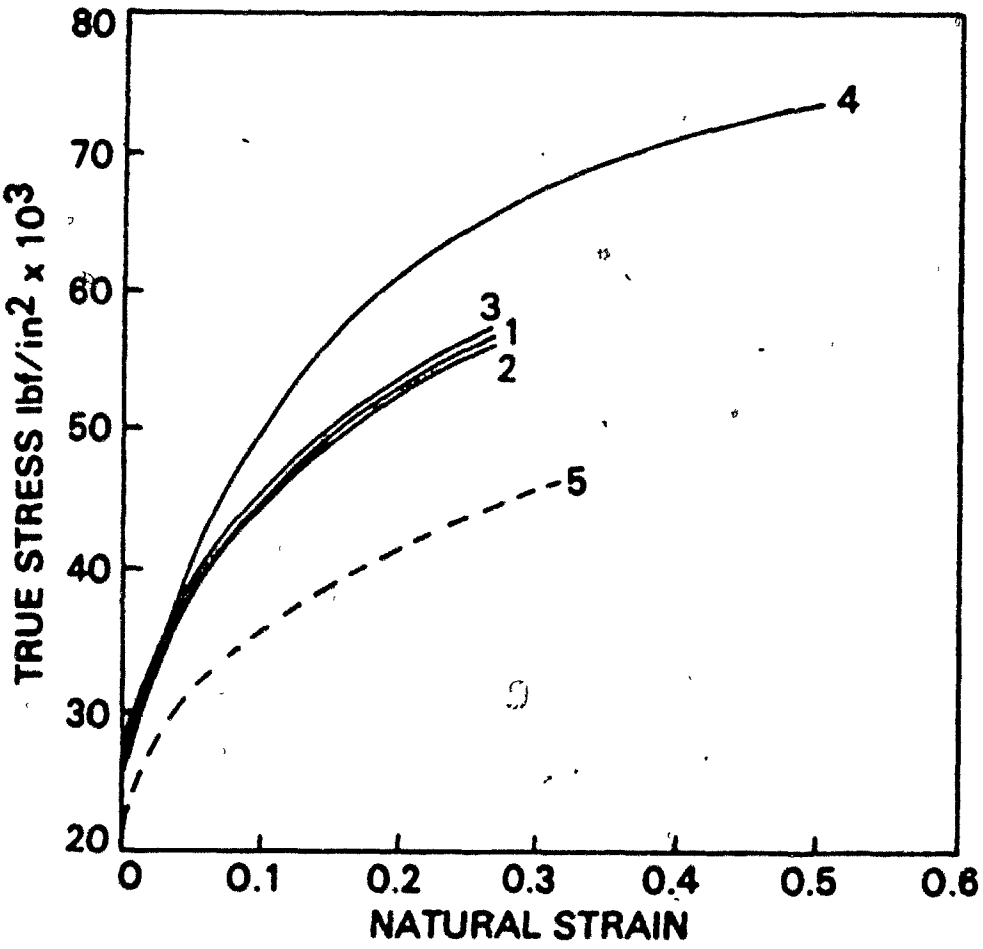

Figure 2.3 Work hardening characteristics for annealed rimmed steel. Measured average r-value is 0.38. Curves 1,2,3 are experimental curves in simple tension at 0°, 45° and 90° to rolling direction, respectively. Curve 4 is experimental curve for balanced biaxial tension. Curve 5 is balanced biaxial curve predicted from average r-value and corresponding work hardening characteristic [38].

not explain the behaviour in biaxial tension where the R-value is less than unity. Dillamore [40], arguing from a crystal plasticity point of view, has concluded that the orthotropic theory is only likely to give reasonable correlations for R-values between 1 and 2.

2.6) Hill's Generalized Criterion:

Hill [41] has proposed a new yield criterion, which will accommodate the results for balanced biaxial tension, and which is of interest for those materials having R-values less than unity. The criterion for plane stress, assuming that there is no planar anisotropy, is:

$$(1 + 2R)\left|\sigma_1 - \sigma_2\right|^m + \left|\sigma_1 + \sigma_2\right|^m = 2(1 + R)Y^m \quad (2.23)$$

where Y is the yield stress in uniaxial tension, R is the usual strain ratio measured in uniaxial tension, and m is a new parameter which must be determined experimentally. For the yield locus to be convex, $m > 1$. When $m < 2$, the locus is elongated in the direction of balanced biaxial tension. The effect of the parameter m is shown in Figure 2.4.

2.7) CMTP (Continuum Mechanics of Textured Polycrystals):

The CMTP approach, combining aspects of both the continuum and crystal plasticity analyses, was proposed recently by Montheillet et al. [42] and applied by Lequeu et al. [43] in order to predict the plastic strain ratio R(α) for

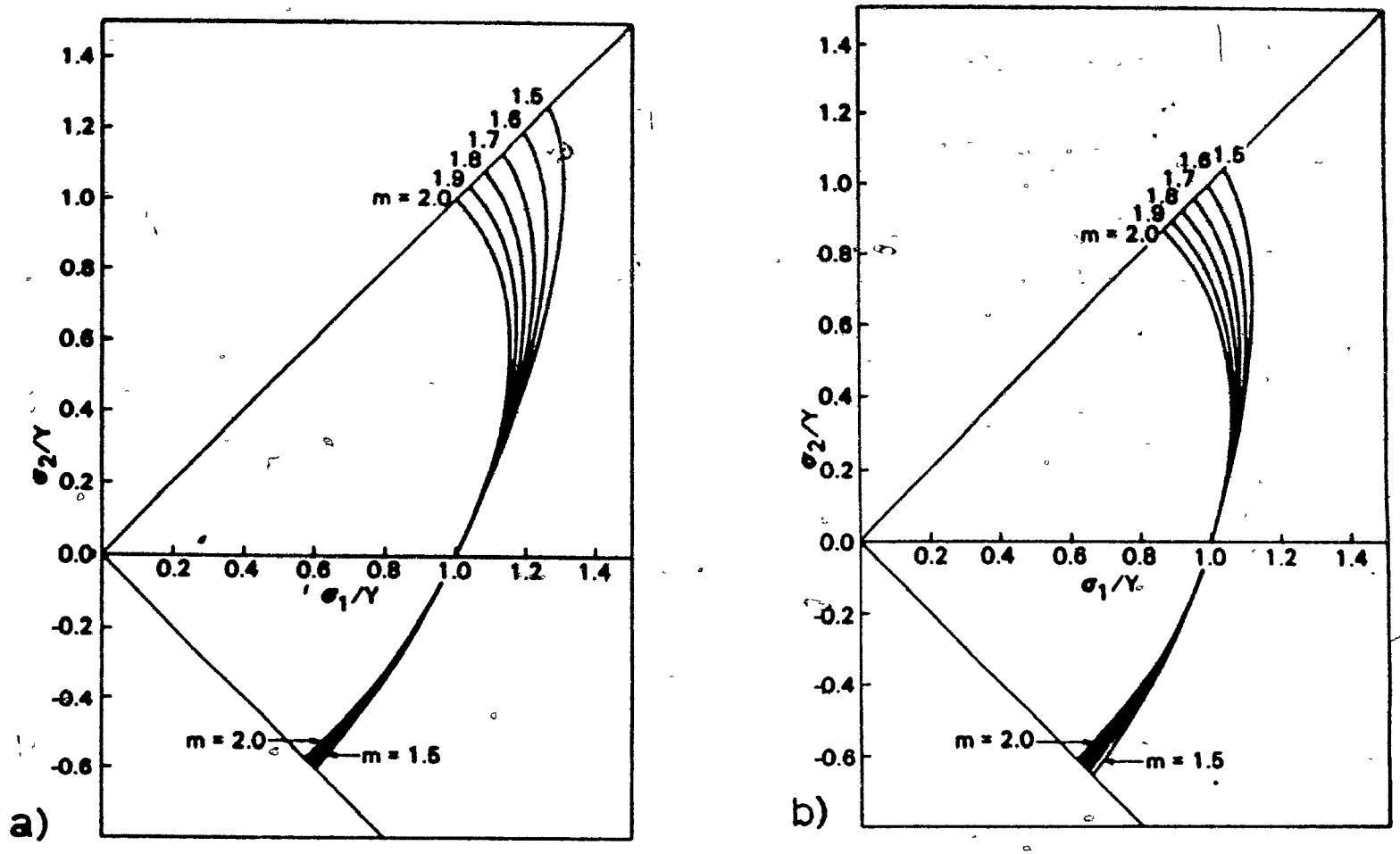

Figure 2.4 Yield loci based on the generalized anisotropic yield criterion proposed by Hill.
(a) r = 1.0
(b) r = 0.5

specific ideal orientations.

The CMTP analysis is only applicable to strongly textured cubic polycrystals which display a single or limited set of ideal orientations. For reasons that will be seen in the discussion, only the analysis based on the quadratic yield criterion is summarized here. For each ideal orientation, the <100> directions are taken as the principal axes of anisotropy. The Hill parameters are adjusted so that they give a best fit to the appropriate yield surface of the single crystal representing the ideal orientation. It was shown that:

$$F = G = H = \frac{\alpha}{6\tau_c^2} \quad \text{and} \quad L = M = N = \frac{\beta}{6\tau_c^2} \qquad (2.24)$$

where $\alpha = 0.49$ and $\beta = 0.66$ and τ_c is the critical resolved shear stress of the crystals. Thus the CMTP yield criterion can be expressed as:

$$F(\$) = 3\alpha(S_{11}^2 + S_{22}^2 + S_{33}^2) + 2\beta(S_{12}^2 + S_{23}^2 + S_{31}^2) = 6\tau_c^2$$

or, setting $\alpha = 1/2$ and $\beta = 2/3$ and taking $\sqrt{6}\,\tau_c$ as the unit of stress, as:

$$F(\$) = \frac{3}{2}(S_{11}^2 + S_{22}^2 + S_{33}^2) + \frac{4}{3}(S_{12}^2 + S_{23}^2 + S_{31}^2) = 1 \qquad (2.25)$$

where S_{ij} are the deviator stress components.

2.8) Prediction of R(α) by the CMTP Method:

Suppose that the rolled sheet has one single ideal orientation, {hkℓ} <uvw>. Let the superscripts S,C, and xyz represent the sheet (RD, TN, ND), crystal <100>, and tensile specimen axes, respectively. Let T_1 be the matrix for transformation from the crystal to the sheet.

$$T_1 = \begin{bmatrix} r_1 & u_1 & n_1 \\ r_2 & u_2 & n_2 \\ r_3 & u_3 & n_3 \end{bmatrix}$$

where $r_1 = u/\sqrt{u^2 + v^2 + w^2}$, $n_1 = h/\sqrt{h^2 + k^2 + \ell^2}$

$r_2 = v/\sqrt{u^2 + v^2 + w^2}$, $n_2 = k/\sqrt{h^2 + k^2 + \ell^2}$

$r_3 = w/\sqrt{u^2 + v^2 + w^2}$, $n_3 = \ell/\sqrt{h^2 + k^2 + \ell^2}$,

and $\vec{u} = \vec{n} \times \vec{r}$

Then, let T_2 be the matrix for transformation from the sheet to the specimen.

$$T_2 = \begin{bmatrix} \cos\alpha & -\sin\alpha & 0 \\ \sin\alpha & \cos\alpha & 0 \\ 0 & 0 & 0 \end{bmatrix}$$

Therefore the matrix for transformation from the crystal to the specimen is:

$$T = T_1 \cdot T_2 = \begin{bmatrix} a_1 & b_1 & n_1 \\ a_2 & b_2 & n_2 \\ a_3 & b_3 & n_3 \end{bmatrix}$$

$$\left.\begin{aligned} \text{where } a_i &= r_i \cos\alpha + u_i \sin\alpha \\ b_i &= -r_i \sin\alpha + u_i \cos\alpha \quad \text{for } i = 1,2,3 \end{aligned}\right\} \qquad (2.26)$$

The stress tensor in the crystal axes can be expressed as:

$$[\sigma]^C = T.[\sigma]^{xyz}.T^{-1} \quad \text{where } [\sigma]^{xyz} = \begin{bmatrix} \sigma & 0 & 0 \\ 0 & 0 & 0 \\ 0 & 0 & 0 \end{bmatrix}$$

which leads to:

$$[\sigma]^C = \sigma \begin{bmatrix} a_1^2 & a_1a_2 & a_1a_3 \\ a_1a_2 & a_2^2 & a_2a_3 \\ a_1a_3 & a_2a_3 & a_3^2 \end{bmatrix}$$

Applying the normality principle to the CMTP yield criterion, we obtain:

$$[d\varepsilon]^C = 2d\lambda\sigma \begin{bmatrix} \frac{3}{2}a_1^2 - \frac{1}{2} & \frac{2}{3}a_1a_2 & \frac{2}{3}a_1a_3 \\ \frac{2}{3}a_1a_2 & \frac{3}{2}a_2^2 - \frac{1}{2} & \frac{2}{3}a_2a_3 \\ \frac{2}{3}a_1a_3 & \frac{2}{3}a_2a_3 & \frac{3}{2}a_3^2 - \frac{1}{2} \end{bmatrix}$$

and finally

$$[d\varepsilon]^{xyz} = T^{-1}[d\varepsilon]^{C}\,T, \text{ or}$$

$$[d\varepsilon]^{xyz} = d\lambda\sigma \begin{bmatrix} \frac{5}{3}\sum(a_i^4) + \frac{1}{3} & * & * \\ \frac{5}{3}\sum(a_i^3 b_i) & \frac{5}{3}\sum(a_i^2 b_i^2)-1 & * \\ \frac{5}{3}\sum(a_i^3 n_i) & \frac{5}{3}\sum(a_i^2 b_i n_i) & \frac{5}{3}\sum(a_i^2 n_i^2)-1 \end{bmatrix}$$

where the summations over the index i are extended from 1 to 3.

The strain rate ratio is therefore

$$R(\alpha) = \frac{d\varepsilon_{yy}}{d\varepsilon_{zz}} = \frac{\frac{5}{3}\sum(a_i^2 b_i^2)-1}{\frac{5}{3}\sum(a_i^2 n_i^2)-1}$$

and finally, with the aid of 2.26, and after symmetry considerations ($R(-\alpha) = R(\alpha)$, and $R(\pi-\alpha) = R(\alpha)$), this leads to:

$$R(\alpha) = \frac{\frac{1}{4}\sum(u_i^4 + r_i^4 - 2u_i^2 r_i^2)\sin^2 2\alpha + \sum(u_i^2 r_i^2)\cos^2 2\alpha - 3/5}{\sum(r_i^2 n_i^2)\cos^2\alpha + \sum(u_i^2 n_i^2)\sin^2\alpha - 3/5}$$

CHAPTER 3

EXPERIMENTAL PROCEDURE

3.1) Experimental Material:

The material investigated was commercial purity aluminium 1100 supplied by Alcan International Ltd., Kingston Laboratories, Kingston, Ontario; its chemical composition is listed in table 3.1. Optical metallography showed that it was produced by hot rolling and had elongated grains. On receipt at McGill, it was annealed at 550°C for one hour, a process which transformed the microstructure into an equiaxed form (see Figure 3.1), and led to a more or less random texture (see Figure 3.2).

The elongated grain structure of the as received material was easily revealed by Keller's reagent (2 ml HF (48%), 3 ml HCl (conc), 5 ml HNO_3 (conc), 190 ml water) [44] after a careful mechanical polish. However, this reagent was not suitable for the observation of the annealed structure. For this reason, another metallographic technique [45] was used. After the usual mechanical polish, the annealed specimen was again polished electrolytically in a solution consisting of 5% perchloric acid (70% $HClO_4$) in pure ethanol. The solution was contained in a stainless steel vessel which acted as a cathode, and was chilled by melting ice. During the one to two minutes of polishing under a current density of 0.5 A/mm^2, the specimen was rotated in order to avoid pit

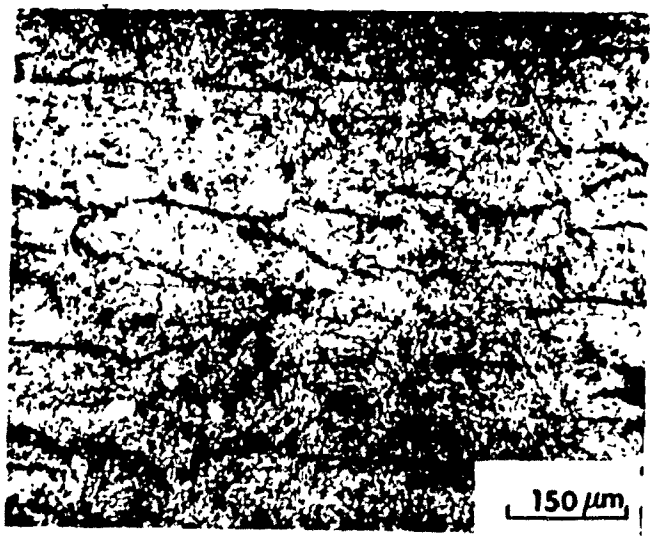

Figure 3.1 a) Optical micrograph of as received aluminium 1100.

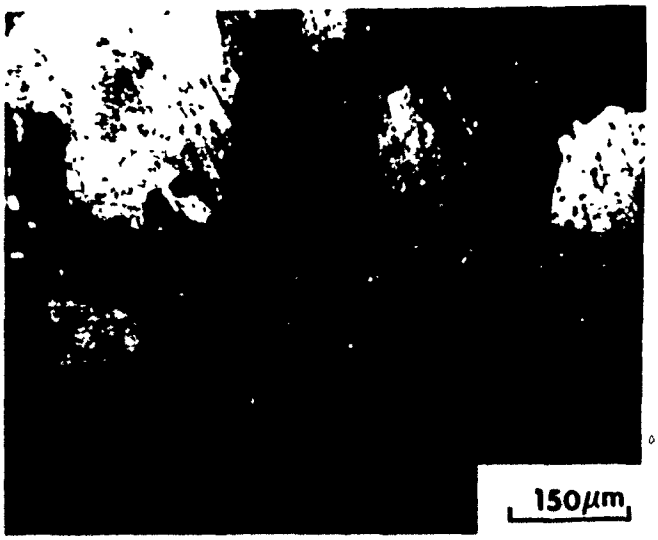

Figure 3.1 b) Optical micrograph of aluminium 1100 annealed at 550°C for 1 hour, and examined under polarized light after anodic oxidation.

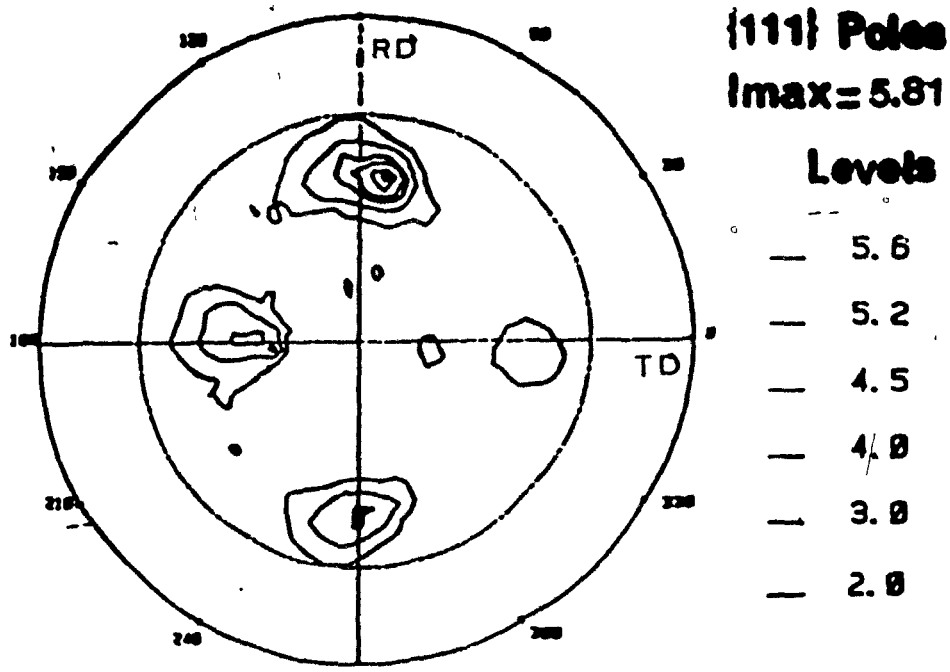

Figure 3.2 a) Texture of as received aluminium 1100.

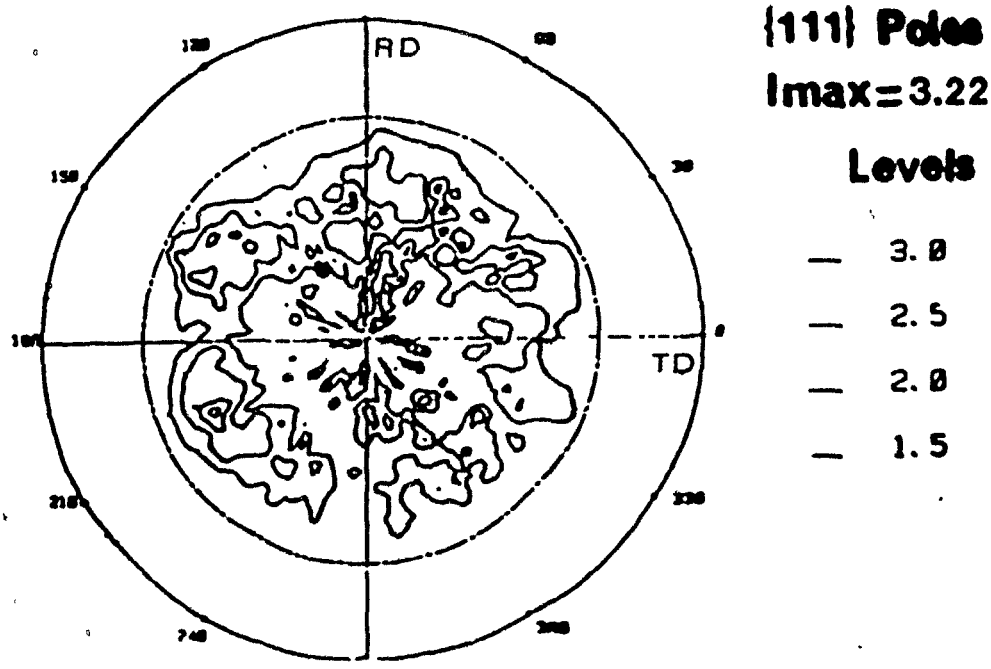

Figure 3.2 b) Texture of aluminium 1100 annealed at 550°C for 1 hour.

formation. The polished specimen was then anodized using Barker's reagent (4 ml HBF_4(48%), 200 ml water) at ambient temperature under about 20 V dc for 40 to 60 seconds, and observed under a microscope with crossed polarizers which finally revealed the grains as seen in figure 3.1b.

The sheet was initially around one inch thick (25.7 mm) and was cold rolled repeatedly in order to obtain ten different strain states ranging from an equivalent strain $\bar{\varepsilon} = 0$ to about 2.6 (see table 3.2). The equivalent strain for each sheet of thickness T is defined as:

$$\bar{\varepsilon} = \frac{2}{\sqrt{3}} \ln \left(\frac{T_o}{T}\right)$$

where T_o is the thickness of the initial sheet (25.7 mm).

Si	Fe	Cu	Mn	Mg	Ni	Zn	Ti	Cr	Al
0.158	0.693	0.063	0.025	0.010	0.003	0.013	0.025	0.007	Bal.

Table 3.1: Chemical Composition of Al 1100 (99.0% Al) - wt.%

Stage of Deformation	Thickness T (mm)	$\bar{\varepsilon} = \frac{2}{\sqrt{3}} \ln \left(\frac{T_o}{T}\right)$
0	25.70	0
1	20.35	0.26
2	16.40	0.52
3	13.15	0.77
4	10.45	1.03
5	8.45	1.28
6	6.60	1.56
7	5.30	1.82
8	4.25	2.07
9	3.35	2.35
10	2.70	2.59

Table 3.2: Stages of Deformation of the Sheet

3.2) Types of Specimens:

For each deformed sheet, as for the initial sheet, the following three types of tests were performed:

i) uniaxial tension along the rolling, transverse and 45° directions;

ii) plane strain tension along the rolling and transverse directions;

iii) uniaxial compression along the sheet normal direction.

Each test was repeated at least twice to ensure reproducibility. The specimen geometries are shown in Figures 3.3.a and 3.3.b. The uniaxial tension specimens were cut according to the subsize type described in ASTM standard, designation: A370. The dimensions of the plane strain specimen were taken from D.P. Clausing's publication [46]. As for the compression specimens, the usual geometry was adopted, the height of the specimen being 1.5 times its diameter. For the first three sheets, the height of the compression specimens was taken as the thickness of the sheet, but for the subsequent sheets, the thickness was too small to permit the use of a diameter equal to two-thirds of the thickness. For this reason, composite specimens were made so that the diameter was maintained larger than about 10 mm. For example, for the last sheet of 2.70 mm thickness, six cylinders were stuck together with super glue in order to obtain a composite specimen 16.20 mm in height and 10.80 mm in diameter. In addition to the difficulty of machining and handling very small specimens, a further reason for not employing them is that the accuracy of load and dimension measurement is not as good as for larger specimens.

3.3) Apparatus:

The various tests were all carried out at ambient temperature on an Instron universal testing machine. This machine incorporates a highly sensitive electronic weighing system with a load cell that uses strain gauges for detecting

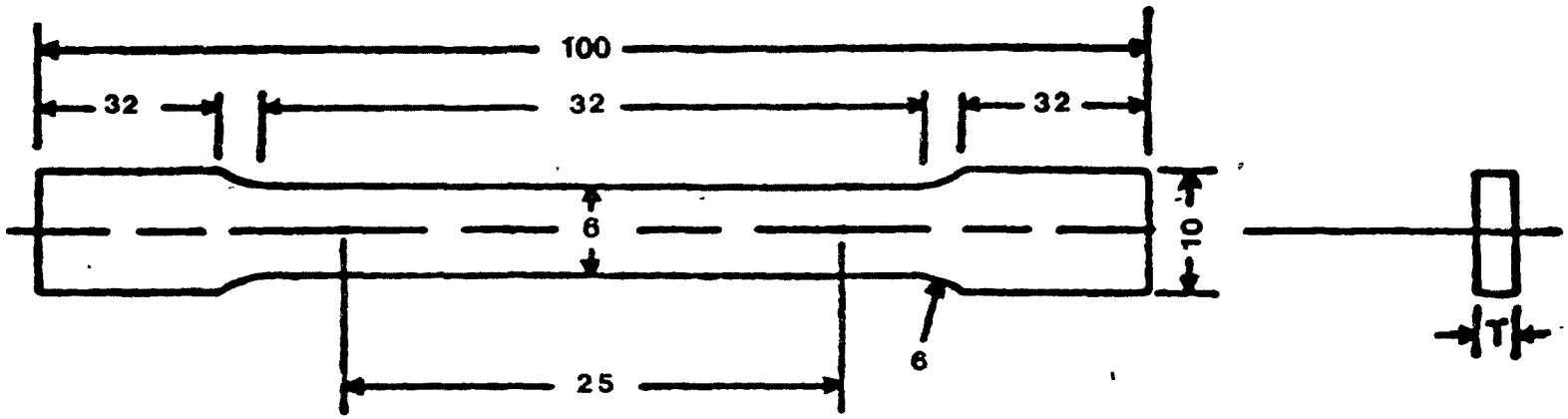

Figure 3.3 a) Geometry of uniaxial tension specimen.

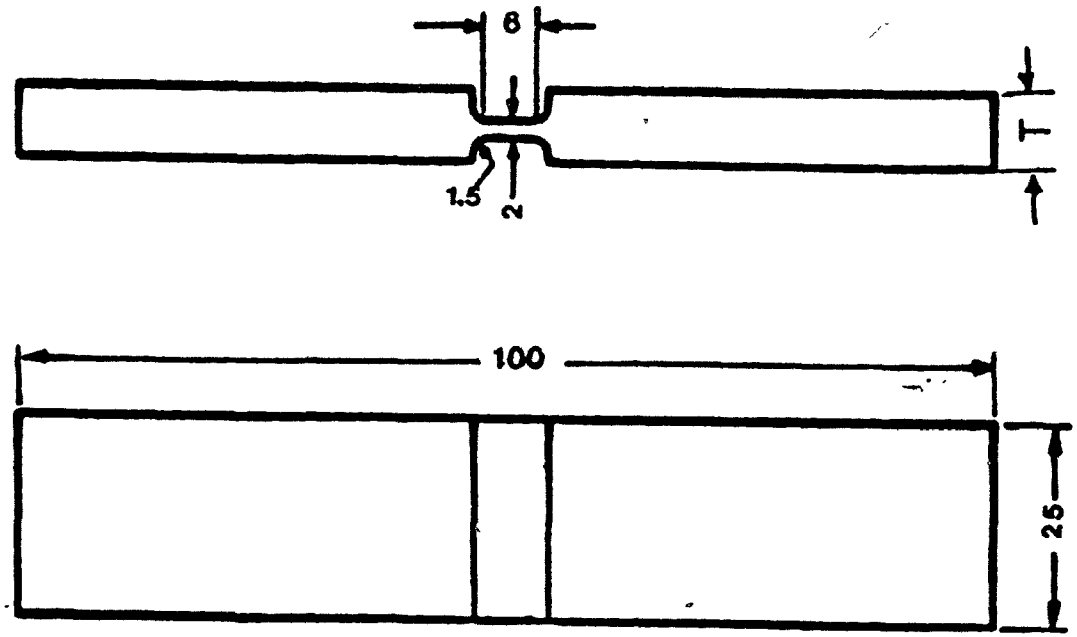

Figure 3.3 b) Geometry of plane strain tension specimen.

and recording tensile and compressive loads. The moving crosshead is operated by two vertical drive screws and a positional servomechanism for good accuracy and flexibility of control over crosshead motion. The chart of the recorder is driven synchronously at a wide variety of speed ratios (with respect to the crosshead) enabling measurement of sample extension or contraction to be made with a large choice of magnifications. Because of this synchronous operation and a low inherent deflection of the load cell as well as of the system as a whole, the time axis of the chart is a fairly accurate measure of grip position and sample extension or contraction. The accuracy of the overall load weighing system is ± 0.5% of the indicated load or ± 0.25% of the recorder scale in use, whichever is greater for all load ranges.

All the tests were carried out at a constant crosshead speed v of 2.5 mm/min. As can be seen below, this is equivalent to a strain rate $\dot{\varepsilon}$ of 1.32×10^{-3} s^{-1} to 1.18×10^{-3} s^{-1} in the case of uniaxial tension and 2.12×10^{-3} s^{-1} to 2.35×10^{-3} s^{-1} in the case of uniaxial compression.

For uniaxial tension,

$$\dot{\varepsilon} = \frac{v}{L} = \frac{v}{L_0 + \Delta L}$$

where L_0 is the gauge length and ΔL is the extension.

If v = 0.0423 mm/s (2.5 mm/min),

$L_0 = 32$ mm

$\Delta L = 0$ at the beginning of the test and $\Delta L = 4$mm at the end, then

$\dot{\varepsilon} = \frac{.0423}{32} = 13.2 \times 10^{-4}\ s^{-1}$ at the beginning of the test, and

$\dot{\varepsilon} = \frac{.042}{36} = 11.8 \times 10^{-4}\ s^{-1}$ at the end.

Doing the same for the compression tests, where in most cases $L_0 \simeq 20$ mm and $\Delta L \simeq 2$ mm, we find:

$\dot{\varepsilon} \simeq \frac{.0423}{20} \simeq 21.2 \times 10^{-4}\ s^{-1}$ at the beginning of the test, and

$\dot{\varepsilon} \simeq \frac{.0423}{18} \simeq 23.5 \times 10^{-4}\ s^{-1}$ at the end.

Obviously this variation in strain rate is small and unimportant for the following reasons: (i) we are primarily concerned here with the yield stress, which is unaffected by the above considerations; and (ii) as the strain rate sensitivity of aluminium is low at room temperature, the effect of the strain rate decrease during straining is small in any event. As for the effect of the difference in strain rate in tension and compression (that in compression being typically

twice as high as that in tension), this is again small for the same two reasons.

3.4) Measurement of Yield Stress:

The yield stress was determined by taking the 0.2% offset on the load/displacement curve (see Figure 3.4) and dividing by the original cross section of the specimen. The 0.2% offset is determined in the following manner: First the total extension of the specimen x_s is found by writing,

$$x_s = x_p \cdot v_s/v_p$$

(supposing the deflection of the machine is negligible). Here v_s is the velocity of one end of the specimen (or cross-head) and v_p that of the paper (or chart). Then the total percentage extension e_s is equal to x_s divided by the gauge length, and the 0.2% extension (distance OA on Figure 3.4) is equal to x_p multiplied by 0.2% divided by e_s.

eg: $x_p = 120$ mm ; $L_s = 30$ mm

$x_s = 6$ mm ; $e_s = 6/30 = 20\%$

then $x_{0.2}(= OA) = \frac{120 \times 0.2\%}{20\%} = 1.2$ mm

The 0.2% offset is found by drawing a line from A parallel to the loading line; it crosses the curve at point B and a

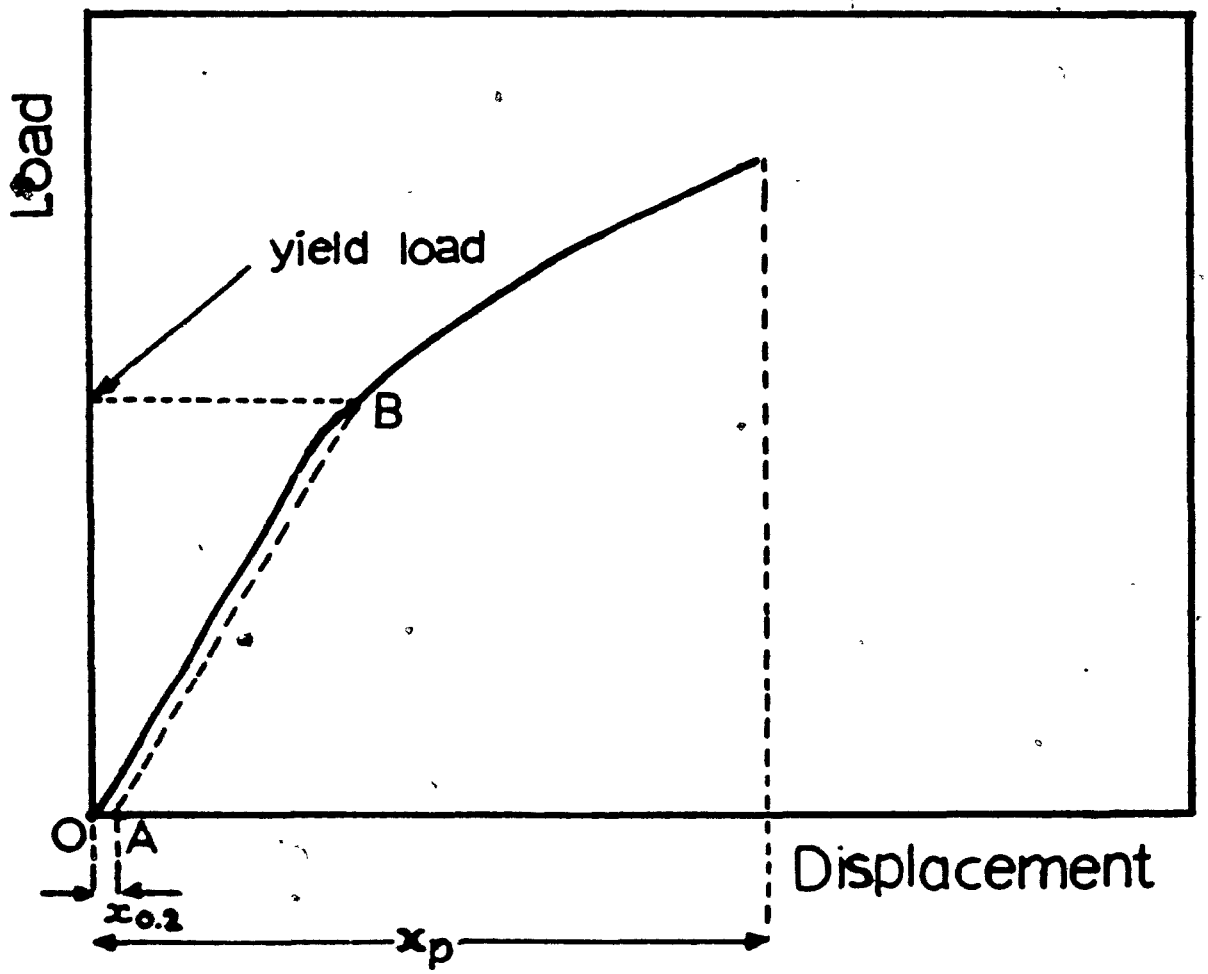

Figure 3.4 Load vs. displacement curve record during uniaxial tension test.

projection of this point on the load axis is then taken (see Figure 3.6).

3.5) Direct Measurement of R-value:

The resistance to thinning, or R-value, was determined in the rolling, transverse and 45° directions for the first three sheets by deforming the uniaxial tension specimen by increasing amounts and measuring the width and thickness after unloading. Some investigators have taken this value as being the ratio of the width to thickness strains, ε_y and ε_z respectively, at the limit of uniform elongation during the uniaxial tension test [9], or at 15% elongation [12]. However, this R-value cannot be compared to any theoretical value since it varies during elongation and does not characterize the behaviour of the undeformed sheet (see Figure 3.5). As can be seen from this figure, it is not easy to extrapolate the curve to zero strain because the error increases as the deformation decreases (note the error bars and see the error analysis below).

This problem is overcome by plotting ε_{yy} vs. ε_{zz} and taking the slope of the curve at zero strain. This is easily done since the curve has to go through the origin (Figure 3.6). This slope $d\varepsilon_{yy}/d\varepsilon_{zz}$ is indeed the current R-value, which can be compared to the theoretical value expressed as a function of the Hill parameters in Chapter 2.

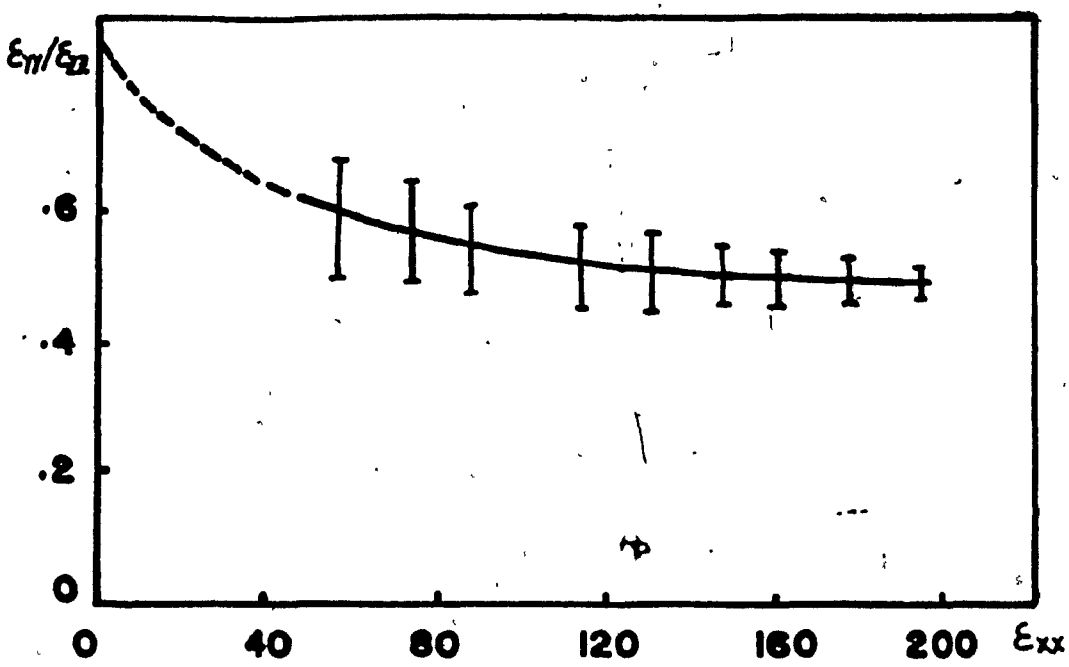

Figure 3.5 Dependence of strain ratio $R_S(=\varepsilon_{yy}/\varepsilon_{zz})$ on elongation strain. Note that error bars decrease with increasing strain.

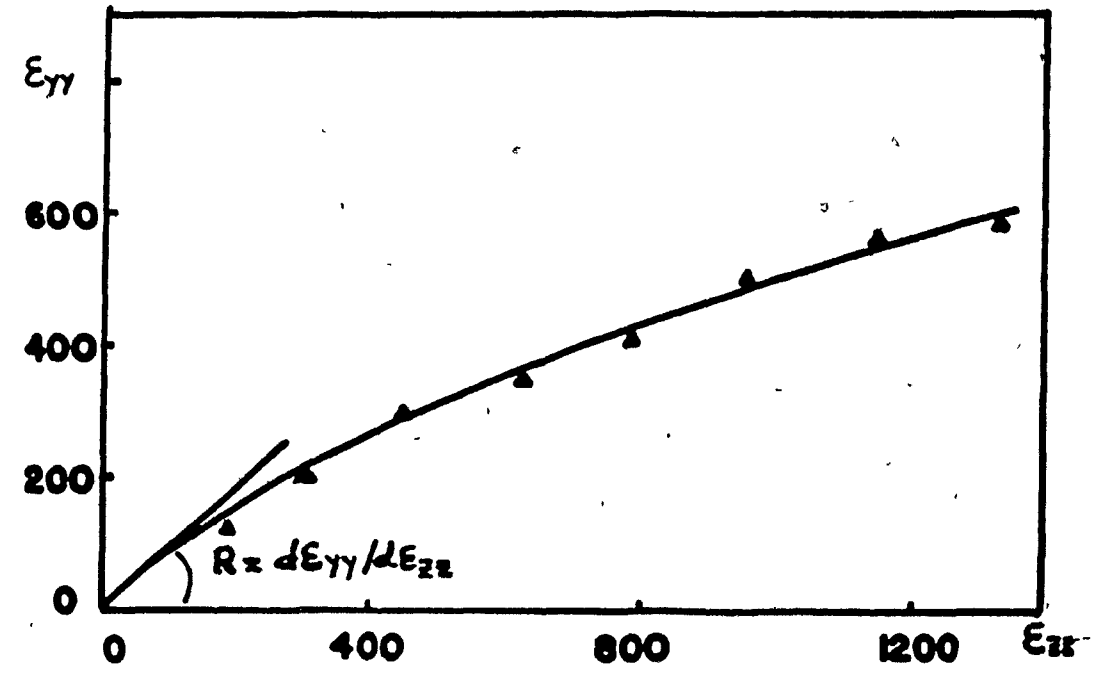

Figure 3.6 Width vs. thickness strains as measured in tensile test. The strain rate ratio $R(=d\varepsilon_{yy}/d\varepsilon_{zz})$ is taken as the slope of the curve at the origin.

3.6) Error Analysis on Experimental R-values:

If

$$R = \frac{\varepsilon_w}{\varepsilon_t} = \frac{\ln(w_o/w)}{\ln(t_o/t)} = \frac{\ln w_o - \ln w}{\ln t_o - \ln t},$$

then,

$$\Delta R = \left(\left|\frac{\partial R}{\partial w_o}\right| + \left|\frac{\partial R}{\partial w}\right|\right) \Delta_w + \left(\left|\frac{\partial R}{\partial t_o}\right| + \left|\frac{\partial R}{\partial t}\right| \Delta t\right.$$

$$= \left(\frac{1}{w_o \ln \frac{t_o}{t}} + \frac{1}{w \ln \frac{t_o}{t}}\right) \Delta w + \left(\frac{\ln(w_o/w)}{t_o(\ln(t_o/t)^2} + \frac{\ln(w_o/w)}{t(\ln(t_o/t)^2}\right) \Delta t$$

$$= \left(\frac{1}{w_o} + \frac{1}{w}\right) \frac{\Delta w}{\ln(t_o/t)} + \left(\frac{1}{t_o} + \frac{1}{t}\right) \frac{\ln(w_o/w)}{(\ln(t_o/t))^2} \Delta t$$

$$\frac{\Delta R}{R} = \left(\frac{1}{w_o} + \frac{1}{w}\right) \frac{\Delta w}{\ln(w_o/w)} + \left(\frac{1}{t_o} + \frac{1}{t}\right) \frac{\Delta_t}{\ln(t_o/t)}$$

Example:

t_o = 6.09 mm

w_o = 6.00 mm

$\Delta w = \Delta t$ = 0.01 mm (the accuracy of the micrometer).

1st strain increment

t = 6.02

w = 5.93 $\quad \frac{\Delta R}{R}$ = 0.285 + 0.222 = .507 = 50.7%

2^{nd} strain increment

$t = 5.92$

$w = 5.82 \qquad \frac{\Delta R}{R} = 0.111 + 0.118 = 0.229 = 22.9\%$

3^{rd} strain increment

$t = 5.65$

$w = 5.54 \qquad \frac{\Delta R}{R} = 0.0435 + 0.0455 = 0.089 = 8.9\%$

As can be seen, the error decreases with increasing deformation.

CHAPTER 4

EXPERIMENTAL RESULTS

4.1) Determination of the Experimental R-value:

The experimental R-value was measured directly for the first three sheets during uniaxial tension tests in the rolling, transverse and 45° directions. Each tensile specimen was deformed to an increasing interval of strain and unloaded after each interval in order to remove the elastic strain; then the thickness and width were measured, and the specimen was reloaded to a further strain. This procedure was repeated as many times as necessary to obtain sufficient points to plot a ε_{yy} vs. ε_{zz} curve, or until the limit of uniform elongation was reached. Note that for the sheets rolled to larger strains ($\bar{\varepsilon} > .52$), the limit of uniform elongation was reached more and more rapidly after the elastic limit, thus making it more and more difficult to make a large enough number of measurements of width and thickness strain before necking occurred. Therefore this method was abandoned after the first two rolling reductions.

For each specimen, the points corresponding to the measurements were reported on a graph having ε_{yy} and ε_{zz} as the y and x axes, respectively, and fitted with a second degree polynomial using the least squares technique. The fact that the error on the strain decreases as the strain increases (see Chapter 3) was taken into account by putting

more weight on the points as the strain increases; this is equivalent to saying that the higher strain points are more reproducible. The curve was made to go through the origin, which it must do since the specimen is a polycrystal, by putting much more weight on this point. If the polynomial fitted to the data has the form:

$$\varepsilon_{yy} = b_1 \varepsilon_{zz}^2 + b_2 \varepsilon_{zz} + b_3 \qquad (4.1)$$

where b_3 is very close to zero, then

$$\left.\frac{d\varepsilon_{yy}}{d\varepsilon_{zz}}\right|_{\varepsilon_{zz}=0} = b_2 = R \qquad (4.2)$$

This is a systematic way of determining the R-value, and it is obviously much better than drawing a curve and taking the slope at the origin by hand, since there is always an error on the experimental points. The R values were determined in this way for the three sheets at angles $\alpha = 0^{\circ}$, 45° and 90°. The program to do this is called RZERO (see Appendix A). The results are shown in Figure 4.1.a to 4.1.i.

4.2) Yield Stress Measurement

For the original sheet and the ten subsequently deformed sheets, the yield stress was measured during uniaxial tension and compression tests as well as by means of

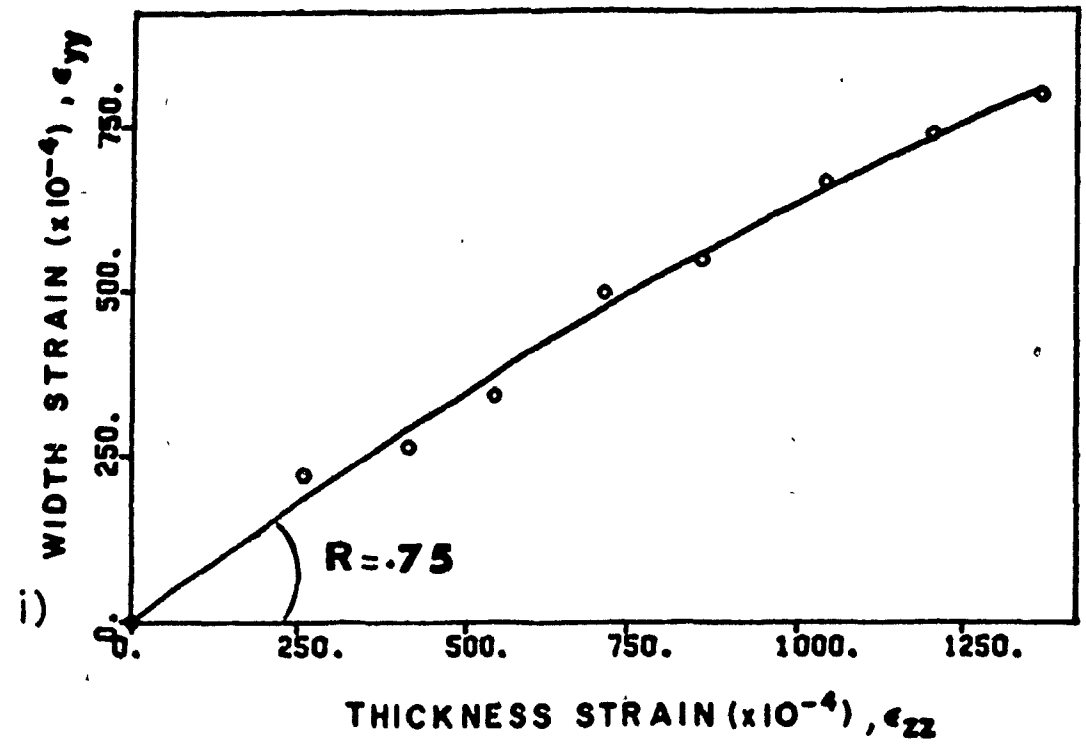

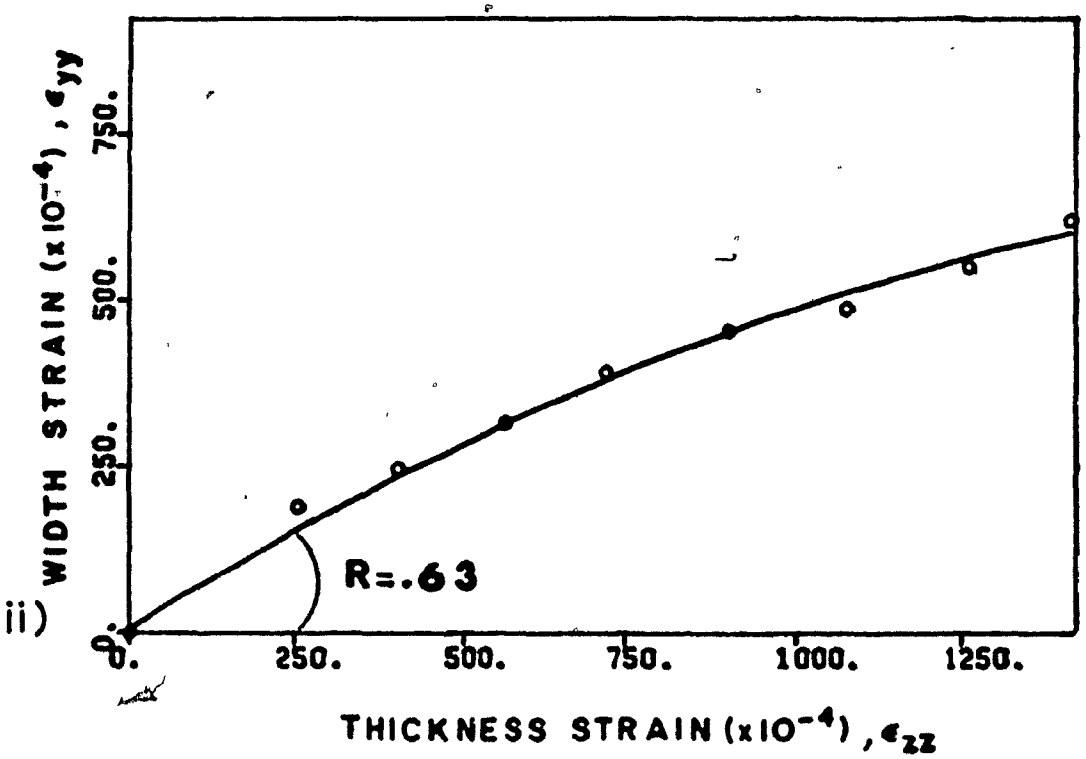

Figure 4.1 a) Width vs. thickness strains measured in tensile specimens cut from the annealed sheet ($\bar{\varepsilon} = 0$) and aligned along the rolling direction. i) Specimen A; ii) Specimen B.

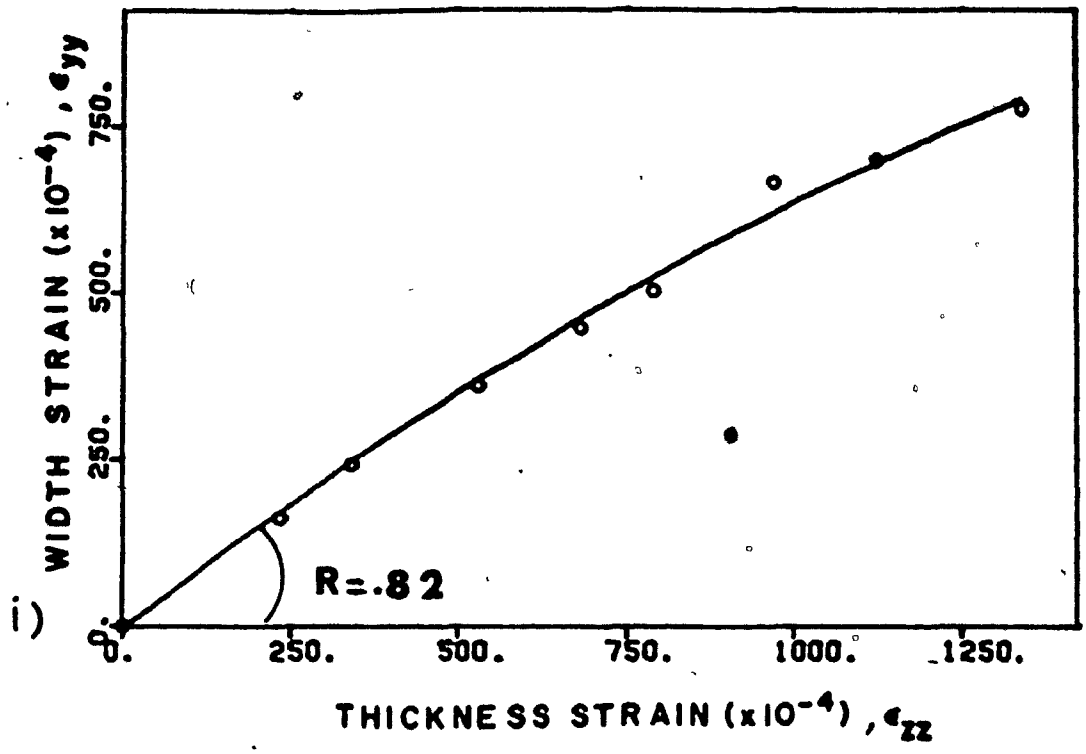

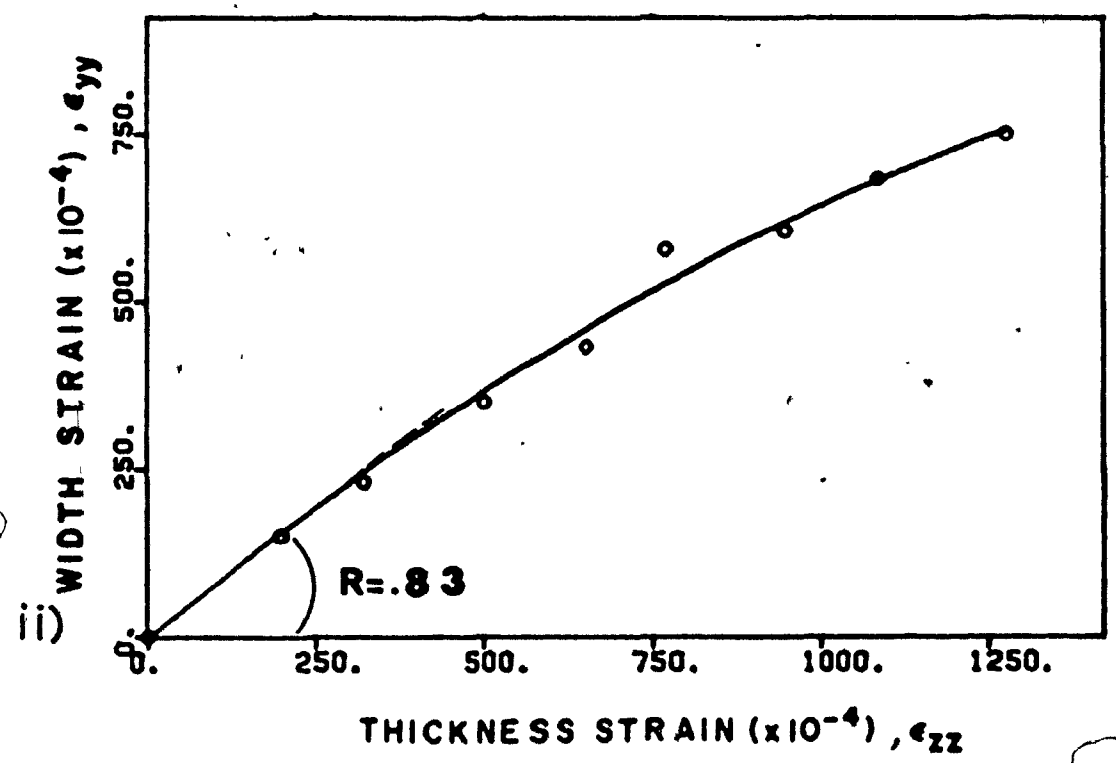

Figure 4.1 b) Width vs. thickness strains measured in tensile specimens cut from the annealed sheet ($\bar{\varepsilon} = 0$) and aligned along the transverse direction. i) Specimen A; ii) Specimen B.

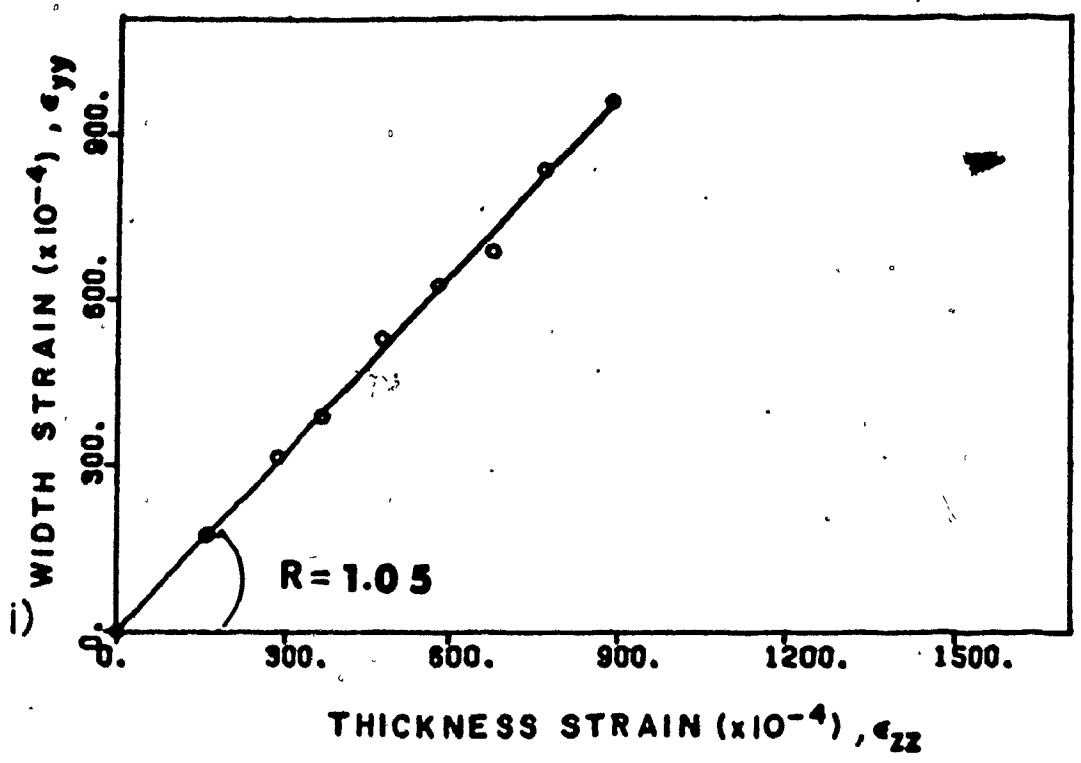

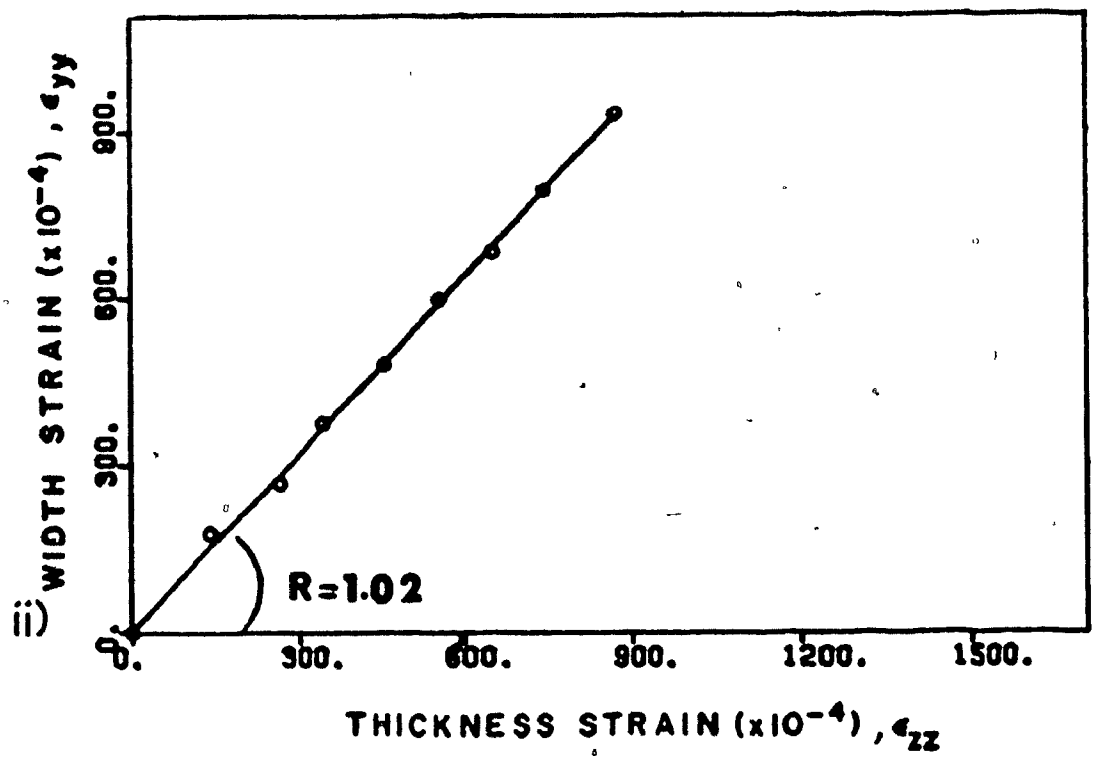

Figure 4.1 c) Width vs. thickness strains measured in tensile specimens cut from the annealed sheet ($\bar{\varepsilon} = 0$) and aligned along an angle $\alpha=45^{\circ}$ to the rolling direction. i) Specimen A; ii) Specimen B.

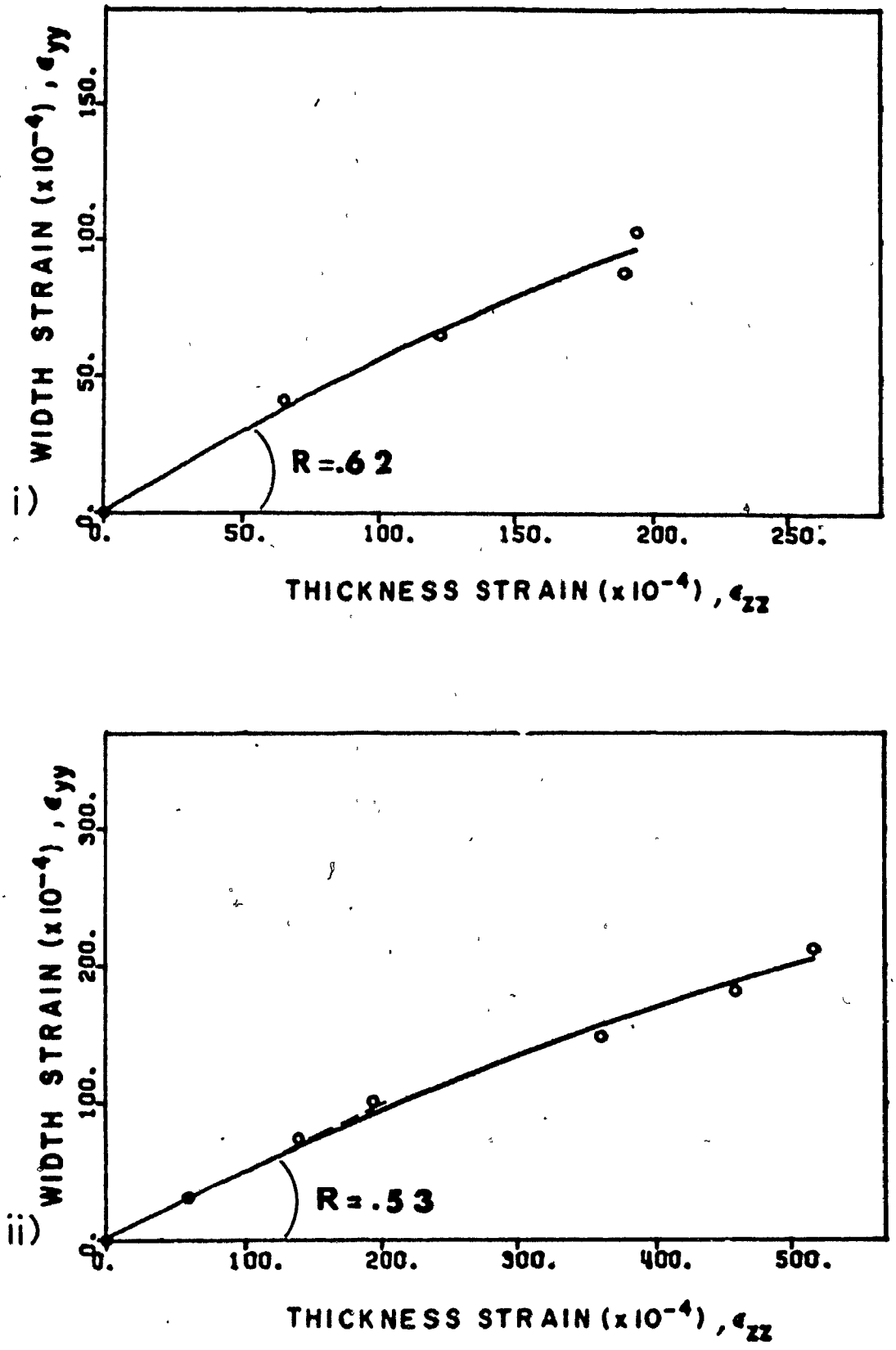

Figure 4.1 d) Width vs. thickness strains measured in tensile specimens cut from sheet rolled to a strain $\bar{\varepsilon}$=.27 and aligned along the rolling direction. i) Specimen A; ii) Specimen B.

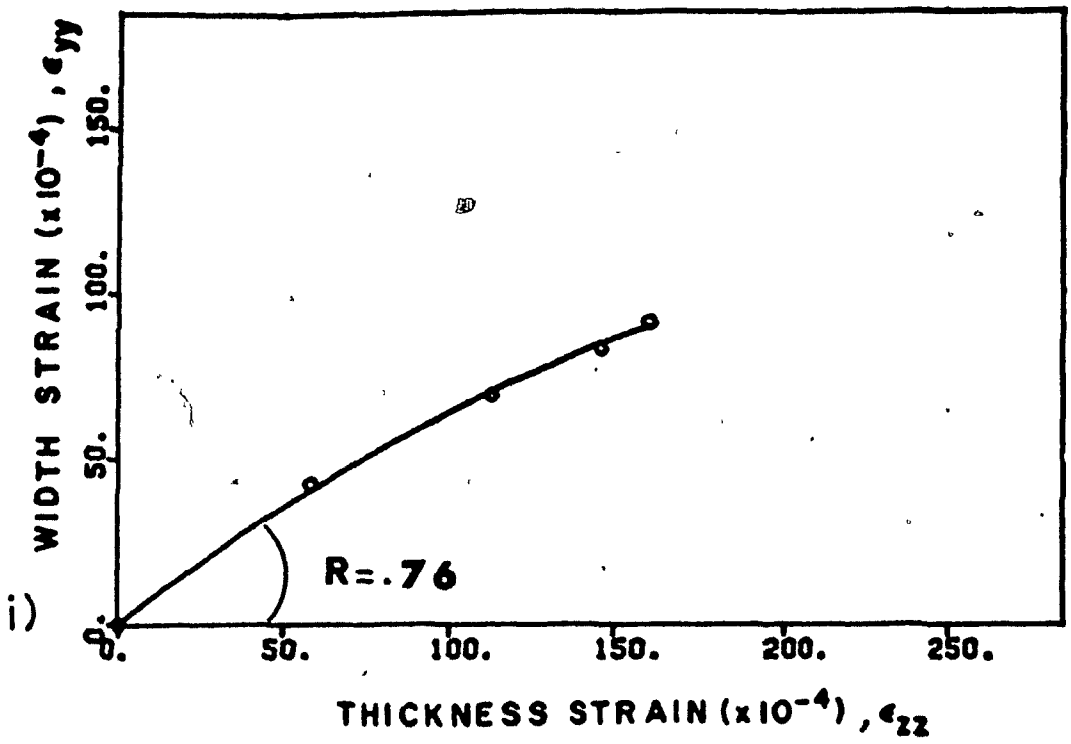

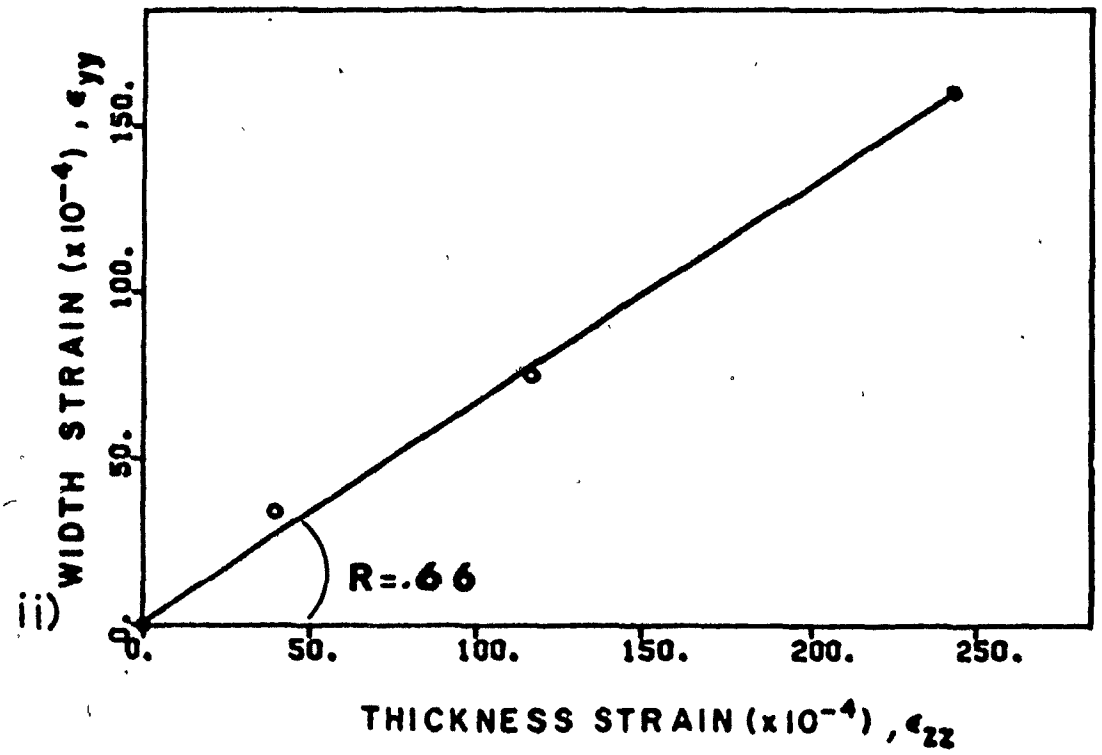

Figure 4.1 e) Width vs. thickness strains measured in tensile specimens cut from sheet rolled to a strain $\bar{\epsilon}=.27$ and aligned along the transverse direction. i) Specimen A; ii) Specimen B.

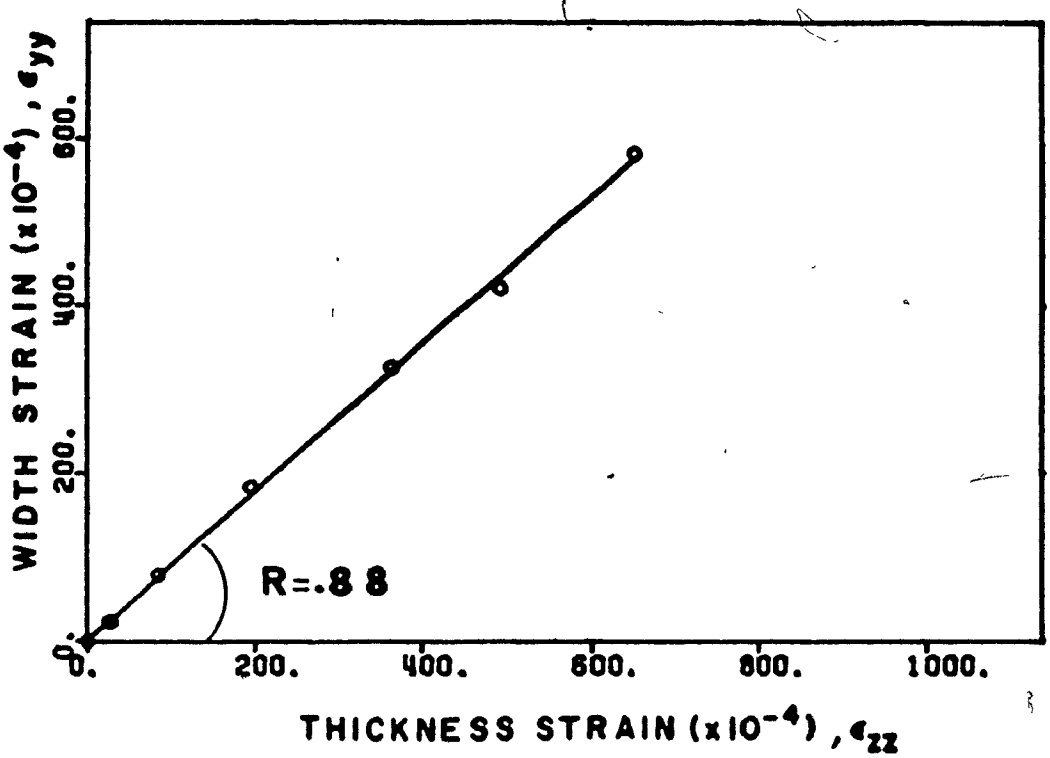

Figure 4.1 f) Width vs. thickness strains measured in tensile specimen cut from sheet rolled to a strain $\bar{\varepsilon} = .27$ and aligned along an angle $\alpha=45°$ to the rolling direction.

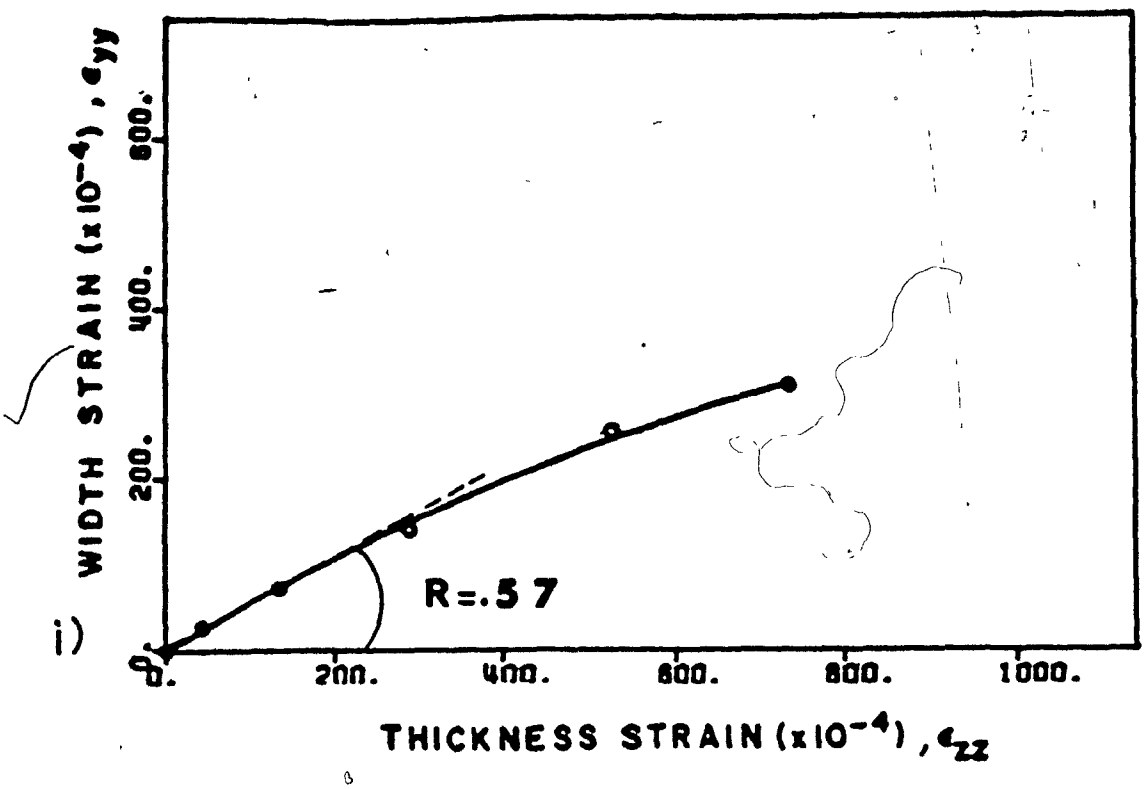

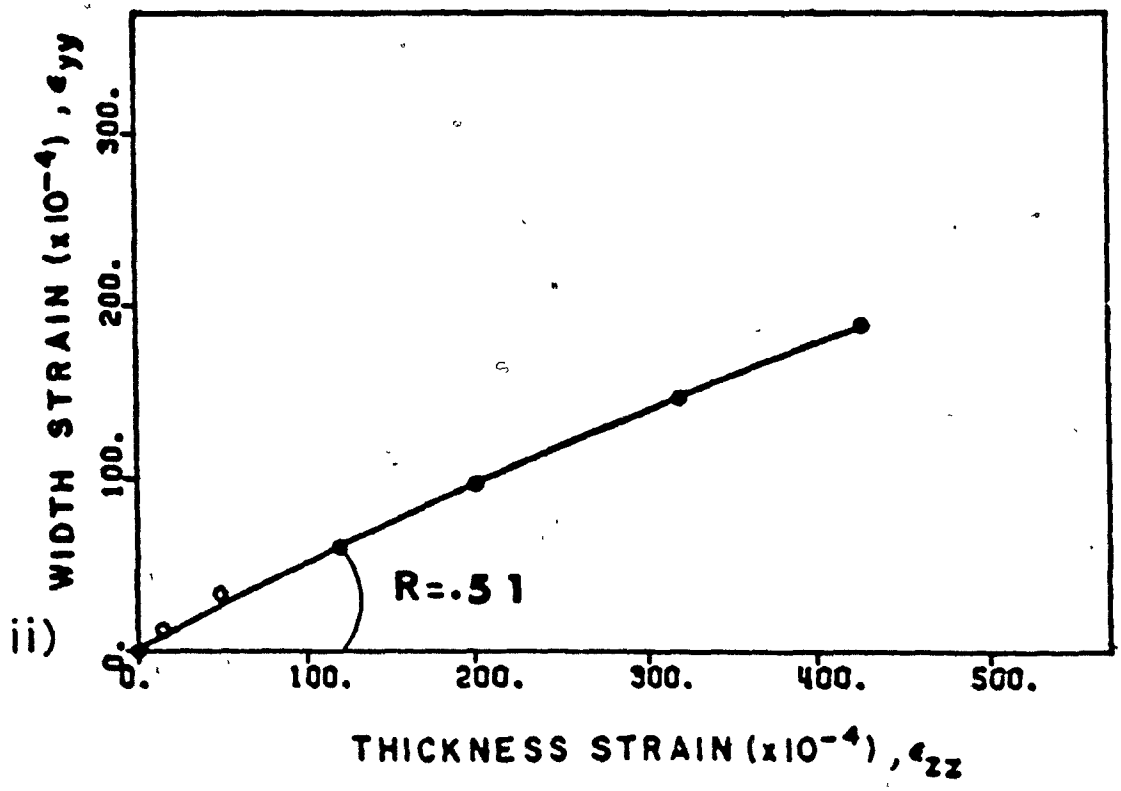

Figure 4.1 g) Width vs. thickness strains measured in tensile specimens cut from sheet rolled to a strain $\bar{\varepsilon}$ = .52 and aligned along the rolling direction. i) Specimen A; ii) Specimen B.

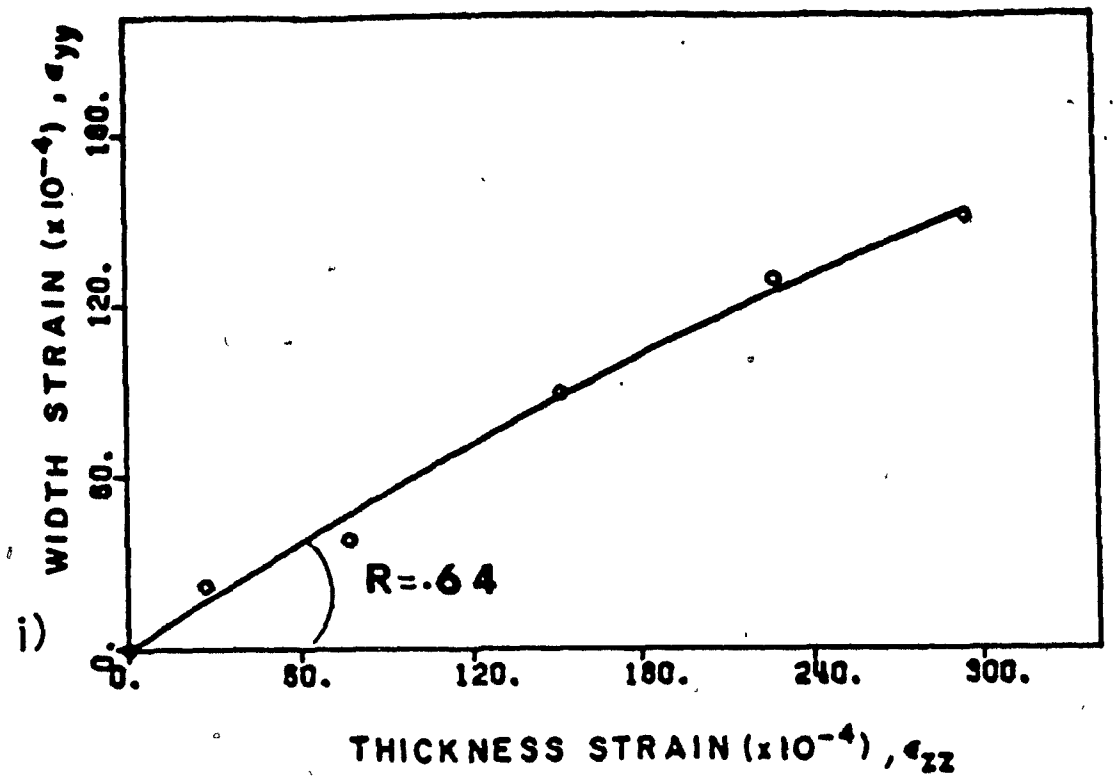

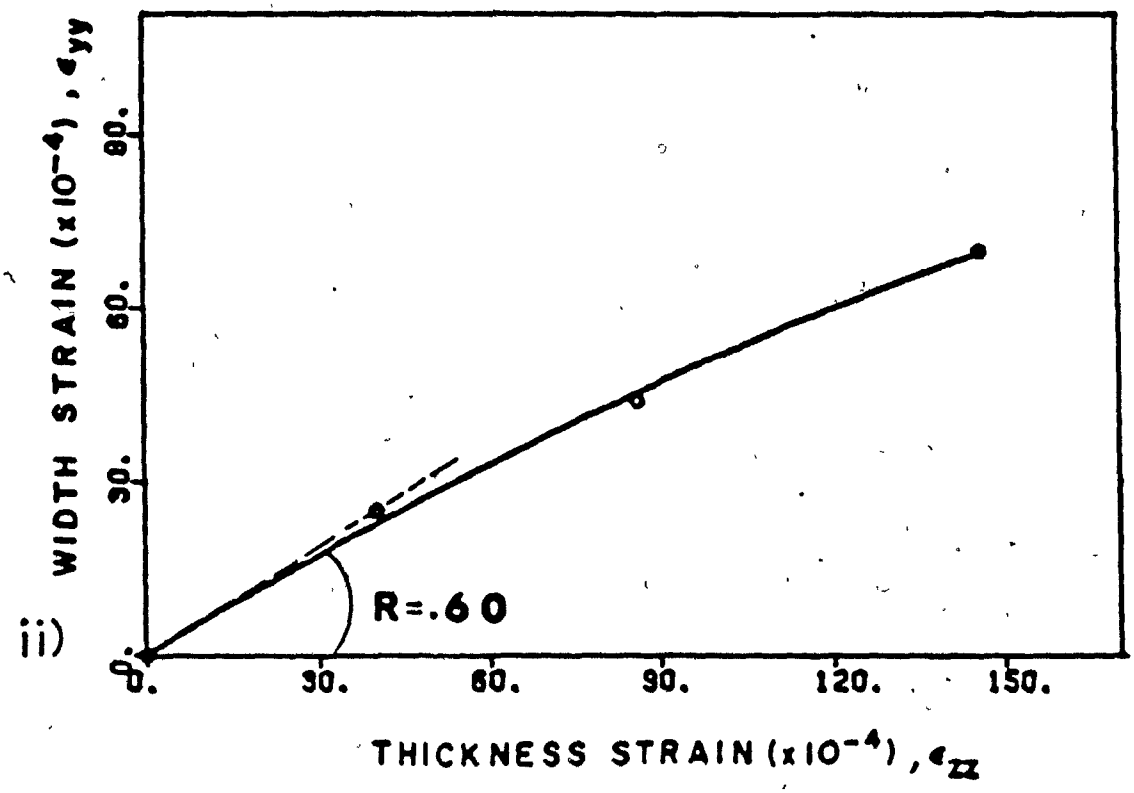

Figure 4.1 h) Width vs. thickness strains measured in tensile specimens cut from sheet rolled to a strain $\bar{\epsilon} = .52$ and aligned along the transverse direction. i) Specimen A; ii) Specimen B.

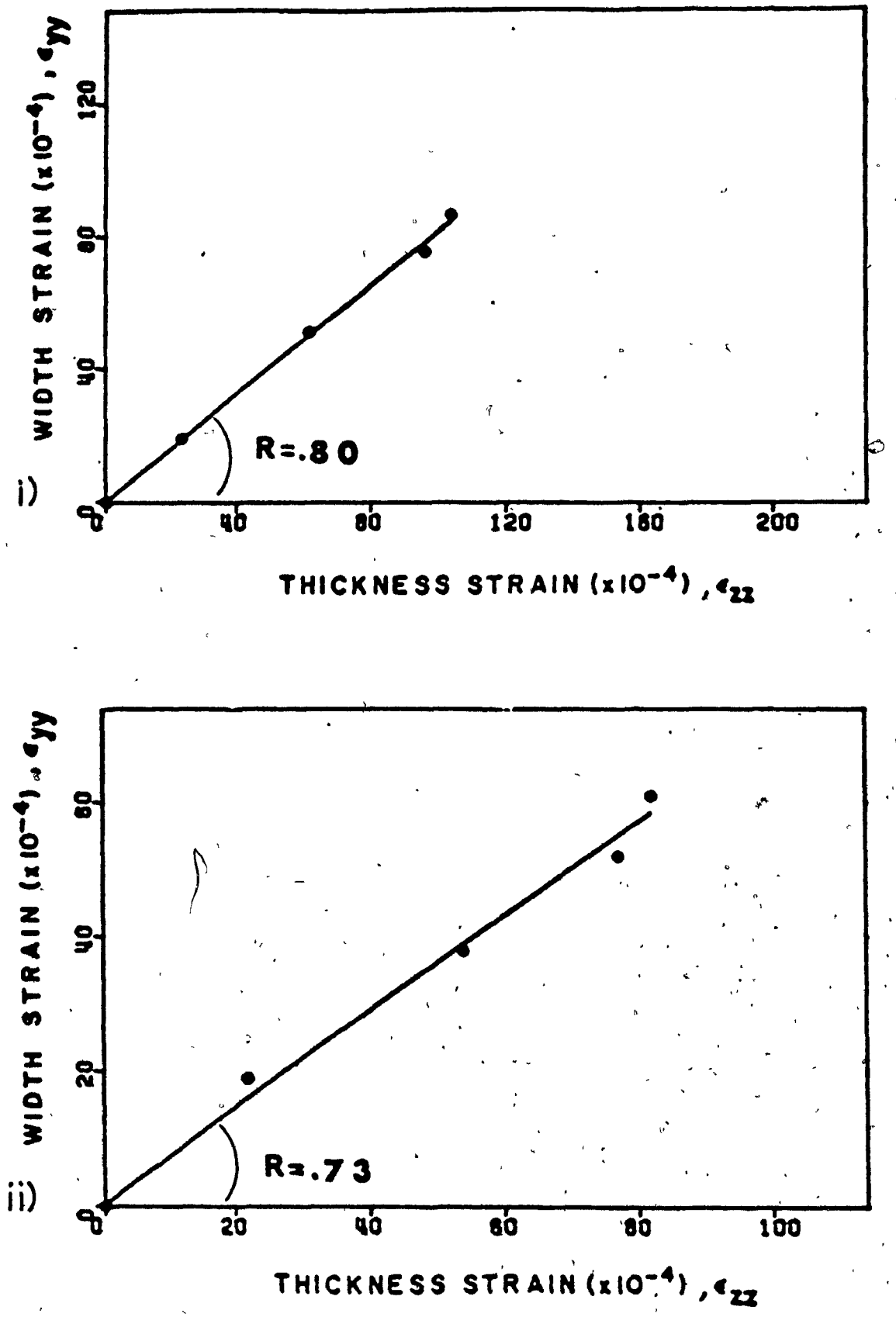

Figure 4.1 i) Width vs. thickness strains measured in tensile specimens cut from sheet rolled to a strain $\bar{\varepsilon} = .52$ and aligned along an angle $\alpha=45°$ to the rolling direction. i) Specimen A; ii) Specimen B.

plane strain tension tests. Uniaxial tension (UT) was carried out in the rolling, transverse and $\alpha = 45°$ directions; plane strain tension (PST) in the rolling and transverse directions only; and finally uniaxial compression (UC) solely in the sheet plane normal direction. In each test, the 0.2% yield stress was determined. The yield stress data for each type of test were fitted, using the least squares technique, with a Ludwik hardening law:

$$\sigma = \sigma_0 + a\bar{\varepsilon}^n$$

where $\bar{\varepsilon}$ is the equivalent rolling strain and σ_0 is the yield stress for $\bar{\varepsilon} = 0$. The parameters a and n as well as the correlation coefficient for the fitting of each data set are listed in table 4.1.

	UT(α=0)	UT(α=90)	UT(α=45)	UC	PST(α=0)	PST(α=90)
a($\times 10^4$)	84.15	84.61	83.71	82.15	93.01	93.68
n	0.477	0.438	0.465	0.430	0.453	0.417
r	0.986	0.977	0.991	0.980	0.984	0.971

Table 4.1: Results of least squares fitting used on yield stress data

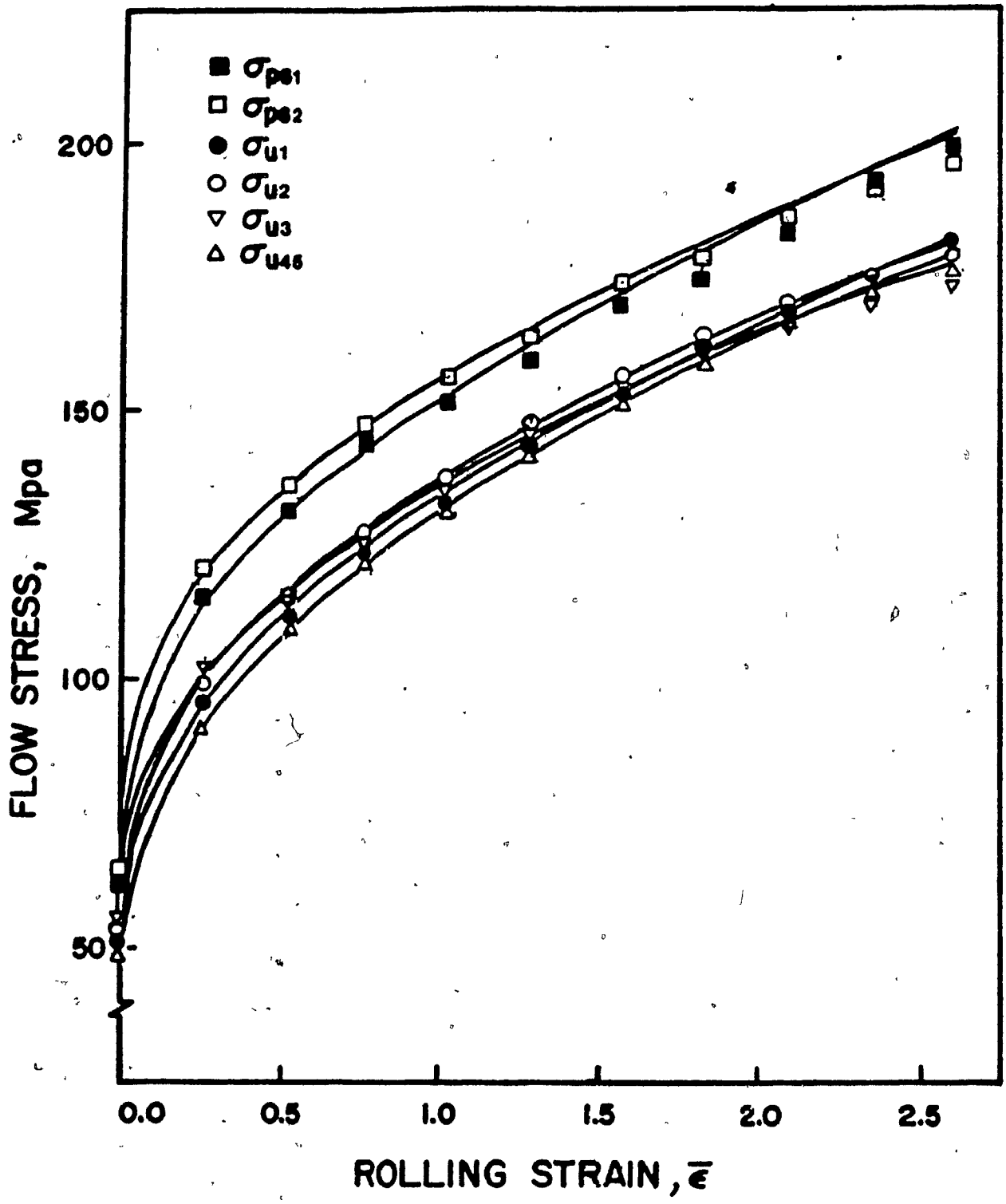

Figure 4.2 Evolution of yield stress components during rolling.

The hardening curves for all size types of test are shown in Figure 4.2. Note that this type of fitting is necessary in order to minimize the scatter when calculating the R values later.

4.3) Construction of the Yield Locus:

The plane stress yield locus can be constructed from the yield stresses measured during the various tests. Five points can be plotted on such a locus: the two uniaxial test measurements represented as A and B on the two axes; the uniaxial compression result, which is equivalent to biaxial tension, and is shown as point C on the locus; and the two plane strain tension results, shown as points D and E. D corresponds to the test where $d\varepsilon_{22} = 0$, i.e. with extension along the 11 direction, and E corresponds to that in which $d\varepsilon_{11} = 0$, i.e. to extension along the 22 direction, see Figure 4.3. On the same figure is shown the theoretical yield locus, with $\bar{R} = .90$, constructed from the computer program shown in Appendix B.

It can be seen that there is a discrepancy between the theoretical and the experimental loci: the quadratic Hill theory underestimates the stress in biaxial and plane strain loading. Thus the anomaly reported previously [37] for commercial purity aluminium is confirmed here.

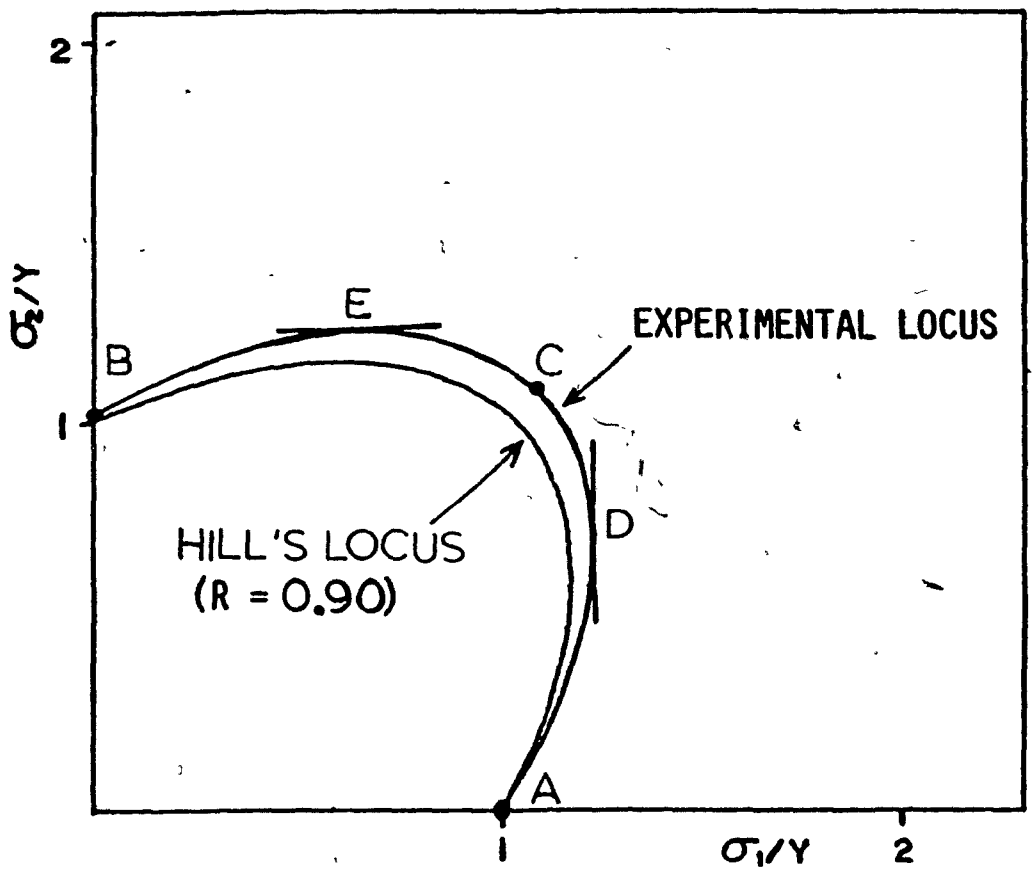

Figure 4.3 Theoretical (quadratic) and experimental yield loci.

4.4) Determination of R(α) from the Hill Quadratic Criterion:

In order to evaluate the R(α) values from the quadratic criterion, the four parameters F, G, H and N must be determined, and this requires at least four test results. Off all the simple tests, the only one leading to an equation which includes the N parameter is the uniaxial tensile test at α ≠ 0° and ≠90°, and for simplicity, the one opted for was α = 45°. For the other three parameters, five further tests were performed: two uniaxial tension tests, two plane strain tension tests and one uniaxial compression test. In fact, only three of these five experimental values are needed, but since the plane strain condition is not exactly satisfied, and since the uniaxial compression test is not very accurate because of friction, it was decided to carry out all five tests and to treat the data with an averaging procedure. The averaging was done by considering only the following three systems of equations:

- two uniaxial tension + one plane strain tension
- two uniaxial tension + other plane strain tension
- two uniaxial tension + uniaxial compression.

Note that two uniaxial tension results are emplcyed in each system because they are the most reliable ones for the reasons mentioned above.

The R-values for α = 0°, 45°, and 90° were calculated

from the parameters F, G, H and N as explained in sections 2.3 and 2.4. The values for the first three sheets were compared to those measured directly and found to be higher. This again indicates that the experimental and fitted (Hill-based) yield loci are different. We therefore conclude that the quadratic criterion does not adequately describe the behaviour of the aluminium sheet, and that a more generalized criterion must be used.

4.5) Generalized Hill Criterion

i) Planar isotropy

Assuming planar isotropy, the generalized Hill criterion can be written as follows:

$$|\sigma_1 + \sigma_2|^m + (1 + 2R)|\sigma_1 - \sigma_2|^m = 2(1 + R)\sigma_u^m \qquad (4.3)$$

Incorporating the expressions for both σ_{ps} and σ_u, the stress ratio can be found to be:

$$\left(\frac{\sigma_{ps}}{\sigma_u}\right)^m = \frac{2^{1-m}(1 + R)\left[(1 + 2R)^{1/m-1} + 1\right]^{m-1}}{(1 + 2R)} \qquad (4.4)$$

Having determined $\bar{\sigma}_{ps}$, $\bar{\sigma}_u$ and $\bar{R}$ (all averages of experimental values at $\alpha = 0°$, $90°$ and $45°$), the above equation can now be solved numerically. A computer program was written (see Appendix C) for this purpose, and gives the results summarized in table 4.2.

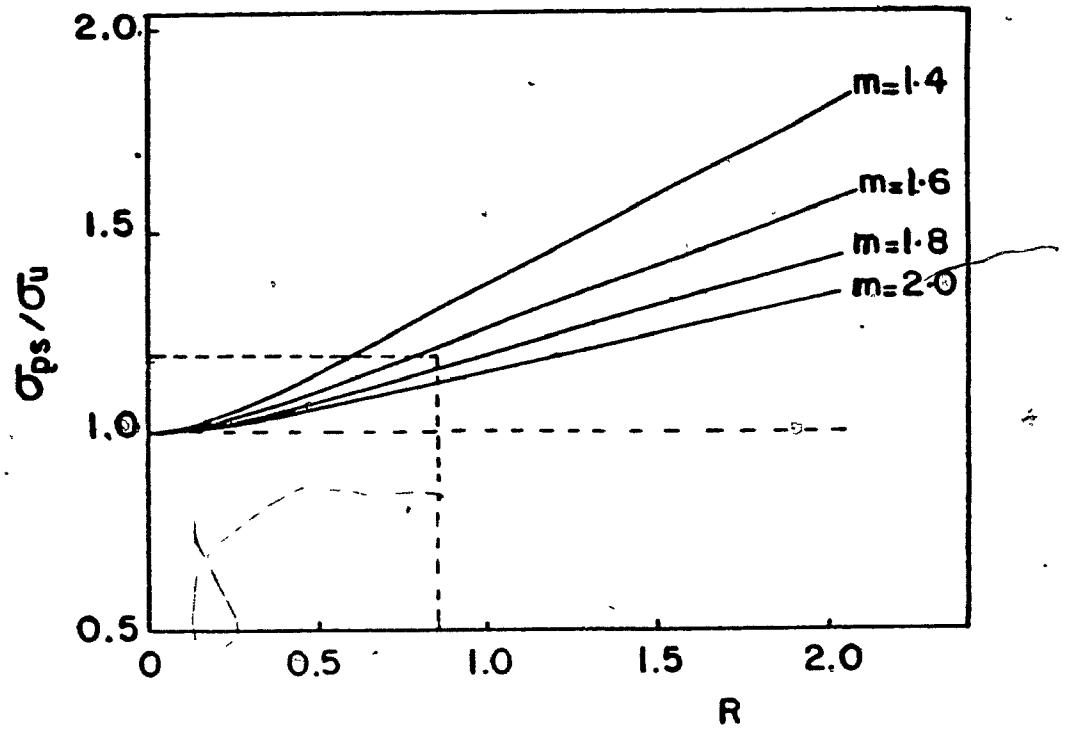

Figure 4.4 Ratio of stress in plane strain tension to uniaxial stress as a function of R (from equation 4.4).

Sheet	$\bar{R}$	$\bar{\sigma}_{ps}/\bar{\sigma}_u$	m
original ($\bar{\varepsilon}$ = 0)	0.90	1.20	1.68
1st rolled ($\bar{\varepsilon}$ = .27)	0.76	1.15	1.73
2nd rolled ($\bar{\varepsilon}$ = .52)	0.67	1.14	1.66

Table 4.2: m values calculated from program

An average value of m was taken equal to 1.7* and, assuming that it is a material property, it will be kept constant for all the rolled sheets, even though this cannot be justified due to the absence of experimental R values for the heavily rolled sheets. Note that planar isotropy was assumed only in order to simplify the problem and to calculate m to a first approximation. Once the value of m is known, the Hill generalized criterion can be reformulated in its most general form, which corresponds to planar anisotropy.

ii) Planar anisotropy

In the literature [47-49], planar isotropy is usually assumed in order to describe the anomalous behaviour in terms of a generalized yield criterion. Although such a criterion does permit an R-value to be defined which is comparable to

*A graphical solution for m is also shown in Figure 4.4

the experimental value, it cannot reflect the variation of this parameter with direction in the sheet which corresponds to the earing behaviour.

To solve this problem, a new criterion is proposed here which takes into account the planar anisotropy. In other words, a criterion is employed which permits the average R-value as well as its variation in the plane of the sheet to be predicted, or described. This criterion is the following one*:

$$2f(\sigma_i) = |F\sigma_1 + G\sigma_2|^m + H|\sigma_1 - \sigma_2|^m + 2N\sigma_{12}^m = 1 \quad (4.5)$$

Applying the normality rule and transforming the coordinates to the specimen axes, as was done before in Chapter 2, it can be shown that:

$$R(\alpha) = \{\sin^2\alpha\,[F|F\sigma_1 + G\sigma_2|^{m-1} + H|\sigma_1 - \sigma_2|^m/(\sigma_1 - \sigma_2)]$$

$$+ \cos^2\alpha\,[G|F\sigma_1 + G\sigma_2|^{m-1} + H|\sigma_1 - \sigma_2|^m/(\sigma_2 - \sigma_1)]$$

$$- 2\cos\alpha\sin\alpha\, N\sigma_{12}{}^{m-1}\}/\{-(F+G)|F\sigma_1 + G\sigma_2|^{m-1}\} \quad (4.6)$$

---

*In this criterion, the superposition of a hydrostatic stress does not influence yielding. This was checked by considering the case where σ_3 is not zero, a form similar to the Hill generalized planar isotropy criterion (equation 4.5 in Ref. 41).

so that:

$$R_0 = \frac{H - GF^{m-1}}{F^m + GF^{m-1}}$$

$$R_{90} = \frac{H - FG^{m-1}}{G^m + FG^{m-1}} \qquad (4.7)$$

$$R_{45} = \frac{N}{(F+G)^m} - \frac{1}{2}$$

In order to determine the above R values, the same procedure as that in section 2.4 can now be employed in order to calculate the parameters F, G, H and N of the new criterion (equation 4.5). The equations developed from this procedure are listed below:

$$F^m + H = 1/x^m \qquad (4.8a)$$

$$G^m + H = 1/y^m \qquad (4.8b)$$

$$(F+G)^m + 2N = (2/x_{45})^m \qquad (4.8c)$$

$$(F+G)^m = 1/z^m \qquad (4.8d)$$

$$\frac{(H^{\frac{1}{m-1}} + G^{\frac{m}{m-1}})^{m-1}}{H(F+G)^m} = P^m \qquad (4.8e)$$

$$\frac{H^{\frac{1}{m-1}} + F^{\frac{m}{m-1}}}{H(F+G)^m} = P^m \qquad (4.8f)$$

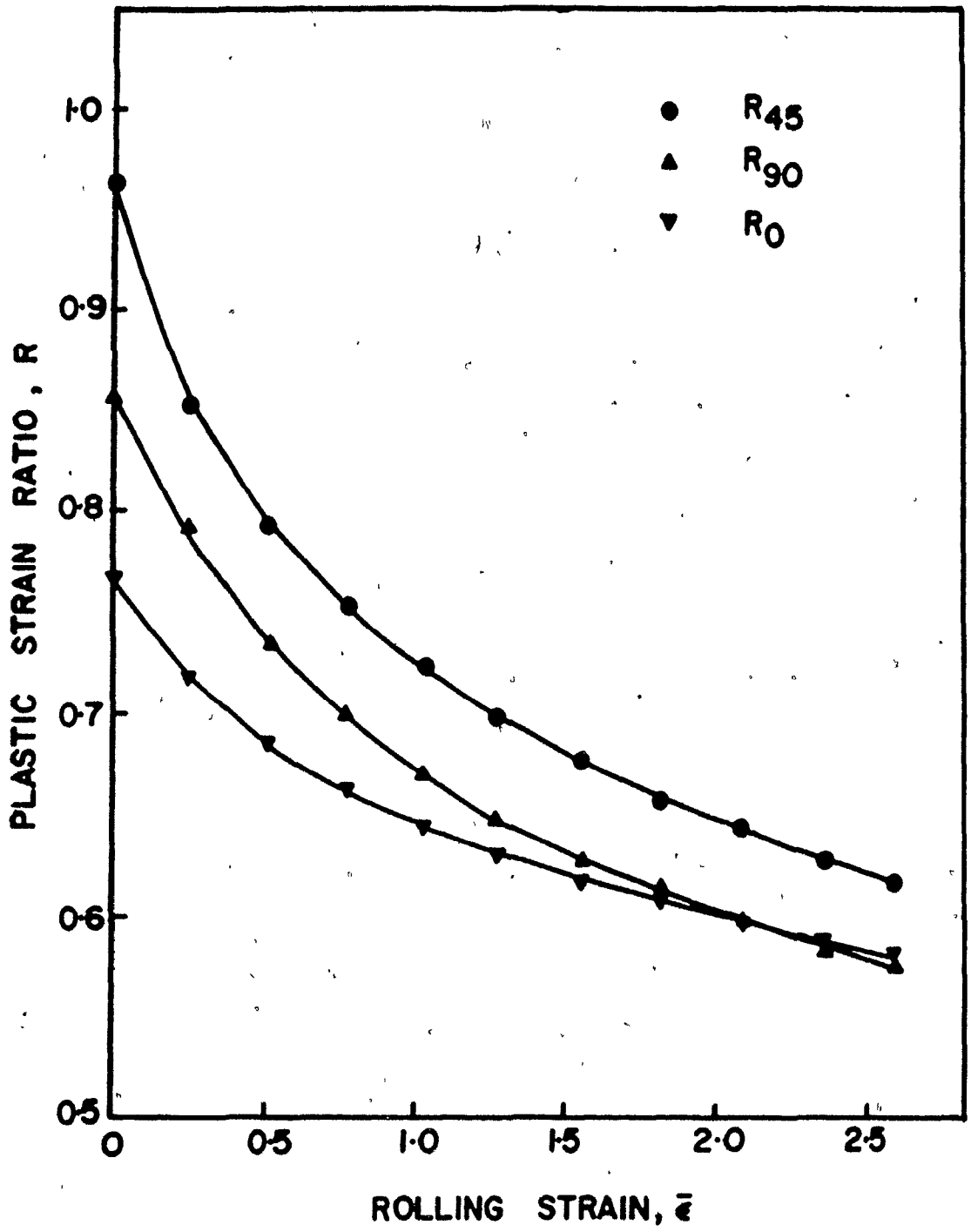

Figure 4.5 Dependence of the three plastic strain ratios on rolling strain.

The following three systems of three equations were solved numerically.

i) System 1: Equations 4.8a, b and d

ii) System 2: Equations 4.8a, b and e

iii) System 3: Equations 4.8a, b and f.

For each system, the parameter N is calculated by substituting for F and G in equation 4.8c. The computer programs called NEW1, NEW2 and NEW3 solving systems 1, 2 and 3 respectively are given in Appendices D, E, and F. Average values of each of the three strain rate ratios obtained from the three systems were taken and are plotted in Figure 4.5.

4.6) R(α) from Experimental Pole Figures and CMTP Analysis:

It is well known that the recrystallization texture of commercially pure aluminium consists of a cube component {100}<001>, components of the rolling texture {110}<112>, {112}<111>, {123}<634> and {110}<001> and a relative large volume of other random components [50-53]. The above main components are shown in Figure 4.6 as well as on each of the experimental {111} pole figures shown in Figure 4.7a to k. Despite the limited information provided by these pole figures, an attempt was made to identify the components present and quantify their volume fractions in each case (see Discussion, 5.3). The volume fractions so determined are plotted in Figure 4.8 as a function of rolling strain. These

are also given in table 4.3.

Since it is not straightforward to include the random texture in the CMTP analysis, it was decided to divide up the amount of this component more or less proportionally among the other components so that the total always adds up to 100%. The fractions obtained in this way are listed in table 4.4. It is these values of the latter table which were used in the CMTP analysis. The corresponding $R(\alpha)$ curves predicted using the CMTP method are shown in Figures 4.9.a and 4.9.b.

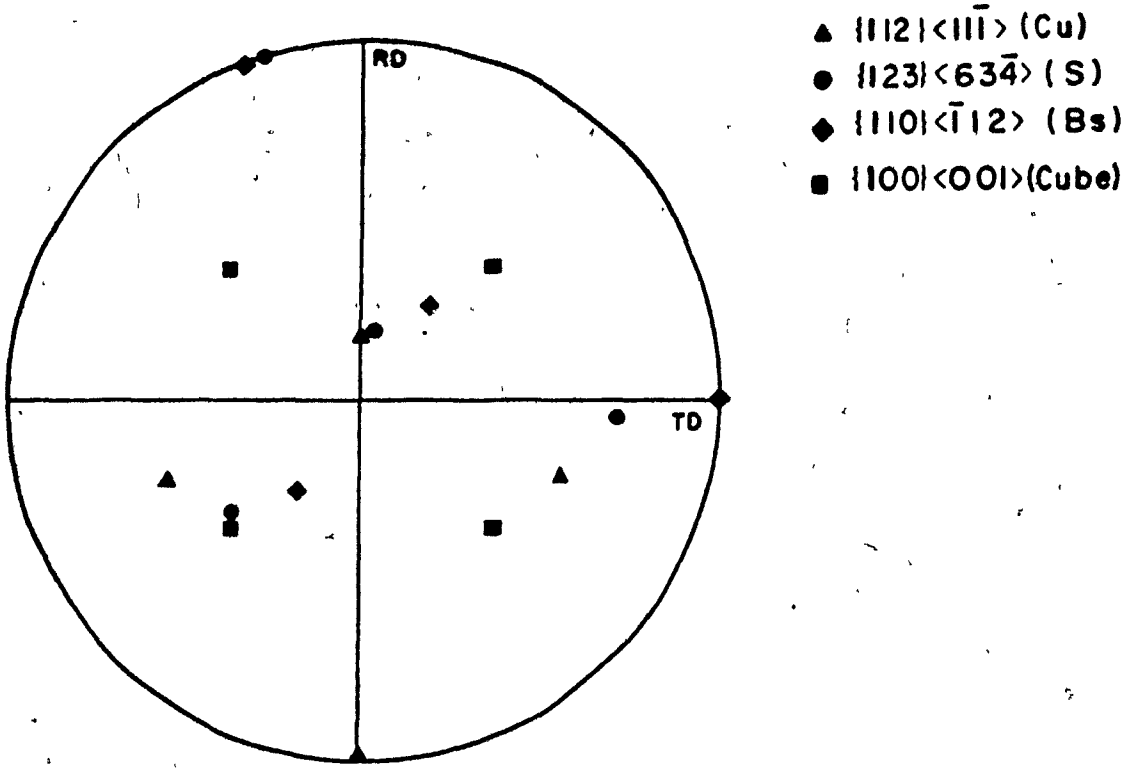

Figure 4.6 Location of {111} poles for the main ideal orientations; one component of each orientation is shown.

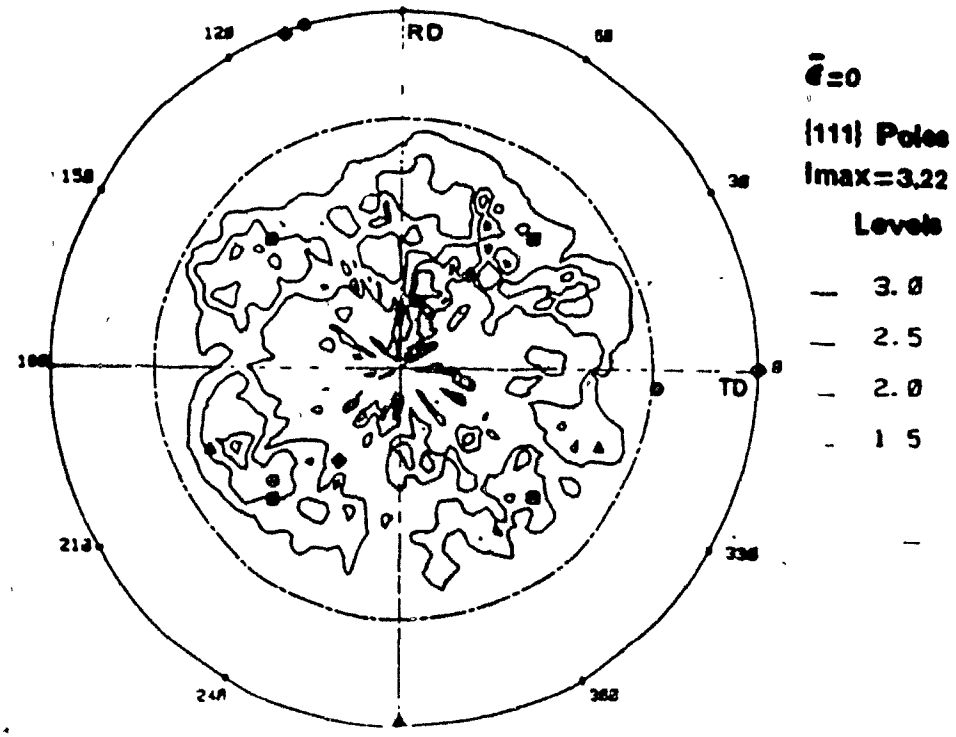

Figure 4.7 a) {111} pole figure for annealed sheet. Ideal orientations are those shown in Figure 4.6.

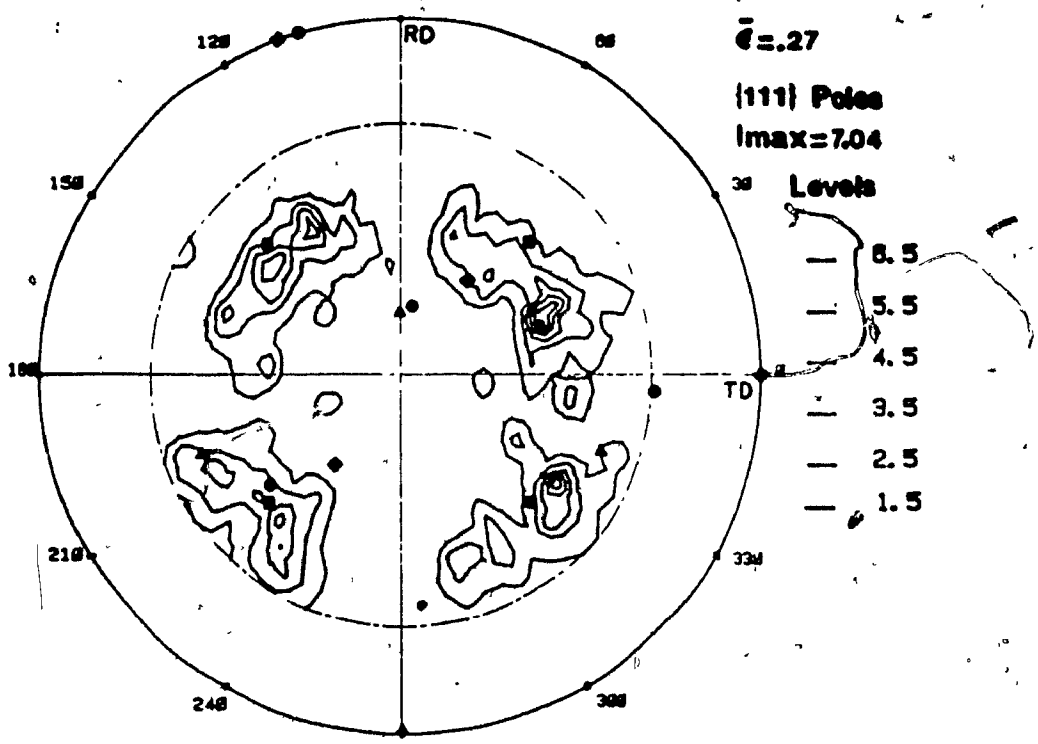

Figure 4.7 b) {111} pole figure for sheet rolled to a strain $\bar{\epsilon}$ = .27. Ideal orientations are those shown in Figure 4.6.

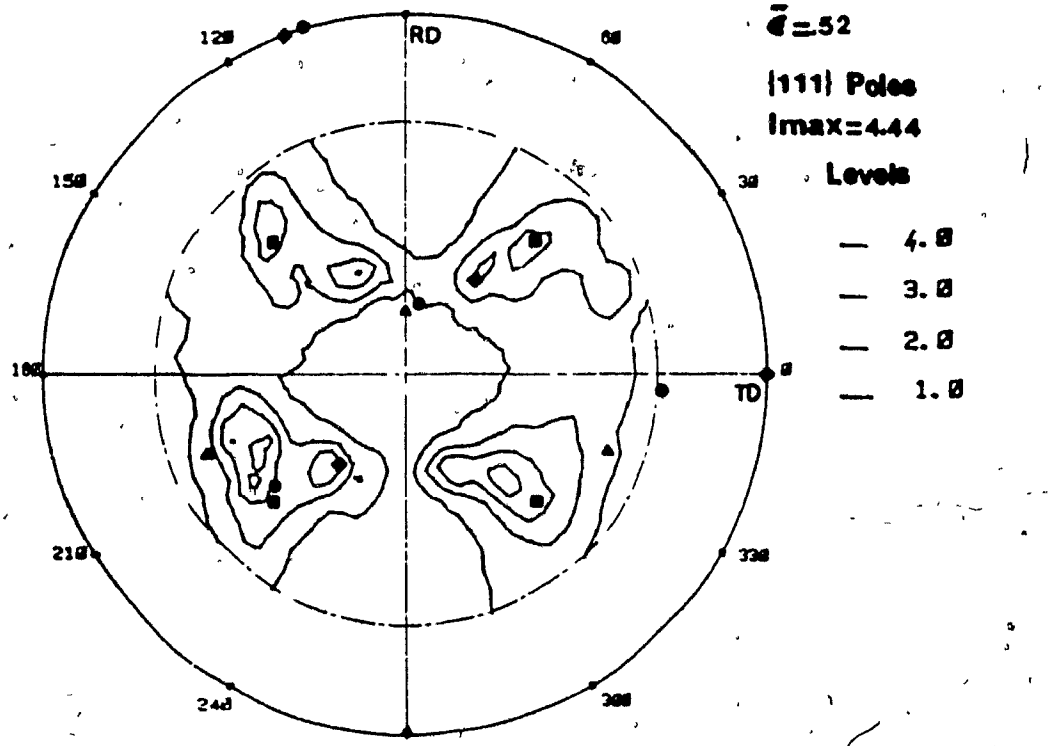

Figure 4.7 c) {111} pole figure for sheet rolled to a strain $\bar{\epsilon}$ = .52. Ideal orientations are those shown in Figure 4.6.

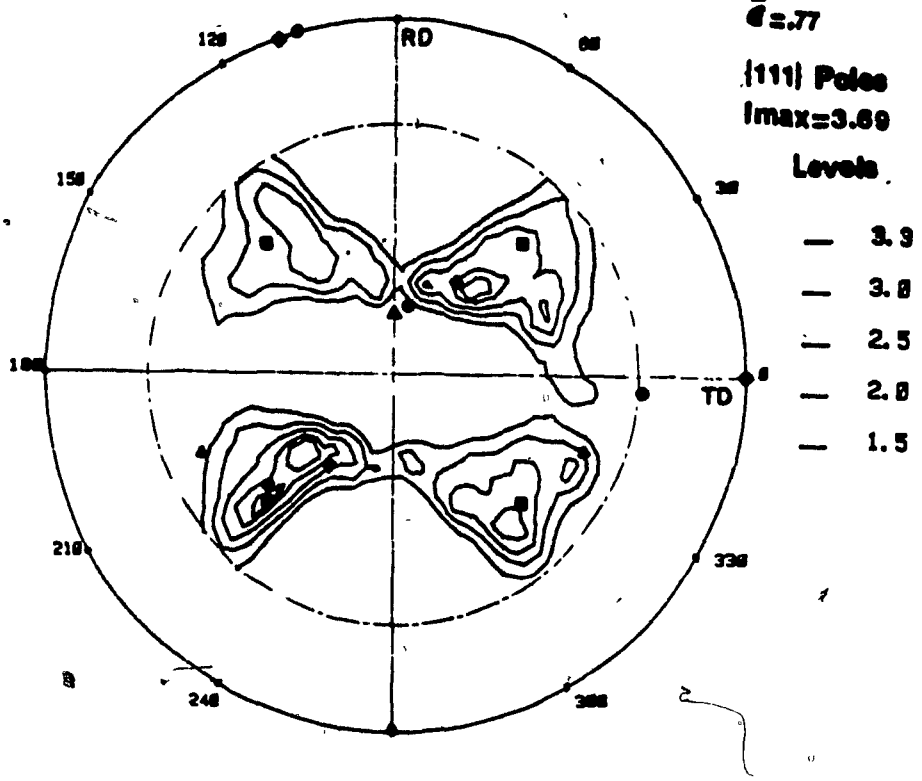

Figure 4.7 d) {111} pole figure for sheet rolled to a strain $\bar{\epsilon}$ = .77. Ideal orientations are those shown in Figure 4.6.

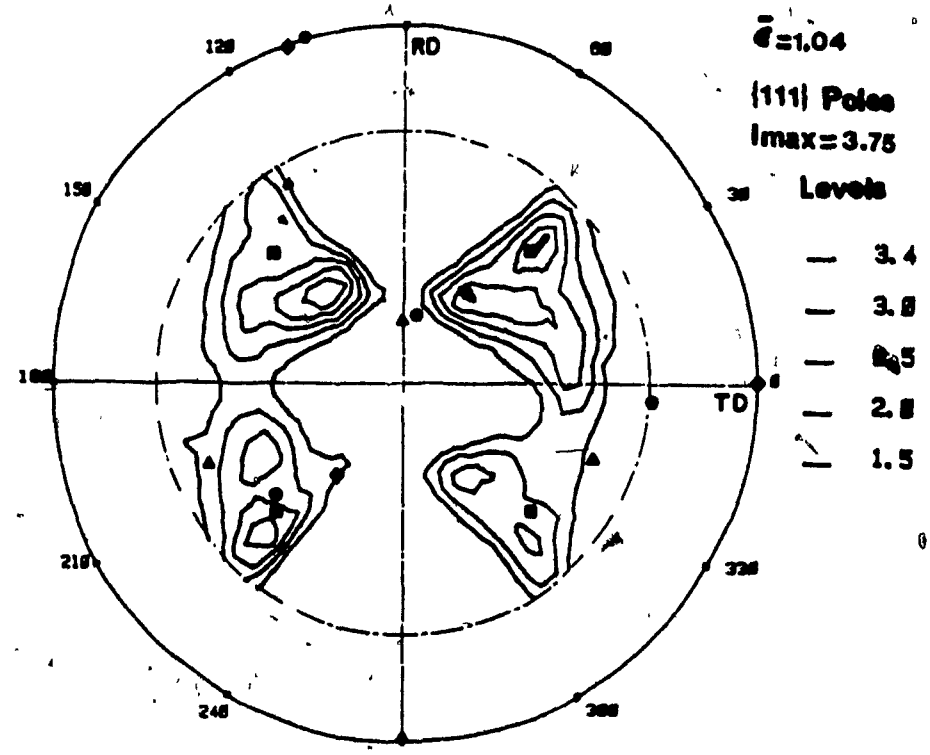

Figure 4.7 e) {111} pole figure for sheet rolled to a strain $\bar{\epsilon}$ = 1.04. Ideal orientations are those shown in Figure 4.6.

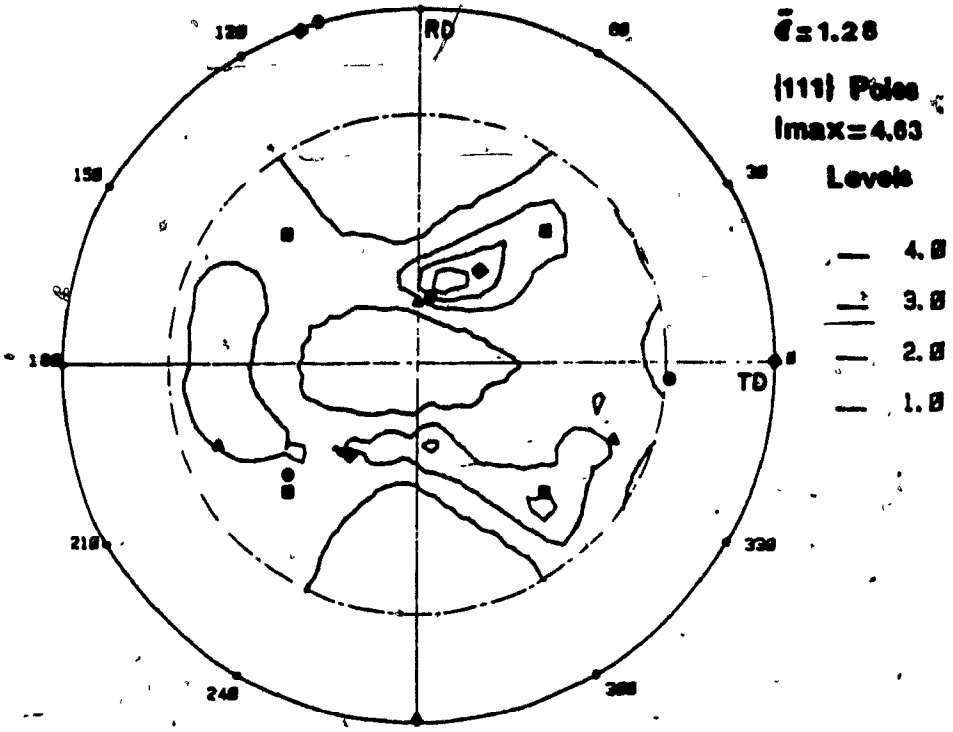

Figure 4.7 f) {111} pole figure for sheet rolled to a strain $\bar{\varepsilon}$ = 1.28. Ideal orientations are those shown in Figure 4.6.

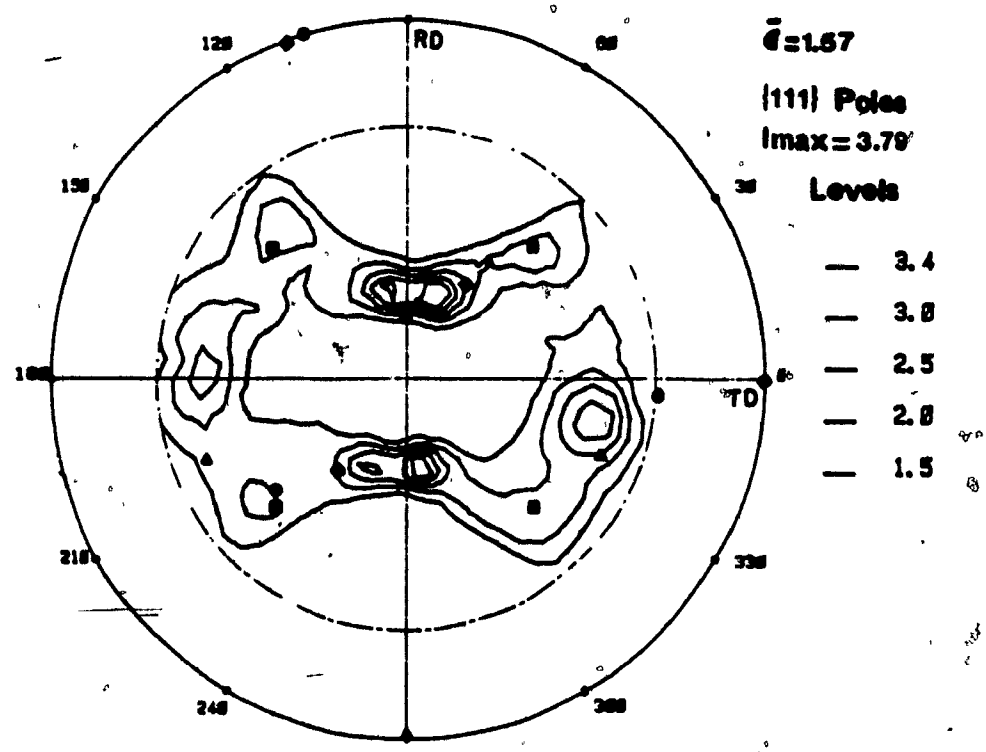

Figure 4.7 g) {111} pole figure for sheet rolled to a strain $\bar{\varepsilon}$ = 1.57. Ideal orientations are those shown in Figure 4.6.

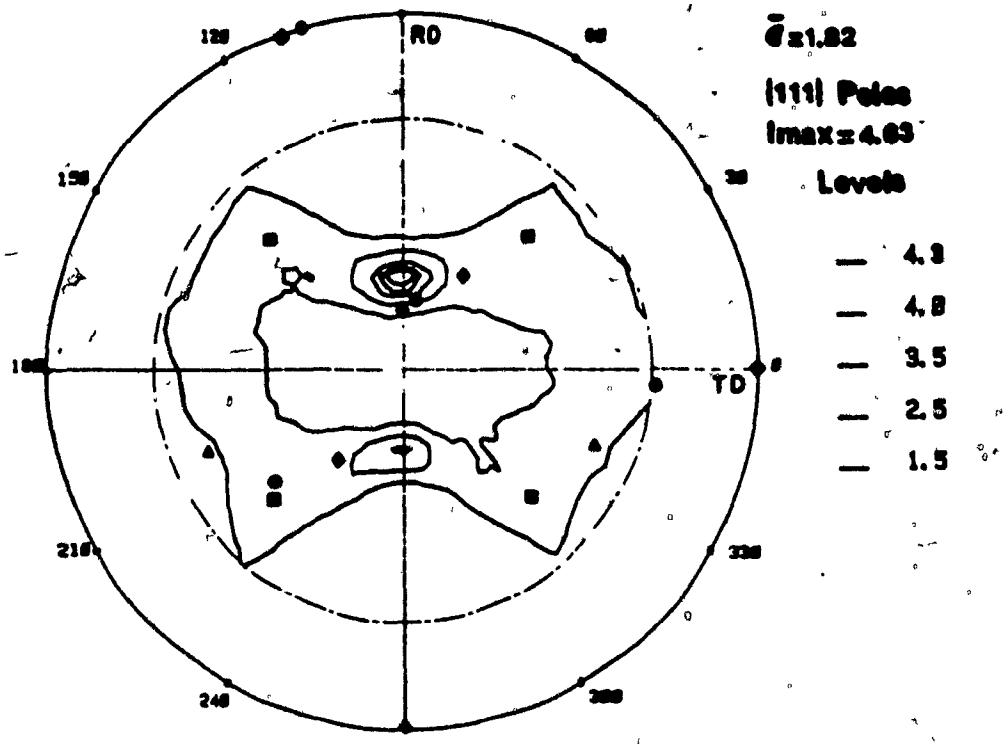

Figure 4.7 h) {111} pole figure for sheet rolled to a strain $\bar{\epsilon}$ = 1.82. Ideal orientations are those shown in Figure 4.6.

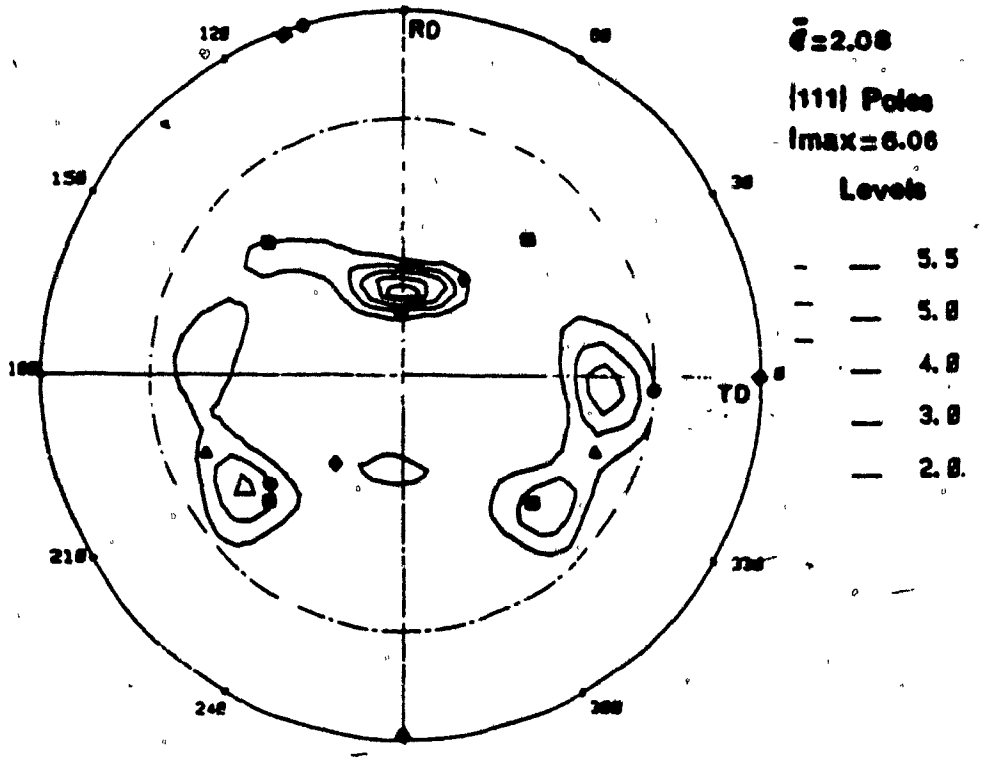

Figure 4.7 i) {111} pole figure for sheet rolled to a strain $\bar{\epsilon}$ = 2.08. Ideal orientations are those shown in Figure 4.6.

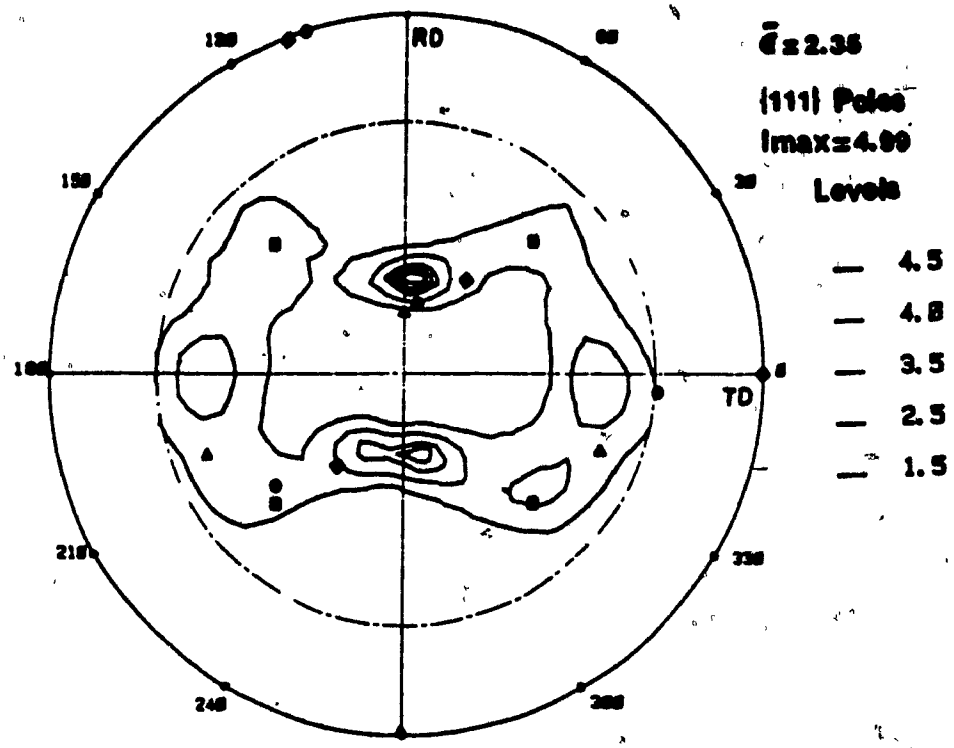

Figure 4.7 j) {111} pole figure for sheet rolled to a strain $\bar{\epsilon}$ = 2.35. Ideal orientations are those shown in Figure 4.6.

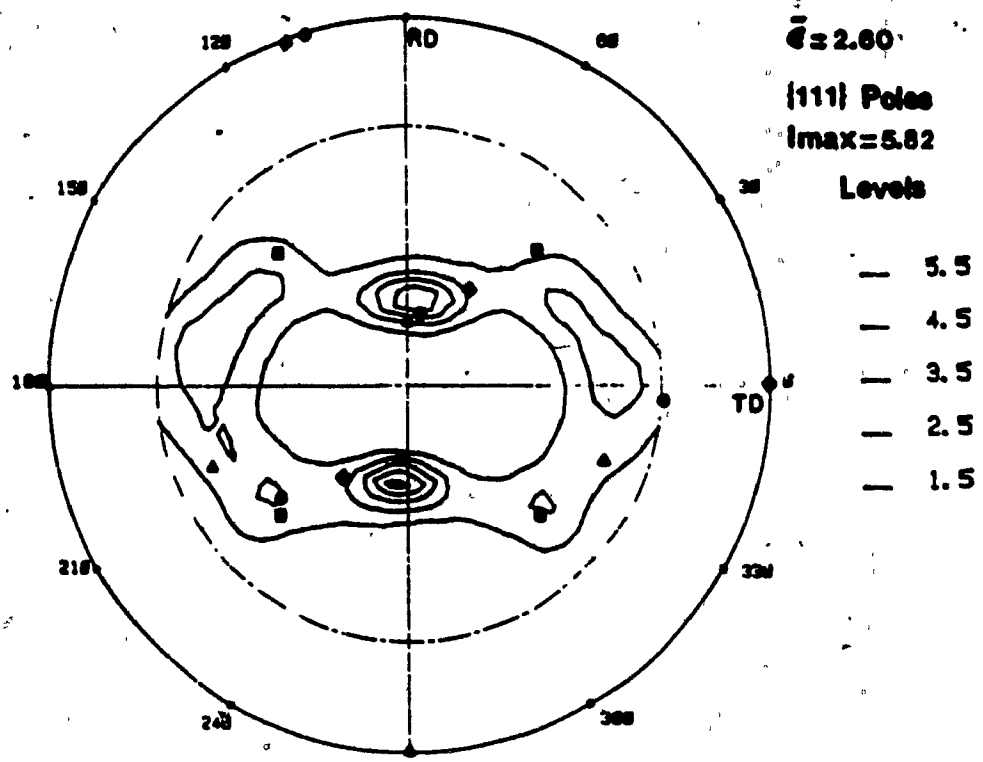

Figure 4.7 k) {111} pole figure for sheet rolled to a strain $\bar{\epsilon}$ = 2.60. Ideal orientations are those shown in Figure 4.6.

Stage of Deformation	Rolling Strain $\bar{\varepsilon}$	Volume Fraction of Texture Components				
		Random	Cube	Bs	S	Cu
0	0	30	25	25	15	5
1	0.26	24	20	26	16	14
2	0.52	20	15	27	18	20
3	0.77	15	12	28	20	25
4	1.03	12	9	29	22	28
5	1.28	9	5	31	24	31
6	1.56	8	3	31	25	33
7	1.82	6	3	31	26	34
8	2.07	4	2	32	27	35
9	2.35	3	1	32	28	36
10	2.59	2	0	33	28	37

Table 4.3: Volume Fractions of Texture Components Present in Each Sheet (Including Random Texture)

Stage of Deformation	Rolling Strain $\bar{\varepsilon}$	Volume Fractions of Texture Components				
		Random	Cube	Bs	S	Cu
0	0	0	32	32	22	14
1	0.26	0	26	32	22	20
2	0.52	0	20	32	23	25
3	0.77	0	16	32	24	28
4	1.03	0	12	32	25	31
5	1.28	0	8	33	26	33
6	1.56	0	6	33	27	34
7	1.82	0	4	33	28	35
8	2.07	0	3	33	28	36
9	2.35	0	1	33	29	37
10	2.59	0	0	34	29	37

Table 4.4: Volume Fractions of Texture Components Present in Each Sheet (Without Random Texture)

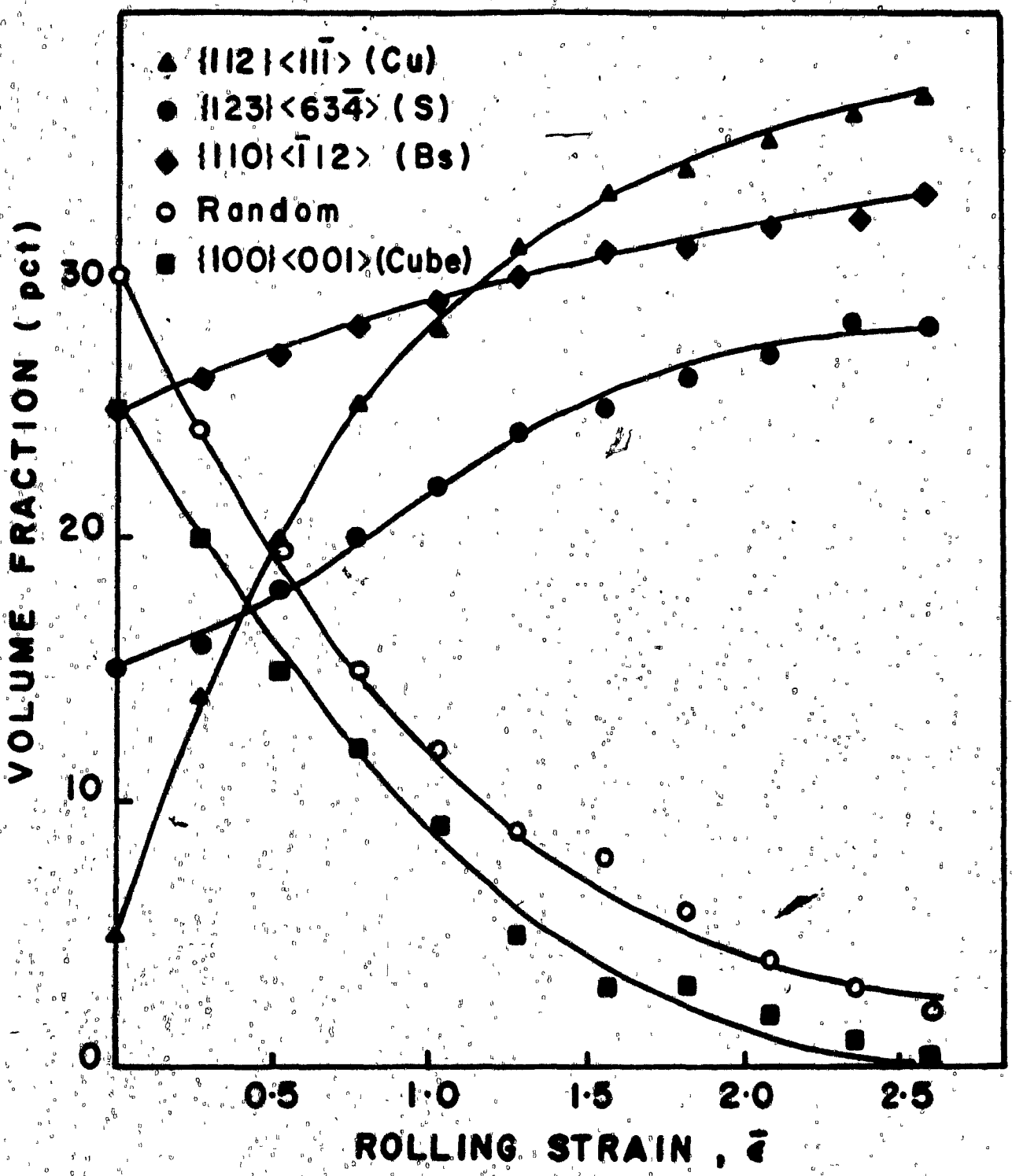

Figure 4.8 Volume fractions of main components as a function of rolling strain $\bar{\varepsilon}$.

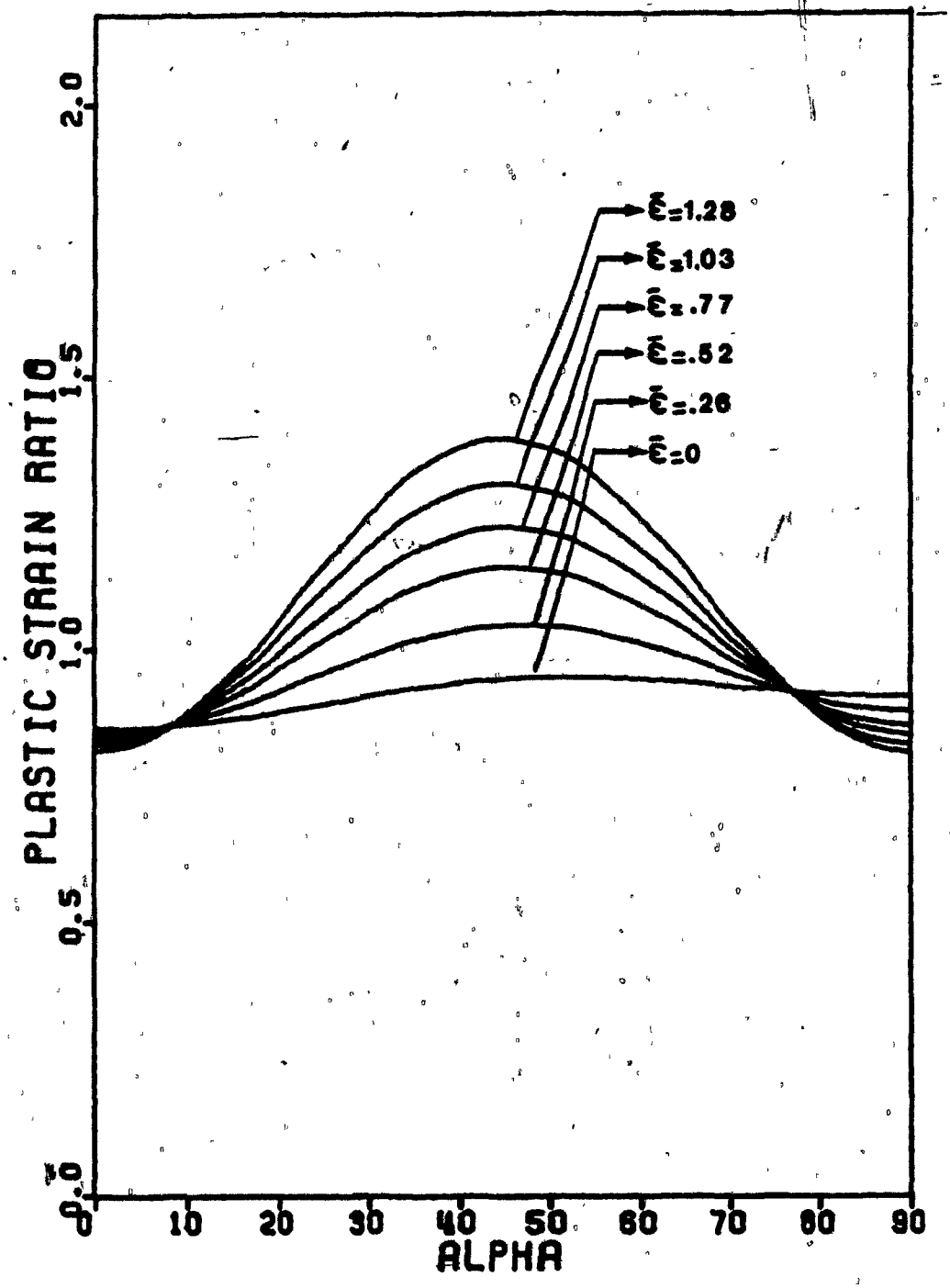

Figure 4.9 a) R(α) curves predicted by the CMTP method for strains $\bar{\epsilon}$ = 0 to $\bar{\epsilon}$ = 1.28. Volume fractions of texture components for each case are those listed in Table 4.4.

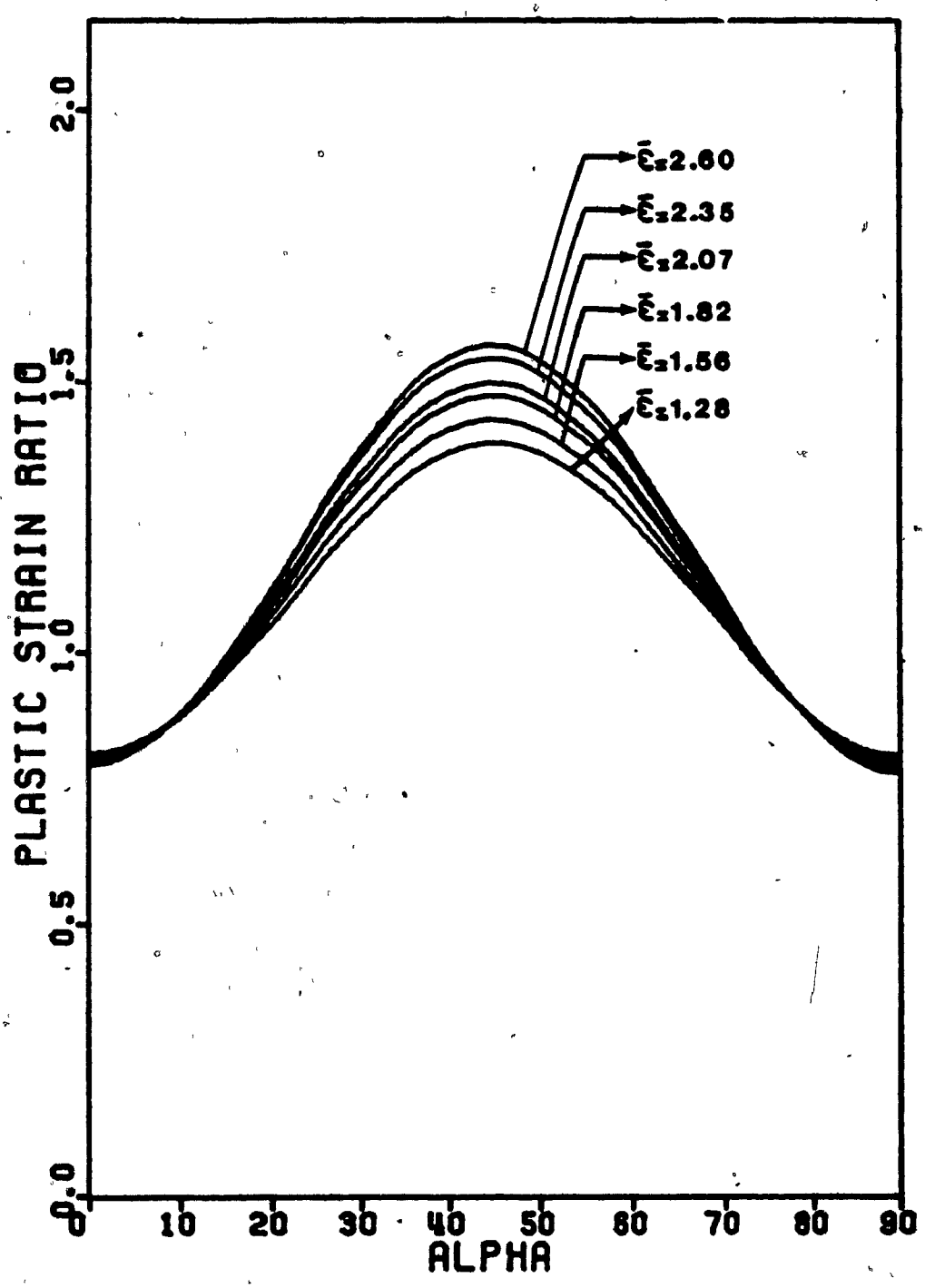

Figure 4.9 b) R(α) curves predicted by the CMTP method for strains $\bar{\varepsilon}$ = 1.28 to $\bar{\varepsilon}$ = 2.60. Volume fractions of texture components for each case are those listed in Table 4.4.

CHAPTER 5

DISCUSSION

5.1) Extrapolated R-value:

In this section it is intended to justify the polynomial fit used in Chapter 4 in order to determine the R-value at zero strain. To do this let us first consider a typical R_s vs. ε_z curve (Figure 5.1), where $R_s = \varepsilon_y/\varepsilon_z$ and ε_y and ε_z are the width and thickness strains, respectively.

The curve in figure 5.1 decreases progressively until it becomes assymptotic to a certain value corresponding to the stabilized tension texture. This type of curve can be described by an exponential function as follows:

$$R_s = Ae^{-B\varepsilon_z} + C \qquad (5.1)$$

Hence if the experimental data are fitted with this curve using the least squares technique, the constants A, B and C can be found, and the R_s value at zero strain, which characterizes the sheet prior to any deformation, can be determined. By examining the above curve and the equation describing it (equation 5.1), it can readily be seen that:

i) $R_s = C$ as ε_z tends to infinity; i.e. C is the value of R_s corresponding to the stabilized tension texture;

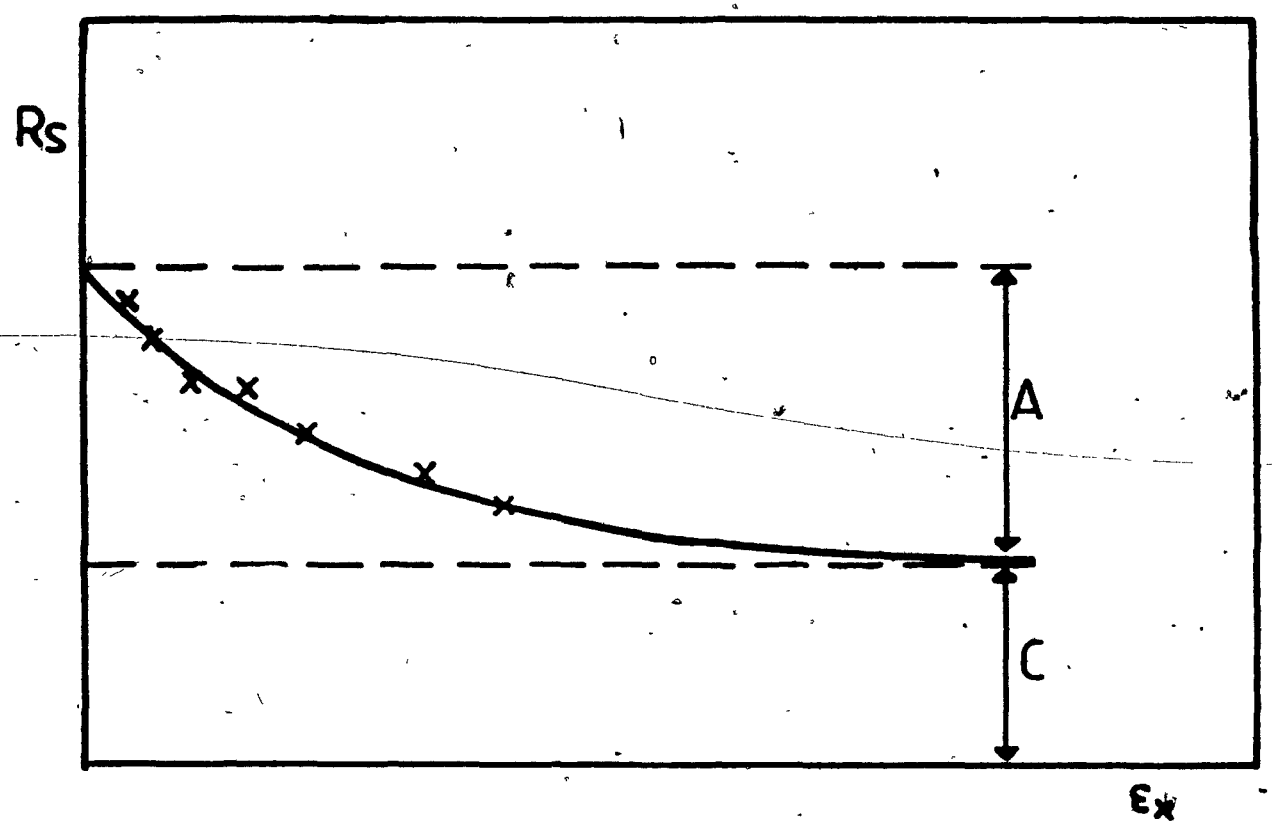

Figure 5.1 Typical dependence of the plastic strain ratio R_S on the tensile strain ε_x.

ii) $R_s = A + C$ at $\varepsilon_z = 0$; i.e. $A + C$ is the value of R_s characterizing the sheet prior to tensile deformation; and

iii) $dR_s/d\varepsilon_z = -AB$ at $\varepsilon_z = 0$; i.e. B is a measure of how fast the curve decreases (the curve decreases faster as B gets larger).

In order to understand the drawback of this exponential fit, it is necessary to write down the main equations used in the least squares method. Basically, this method consists of trying to make the curve pass through the data points so that the sum of the magnitudes of the residuals under the curve will be equal to the sum of the magnitude of those above the curve. (A residual is the distance between a data point and the curve). In other words, it is desired to minimize the following:

$$S = \sum_{i=1}^{N} w_i [Ae^{-B\varepsilon_{zi}} + C - R_{si}]^2 \qquad (5.2)$$

where w_i is the weight or reproducibility of point i and N is the number of data points.

Differentiation of equation (5.2) with respect to A, B and C results in the following:

$$\frac{\delta S}{\delta A} = 2\sum w_i [Ae^{-B\varepsilon_{zi}} + C - R_{si}]e^{-B\varepsilon_{zi}} = 0 \qquad (5.3)$$

$$\frac{\partial S}{\partial B} = -2\sum w_i [Ae^{-B\varepsilon_{zi}} + C - R_{si}]\varepsilon_{zi} Ae^{-B\varepsilon_{zi}} = 0 \quad (5.4)$$

$$\frac{\partial S}{\partial C} = 2\sum w_i [Ae^{-B\varepsilon_{zi}} + C - R_{si}] = 0 \quad (5.5)$$

Development of the above equations leads to:

$$A\sum w_i e^{-2B\varepsilon_{zi}} + C\sum w_i e^{-B\varepsilon_{zi}} - \sum w_i R_{si} e^{-B\varepsilon_{zi}} = 0 \quad (5.3a)$$

$$A\sum w_i \varepsilon_{zi} e^{-2B\varepsilon_{zi}} + C\sum w_i \varepsilon_{zi} e^{-B\varepsilon_{zi}} - \sum w_i R_{si} \varepsilon_{zi} e^{-B\varepsilon_{zi}} = 0$$

(5.4a)

$$A\sum w_i e^{-B\varepsilon_{zi}} + C\sum w_i - \sum w_i R_{si} = 0 \quad (5.5a)$$

or,

$$AS_1 + CS_2 - S_3 = 0 \quad (5.3b)$$

$$AS_4 + CS_5 - S_6 = 0 \quad (5.4b)$$

$$AS_7 + CS_8 - S_9 = 0 \quad (5.5b)$$

Proceeding by substitution results in the following:

$$C = (S_9 - AS_7)/S_8 \tag{5.6}$$

$$A = (S_3S_8 - S_2S_9)/(S_1S_8 - S_2S_7) \tag{5.7}$$

$$(S_3S_8 - S_2S_9)(S_4S_8 - S_5S_7) - S_9(S_8 - S_5)(S_1S_8 - S_2S_7) = 0 \tag{5.8}$$

Equation 5.8, where the only unknown is B, can now be solved by the secant method. The program, called EXPO, which uses this method to solve for B, then A and C, is shown in the Appendix G.

Normally, for most functions, the root can be found by this method even if the interval of the root is not known a priori. But for this function (Equation 5.8), one needs to have a good idea of the magnitude of B; otherwise, for every interval given, a different solution is obtained. To illustrate this problem, a sketch is given in Figure 5.2.

The results from the EXPO program for three sets of data are also shown in Table 5.1; R_s at zero strain is seen to be in good agreement with the result from the polynomial fit.

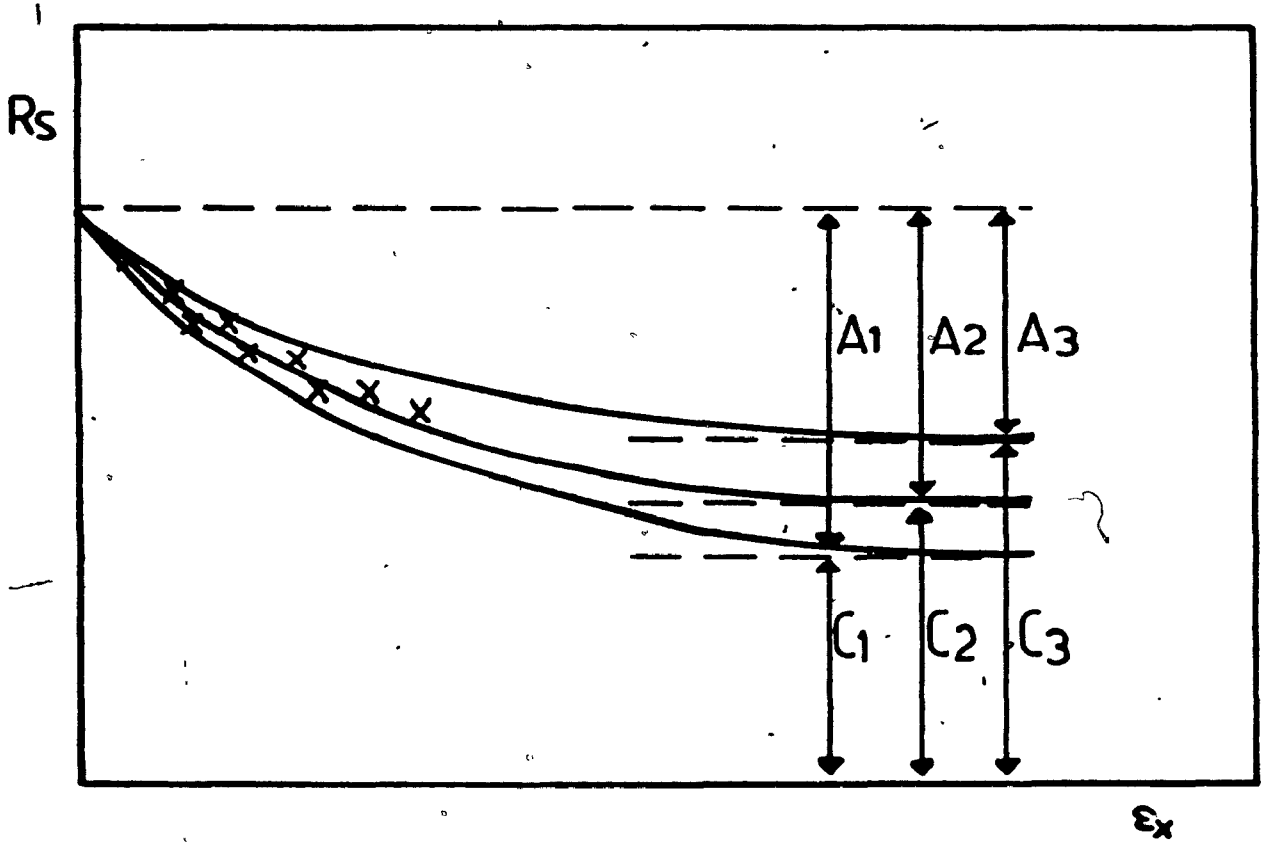

Figure 5.2 Possible solutions fitting the experimental data obtained from program EXPO shown in Appendix F.

Specimen	B1	B2	B	A	C	A+C(=R_s)	R value from polynomial fit
R01	10	4	1.05	.99	-.26	.73	.75
	10	20	1.29	.82	-.09	.78	
	1	2	.83	1.23	-.50	.73	
A11	1	6	.97	2.68	-1.70	.98	.88
	5	10	3.90	.72	.26	.98	
	10	20	6.46	.48	.51	.99	
T21	1	6	.97	3.98	-3.35	.63	.64
	5	10	4.00	1.02	-.38	.64	
	10	20	7.21	.60	+.04	.64	

Table 5.1: Examples of R_s-values from exponential fit

It is worth noting here that, despite the fact that a different B (and hence a different A and C) is obtained for every starting interval [B1, B2], the sum A + C is always constant. This is normal, since most data points are in the vicinity of zero and there are none at large ε_z. Therefore the curve always starts at a more or less constant value and becomes assymptotic at a value which depends on the initial slope.

For this reason it was thought better to use a polynomial fit of degree less than the number of data points so that there is a unique solution. As the exponential function can always be approximated by a finite degree polynomial,

equation (5.1) can be written:

$$R_s = \frac{\varepsilon_y}{\varepsilon_z} = A\,(1 - B\varepsilon_z + \ldots) + C$$

$$\text{or,} \quad \varepsilon_y = (A + C)\,\varepsilon_z - AB\varepsilon_z^2 \qquad (5.9)$$

Equation (5.9) is the second degree polynomial used in Chapter 4 in order to fit the $(\varepsilon_y, \varepsilon_z)$ data and find the slope at the origin. Note that the slope at the origin of the curve representing equation (5.9) is $\frac{d\varepsilon_y}{d\varepsilon_z} = R = A + C$, which is equal to R_s at 0.

5.2) Comparison of the Non-Quadratic Hill and Hosford Criteria:

For the complete analysis of sheet metal forming, an anisotropic yield criterion must be assumed. To be useful for engineering purposes, it must reasonably describe the material behaviour but be straightforward enough so its parameters can be evaluated by simple mechanical tests. Although several non-quadratic criteria have been proposed in the past, only two are compared here and the limitations of one of them are pointed out.

The two considered are (i) a criterion suggested by Hosford in 1979 [54], and (ii) one of the four special cases of Hill's 1979 generalized criterion [41]. These are given in equations 5.10 and 5.11 respectively.

$$F\sigma_1^a + G\sigma_2^a + H|\sigma_1 - \sigma_2|^a = 1 \qquad (5.10)$$

$$C|\sigma_1 + \sigma_2|^m + H|\sigma_1 - \sigma_2|^m = 1 \qquad (5.11)$$

In order to study planar anisotropy, these two criteria must be modified. The first criterion does recognize planar anisotropy but is restricted in its present form to loading along the principal axes of anisotropy. Attempts to generalize this formulation to include a shear stress term σ_{12} were made by Hosford in his 1985 paper [55], but lead to an "unreasonable" formulation. This can be shown by considering a 45° tension test, for which the criterion can be rearranged and written in the following form:

$$(2Q + 1)(R + P)\sigma_{12}^a + P\sigma_1^a + R\sigma_2^a + RP(\sigma_1 - \sigma_2)^a = P(R + 1)Y_o^a \qquad (5.12)$$

where P, R, and Q are the strain rate ratios in the 90°, 0° and 45° directions, respectively, and Y_o is the yield stress along the 1 direction ($\alpha = 0°$). For a 45° tension test (where $\sigma_1 = \sigma_2 = \sigma_{12} = Y_{45}/2$), the flow stress should be:

$$Y_{45} = 2\left[\frac{P(R + 1)}{2(Q + 1)(R + P)}\right]^{1/a} \cdot Y_0 \qquad (5.13)$$

According to Hosford, for the criterion given in

(5.12) to be reasonable, it must include the planar isotropy case. Hence he argued that if planar isotropy is assumed (P = R = Q), one should obtain $Y_{45} = Y_0$ for any a. But, from equation (5.13) above, it is seen that this is true only if a = 2, which is not a satisfactory conclusion.

Now, the second criterion (equation 5.11) is considered in turn. When planar anisotropy is assumed ($R_0 \neq R_{90}$) and a shear stress term σ_{12} is included, the criterion can be re-written as follows:

$$|F\sigma_1 + G\sigma_2|^m + H|\sigma_1 - \sigma_2|^m + 2N\sigma_{12}^m = 1 \qquad (5.14)$$

Note that this is the function used in order to calculate R_0, R_{45} and R_{90} in the Results chapter (Chapter 4).

For this formulation, the expressions for R and the yield stress (Y) values at $\alpha = 0°$, $45°$ and $90°$ are listed below.

$$R_0 = \frac{H - GF^{m-1}}{F^m + GF^{m-1}} \qquad (i)$$

$$R_{90} = \frac{H - FG^{m-1}}{G^m + FG^{m-1}} \qquad (ii)$$

$$R_{45} = \frac{N}{(F+G)^m} - \frac{1}{2} \qquad (iii)$$

$$Y(0) = \left(\frac{1}{F^m + H}\right)^{1/m} \qquad \text{(iv)}$$

$$Y(90) = \left(\frac{1}{G^m + H}\right)^{1/m} \qquad \text{(v)}$$

$$Y(45) = 2\left(\frac{1}{(F+G)^m + 2N}\right)^{1/m} \qquad \text{(vi)}$$

In what follows, a similar type of check is performed as was done for Hosford's criterion above. From equations (i), (ii) and (iii), when we set $R_0 = R_{90} = R_{45}$, the following relation is obtained,

$$N = 2^{m-1}H \qquad (5.15)$$

Then, substituting this into equation (vi), it can be seen that:

$$Y(45) = 2\left(\frac{1}{(2F)^m + 2^m H}\right)^{1/m}$$

$$= \left(\frac{1}{F^m + H}\right)^{1/m} \qquad (5.16)$$

and remembering that $F = G$ (since $R_0 = R_{90}$), then

$$Y(0) = Y(90) = Y(45) \text{ for any } m.$$

Therefore, it can be concluded that this criterion (5.14) is satisfactory for predicting the R-value at 45°. However, in directions other than 45°, where shear components are also present, the criterion seems to be unsatisfactory since, if planar isotropy is assumed, the exponent m will have to be equal to 2. This is illustrated below by taking $\alpha = 30°$.

$$R(30) = -\frac{F + 3G}{4(F+G)} + \frac{2^m H + 3N\, 2^{2m-3}}{4(F+G)(3F+G)^{m-1}} \qquad (5.17)$$

If we set $R(0) = R(90) = R(30)$, the following is obtained:

$$N = \frac{1}{3}\,(2^3 - 2^{3-m})H \qquad (5.18)$$

and,

$$Y(30) = \left[F^m + H\left\{\left(\frac{1}{2}\right)^m + \frac{1}{3}(2^4 - 2^{4-m})\left(\frac{\sqrt{3}}{4}\right)^m\right\}\right]^{-1/m} \qquad (5.19)$$

Finally, setting $Y(30) = Y(0)$

$$\left(\frac{1}{2}\right)^m + \frac{1}{3}\,(2^4 - 2^{4-m})\,\left(\frac{\sqrt{3}}{4}\right)^m = 1 \,,$$

or $$3(2)^m + (2^4 - 2^{4-m})\,(\sqrt{3})^m = 3(4)^m \qquad (5.20)$$

For equation (5.20) to be valid, m must be equal to 2.

Having shown that the present version of Hill's criterion (equation 5.14) is not satisfactory for all tests giving rise to shear stress terms, it can nevertheless be stated that for R-value predictions at 0°, 90° and 45°, it is perfectly suitable.

5.3) Comparison of Calculated R-values with CMTP Predictions:

The agreement between the $R(\alpha)$ values determined by mechanical testing and the CMTP predictions based on experimental pole figures is only qualitative. Nevertheless, the two methods give similar results for the following quantities (see Figure 5.3).

i) The R-values at 0° and 90°, which both decrease with rolling strain;

ii) R_{45}, which is larger than R_0 and R_{90} in all the experiments, as well as in the predictions;

iii) R_{90}, which is larger than R_0 and becomes less than R_0 at a rolling strain of about 2 (experimentally) and about 1.5 (CMTP method).

However, the CMTP R-values are always higher than the experimental ones. The most important discrepancy is at 45°, and as can be seen from Figures 5.3 a to c, this becomes larger as the rolling strain is increased. The reasons for this discrepancy can be summarized as follows:

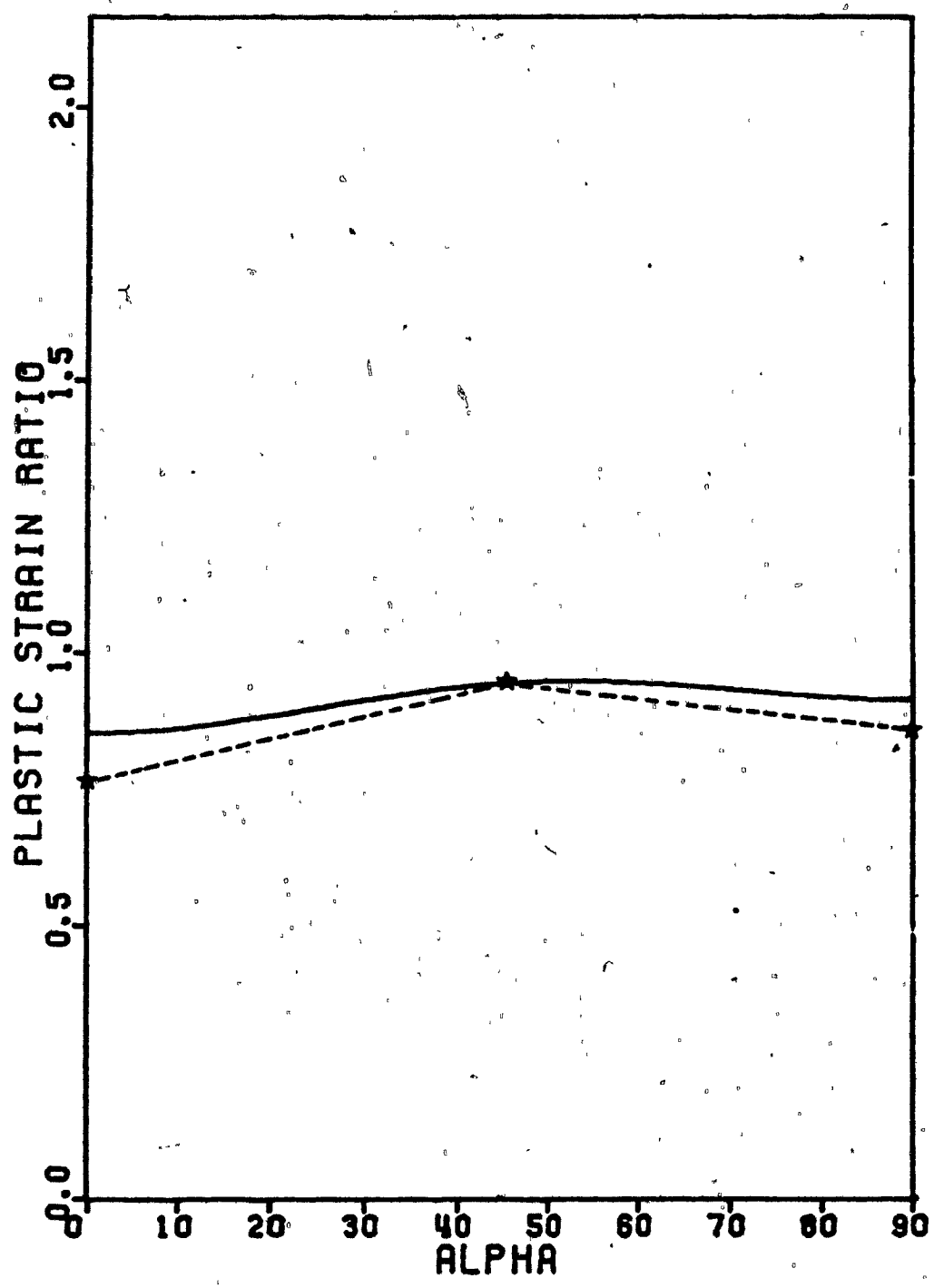

Figure 5.3 a) Comparison of the experimental R(α) values with those calculated using the CMTP method; annealed sheet ($\bar{r}$ = 0).

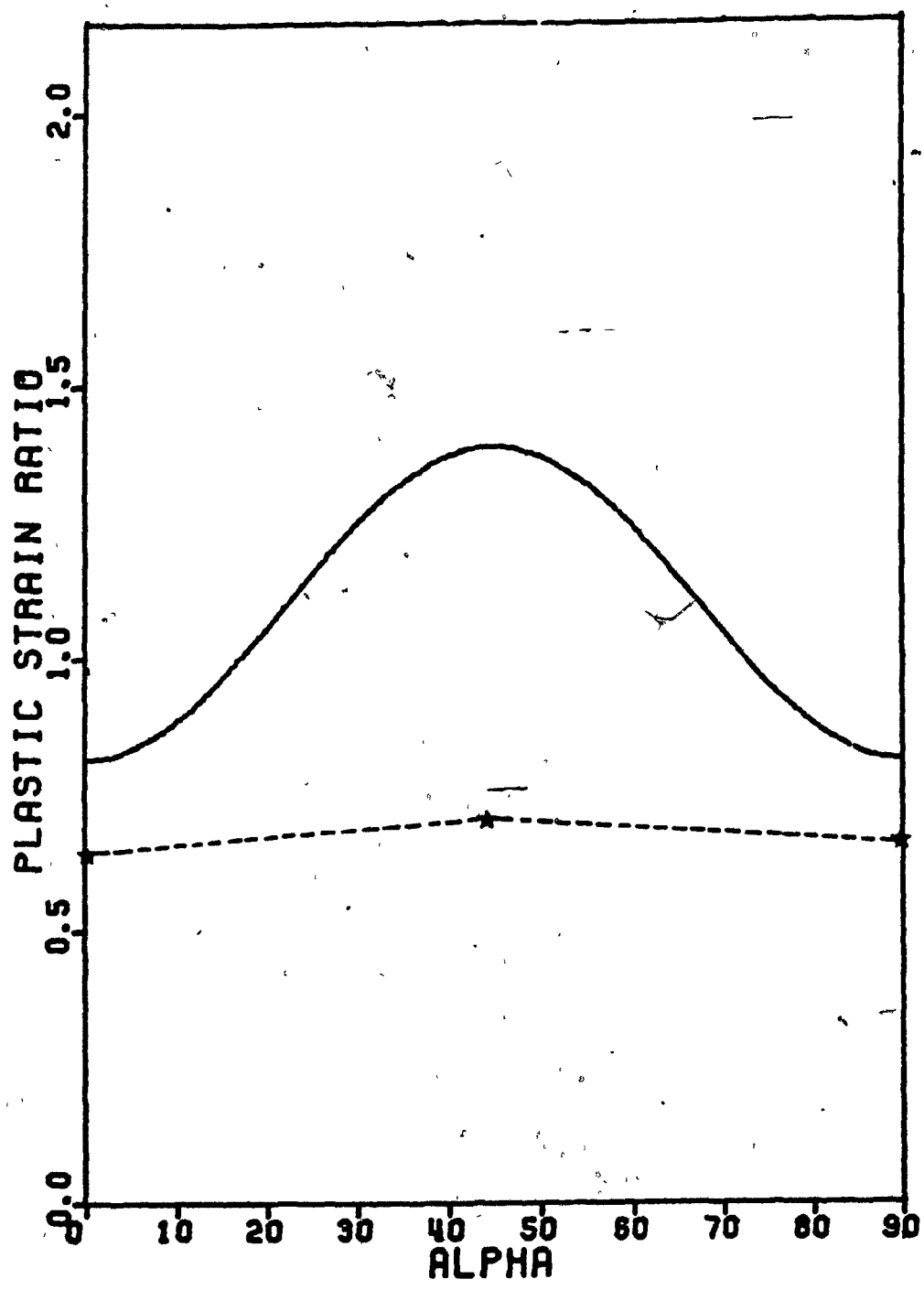

Figure 5.3 b) Comparison of the experimental R(α) values with those calculated using the CMTP method; sheet rolled to a strain $\bar{\varepsilon} = 1.28$.

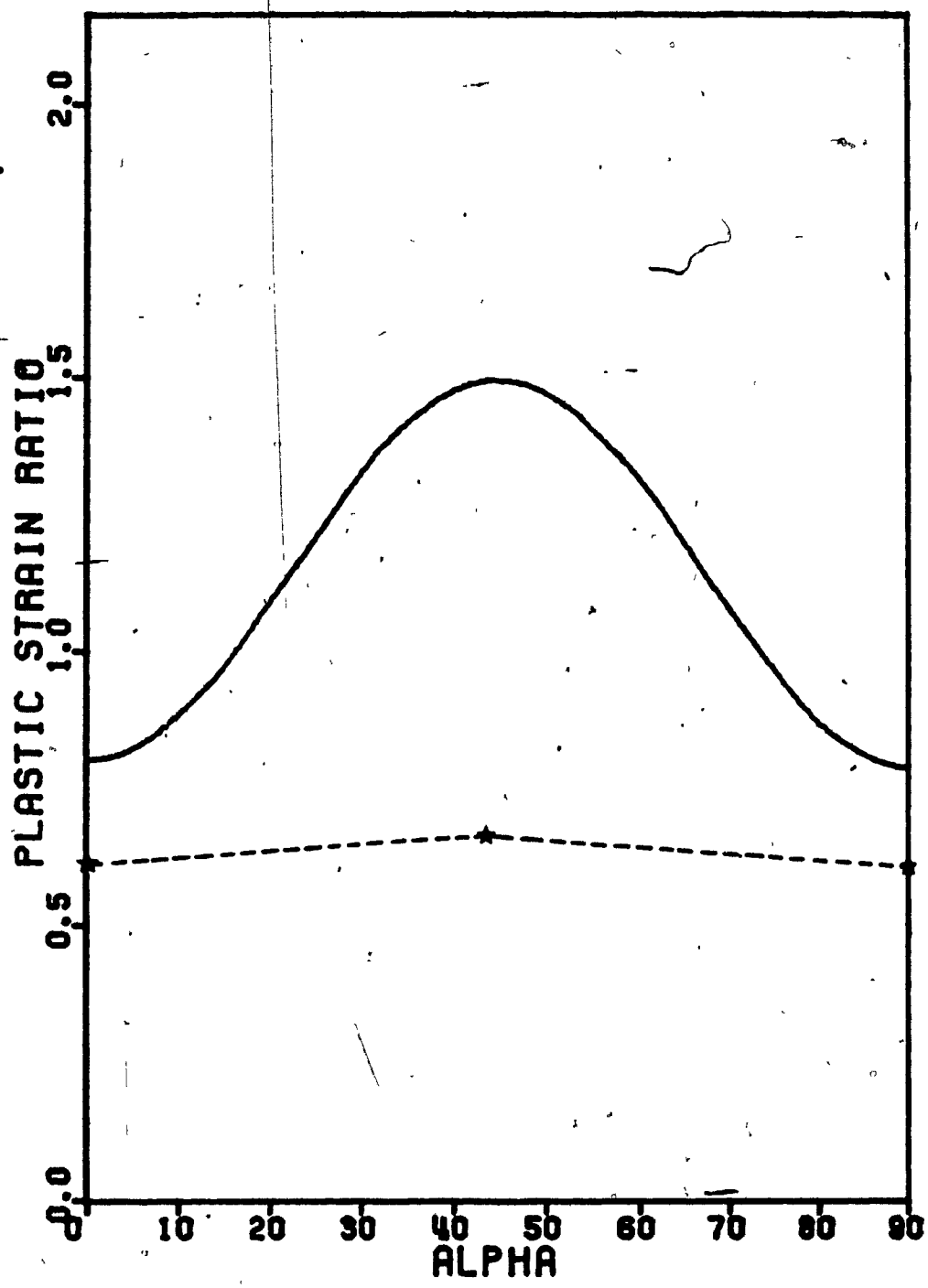

Figure 5.3 c) Comparison of the experimental R(α) values with those calculated using the CMTP method; sheet rolled to a strain $\bar{\varepsilon} = 2.08$.

i) First, there is the experimental error in the measurement of the strains and yield stresses. This remains the smallest source of error, especially for the first three sheets for which the extrapolation procedure was used in order to determine the R-value at zero strain.

ii) Second, there is the basic limitation of the CMTP method in that approximating the Bishop and Hill polyledron by a smooth rounded yield surface can lead to more or less significant errors in the details of the strain rate tensor which are related to small differences between the crystallographic and CMTP yield loci. For example, for the cube texture, the prediction is good at 0° and 90°, but there is larger error in the directions (eg. 45°) where there is shear [56].

iii) Third, the largest source of error is certainly the inherently semi-quantitative nature of texture characterization by means of pole figures and ideal orientations. The problems that arise from this form of description are obvious when it is seen that, for example, for the {111}<112> and {554}<225> texture components, which are very close in a pole figure, the R-values differ considerably (eg. 1.61 and 2.14 respectively at $\alpha = 90°$) [43].

The discrepancy found in our results can be reduced if the amount of the brass texture is decreased and the proportion of the cube texture increased for the heavily rolled sheets. In fact, in (111) pole figures

such as those determined in the present study, in which the outer part is missing, these two texture components can be easily mistaken for each other because they both involve poles in the central region of the figure. Also, apart from the cube texture, the only rolling texture component which can lower the R-value at 45° is the Goss texture [43]. However, this component is certainly not observed in either the annealed or the lightly deformed sheets. It may become important in the heavily rolled sheets, as shown by Pochettino [57], who reported a volume fraction of around 10%. This observation is not in contradiction with our partial pole figures since the Goss component is rather close to the copper texture in the central part of the (111) pole figure. However, even if 15% of this Goss component is included in the CMTP calculation, only a small decrease in R_{45} is obtained (see Figure 5.4).

iv) Fourth, some textures have been reported [56] which may be called 'anomalous textures', because they lead to $\bar{R} < 1$ and $\sigma_b/\sigma_u > 1$. For example, the texture (-.4048, .9020, .1503) [.9128, .4083, .0084] results in $\bar{R} = .92$ and $\sigma_b/\sigma_u = 1.02$. Such a component would be fairly consistent with our experimental results, but unfortunately it is not easily identified in the pole figures.

v) Finally, the CMTP predictions could be much improved if the volume fractions of a large number of ideal orientations were known, such as can be obtained from CODF

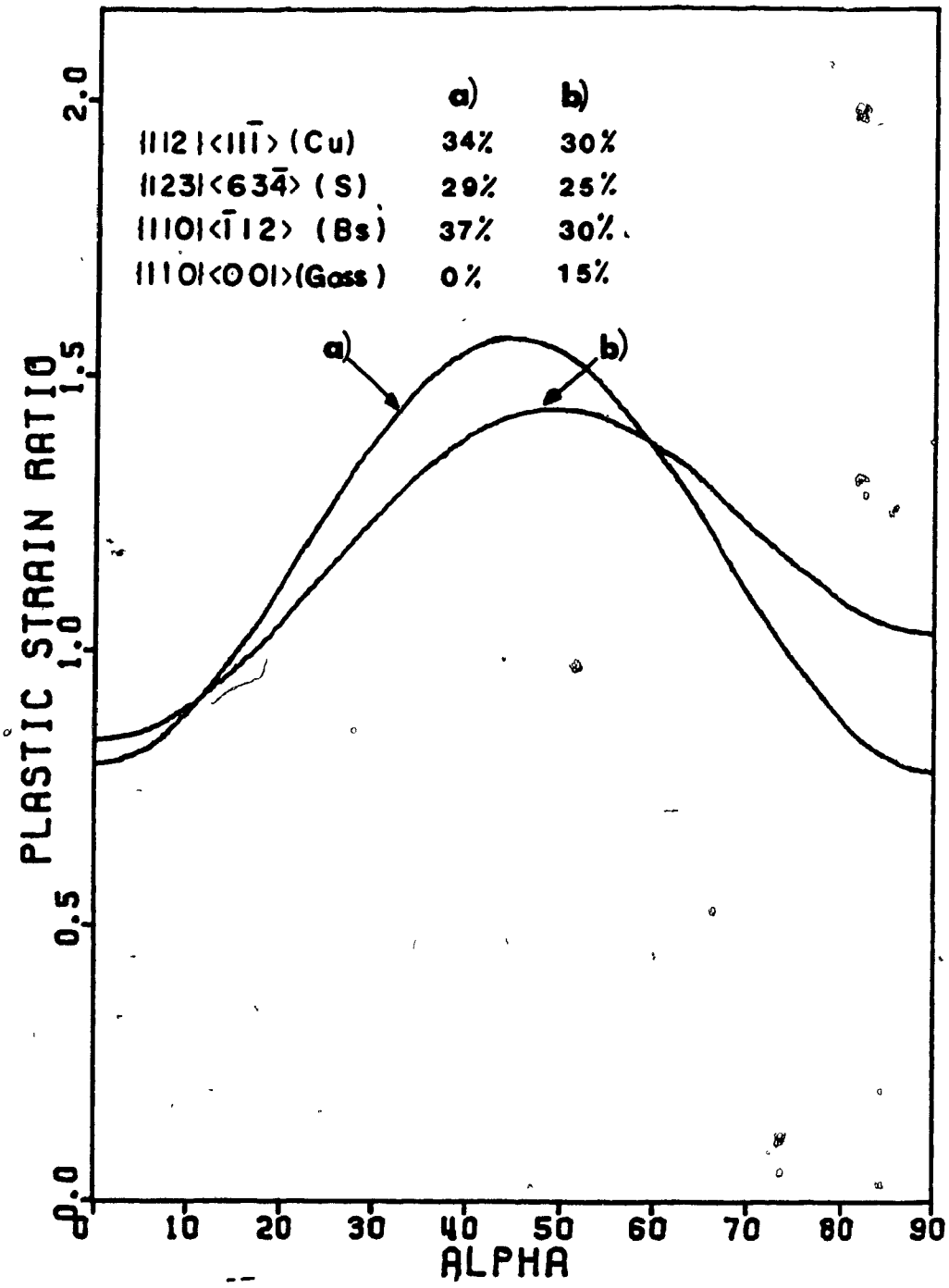

Figure 5.4 Effect of including a 15% volume fraction Goss component on $R(\alpha)$.

methods of texture representation.

5.4) Some Comments on the Texture of the Present Al Sheet:

Although some investigators have reported 0° and 90° earing in annealed commercial purity aluminum [58,59], it is generally known that the earing behaviour of a given sheet is directly dependent on the relative proportions of the cube and 'retained rolling' textures. The main factors which influence the annealing texture are the previous rolling texture, the annealing temperature and the impurity content [2].

For the aluminium sheet investigated, it was found experimentally that R_{45} is larger than both R_0 and R_{90}, and thus 45° earing is expected. Moreover, the CMTP analysis predicts the same result since, as can be seen from the pole figure, the cube texture which would give rise to 0° and 90° earing is not predominant. There are two reasons for this. First the iron content is higher than that of other commercially pure Al sheets [60,61], and it has been reported [62,63] that a high Fe content inhibits the growth of the cube component. Second, the sheet investigated was annealed at a fairly high temperature (550°C), and this is believed to suppress the formation of the cube texture even more. In fact, D.J. Jensen and N. Hansen [60] have reported that an increase in annealing temperature from 250° to 300°C results in a decrease in the amount of cube texture and an increase in the amount of retained rolling texture.

CONCLUSIONS

As a result of this study, the following general conclusions were reached:

1) The anisotropy coefficient characterizing the real behaviour of a rolled sheet is the value corresponding to zero deformation and not the one measured at the limit of uniform elongation. This is why the extrapolation procedure should be used on the width vs. thickness strain (ε_y vs. ε_z) curve recorded from tensile tests in order to determine the slope at the origin $d\varepsilon_y/d\varepsilon_z$. It is this extrapolated value that can be compared to the one obtained from the application of the yield criterion and normality rule.

2) The present sheet is characterized by 'anomalous' behaviour in that the average R-value is less than unity while $\sigma_{ps}/\sigma_u > 1.15$ or $\sigma_b/\sigma_u > 1$. This is consistent with earlier reports [37] regarding such commercial purity Al sheets. As a result, its behaviour is better described by a generalized than a quadratic criterion. Assuming planar <u>isotropy</u> as a first approximation, the exponent m of the criterion is found to be equal to 1.7. A more general criterion which takes planar <u>anisotropy</u> into account is proposed. Such a criterion is useful because the prediction of earing is as important as that of drawability.

3) By using this new yield locus fitted to the experimental

yield stresses, R(α) values (and hence earing and drawability tendencies) can be predicted even for heavily rolled sheets where R-values cannot be measured directly due to plastic instability.

4) The R-values at α = 0°, 45° and 90° decrease continuously with rolling strain and this is in agreement with what is reported experimentally [37] as well as theoretically [64] for FCC metals.

5) The R-values at 45° are larger than both R_0 and R_{90} for all rolled sheets; thus $\Delta R<0$, so that 45° earing is expected. Even though this is in fact generally observed for cold rolled Al, it is not usually the case for the annealed state. In our case $\Delta R<0$ even for the original annealed sheet, apparently because the cube texture which gives rise to 0° and 90° earing ($\Delta R>0$) is not predominant. This can be seen from the corresponding pole figure, the features of which are probably associated with the high Fe content and the high temperature at which the sheet was annealed [62,65].

6) The CMTP predictions (based on incomplete pole figures) are not always in full agreement with the experimental results. For the predictions to be improved, more detailed information regarding the texture components is required, including either the volume fraction of each ideal component, or the full CODF.

REFERENCES

1. J.W. Rogers, Jr. and W.A. Anderson: Proc. of a Symposium on the Relation Between Theory and Practice of Metal Forming, Cleveland, Ohio, Oct. 1970, p. 185.

2. F.A Underwood: "Textures in Metal Sheets", McDonald & Co., London, 1961.

3. S. Mishra and C. Darmann: Int. Met. Rev. 27 N^{O} 6 (1982), p. 307.

4. R. Sowerby: Proc. Symp. on Textures in Non-Ferrous Metals and Alloys, Detroit, Michigan, Sept. 1984, p. 99.

5. P. Gangli and T. Leffers: Proc. ICOTOM 5, 1978, Aachen (Germany), Vol. I, p. 209.

6. R.L. Whiteley: Trans. ASM, 52 (1969), p. 154.

7. W.F. Hosford: Proc. ICSMA 3, 1973, Cambridge, England, Vol. 2, p. 137.

8. P.B. Mellor: "Mechanics of Solids: The Rodney Hill 60th Anniversary Volume", ed. H.G. Hopkins and M.J. Sewell, Manchester, Pergamon Press, April 1980, p. 383.

9. W.T. Lankford, S.C. Snyder and J.A. Bauscher: Trans. ASM, 42 (1950), p. 1197.

10. J. Gronostajski and C. Banasiak: "Sheet Metal Forming and Energy Conservation", ASM, Metals Park, Ohio, (1976), p. 81.

11. S.Y. Chung and H.W. Swift: Proc. Inst. Mech. Eng., 165 (1951), p. 199.

12. J.A. Elias, R.H. Heyer and J.H. Smith: AIME Trans., 224 (1962), p. 678.

13. R.P. Arthey and W. B. Hutchinson: Met. Trans. A, 12A (1981), p. 1817..

14. H. Hu: Met. Trans. A, 6A (1975), p. 2307.

15. H. Hu: Met. Trans. A, 6A (1975), p. 945.

16. H.J. Kleemola and N.G. Mattfolk: Scandinavian Journal of Metallurgy, 7 (1978), p. 161.

17. Y.C. Liu: Met. Trans. A, 14A (1983), p. 1199.

18. W. Truszkowski: Met. Trans. A, 7A (1976), p. 327.

19. W. Truszkowski and J. Jarominek: Mém. Sci. Rev. Met., 70 N° 6 (1973), p. 433.

20. D.H. Lloyd: Sheet Metal Ind., 39 (1962), p. 82.

21. D.V. Wilson and R.D. Butler: J. Inst. Metals, 90 (1963), p. 473.

22. W.F. Hosford: "Formability: Analysis, Modelling, and Experimentation", Proc. of a Symposium held in Chicago, Illinois, Oct. 1977, p. 78.

23. R. Hill: Proc. Roy. Soc. London, A193 (1948), p. 281.

24. H.R. Piehler and W.A. Backofen: "Textures in Research and Practice", ed. Wasserman and Grewen, Springer, Berlin, 1969, p. 436.

25. G.J. Davies, D.J. Goodwill, J.S. Kallend and T. Ruberg: J. Inst. Metals, 101 (1973), p. 270.

26. S. Nagashima, H. Takechi and H. Kato: "Textures in Research and Practice", ed. Wasserman and Grewen, Springer, Berlin, 1969, p. 444.

27. M. Fukuda: Trans. ISIJ (Iron Steel Inst. Japan), 8 (1968), p. 68.

28. G.I. Taylor: J. Inst. Metals, 62 (1938), p. 307.

29. J.F.W. Bishop and R. Hill: Phil. Mag., 42 (1951), p. 414.

30. W.F. Hosford and W.A. Backofen: "Fundamentals of Deformation Processing", Proc. of the 9th Sagamore Army Materials Research Conference, Aug. 1962, p. 259.

31. W.F. Hosford: "Advances in Deformation Processing", Proc. of the 21st Sagamore Army Materials Research Conference, Syracuse, New York, Aug. 1974, p. 187.

32. W.F. Hosford and C. Kim: Met. Trans. A, 7A (1976), p. 468.

33. W.A. Backofen: "Deformation Processing", Addison-Wesley, Reading, Mass., 1972.

34. W.F. Hosford and R.M. Caddell: "Metal Forming: Mechanics and Metallurgy", Prentice-Hall, Inc., Englewood Cliffs, N.J., 1983.

35. A.N. Bramley and P.B. Mellor: Int. J. Mech. Sci., 8 (1966), p. 101.

36. A.N. Bramley and P.B. Mellor: Int. J. Mech. Sci., 10 (1968), p. 211.

37. J. Woodthorpe and R. Pearce: Int. J. Mech. Sci., 12 (1970), p. 341.

38. R. Pearce: Int. J. Mech. Sci., 10, (1968), p. 995.

39. P.B. Mellor and A. Parmar: Proc. of a Symposium on Mechanics of Sheet Metal Forming, held at the General Motors Research Laboratories, Warren, Michigan, Oct. 1977, p. 53.

40. I.L. Dillamore: J. Phys., D. Appl. Phys., 7 (1974), p. 979.

41. R. Hill: Math. Proc. Camb. Phil. Soc., 85 (1979), p. 179.

42. F. Montheillet, P. Gilormini and J.J. Jonas: Acta Met., 33 (1985), p. 705.

43. Ph. Lequeu, F. Montheillet and J.J. Jonas: Proc. Symp. on Textures in Non-Ferrous Metals and Alloys, Detroit, Michigan, Sept. 1984, p. 189.

44. P.R. Sperry and M.H. Bankard: Metallography, Structures and Phase Diagrams, ASM Metals Handbook, 8th Edition, 8 (1973), American Society for Metals, Metals Park, Ohio, p. 120.

45. Ch. Perdrix: Thèse de Docteur-Ingénieur, CEMEF, Ecole des Mines de Paris, Sophia-Antipolis (1983).

46. D.P. Clausing: Int. Jour. Fract. Mech., 6, N° 1 (1970), p. 71.

47. S. Kobayashi, R.M. Caddell and W.F. Hosford: Int. J. Mech. Sci., 27 N° 718 (1985), p. 509.

48. J.L. Bassani: Int. J. Mech. Sci., 19 (1977), p. 651.

49. P.B. Mellor: Int. Met. Rev., 27 N° 1 (1981), p. 1.

50. N. Hansen and D.J. Jensen: Met. Trans. A., 17A (1986), p. 253.

51. M. Hatherley and W.B. Hutchinson: "An Introduction to Textures in Metals", The Institute of Metallurgists, Chameleon Press Ltd., London, 1979.

52. J. Hirsch, Doktorarbeit, RWTH, Aachen (Dec. 1984).

53. H. Mecking: "Preferred Orientation in Deformed Metals and Rocks: An Introduction to Modern Texture Analysis", Ed. Hans-Rudolf Wenk, Academic Press, 1985, p. 267.

54. W.F. Hosford: Proc. 7th North Am. Metalworking Conf. SME, Dearborn, Michigan, USA, 1979, p. 191.

55. W.F. Hosford: Int. J. Mech. Sci., 27 (1985), p. 423.

56. Ph. Lequeu: Ph.D. Thesis, McGill University (1986).

57. A. Pochettino: Thèse de Docteur-Ingenieur, Paris XI (1981).

58. J.C. Blade: Proc. Symp. on Textures in Non-Ferrous Metals and Alloys, Detroit, Michigan, Sept. 1984, p. 1.

59. N. Kanetake, Y. Tozawa and T. Otani: Int. J. Mech. Sci, 25 N° 5 (1983), p. 337.

60. D.J. Jensen and N. Hansen: Proc. ICSMA 7, Aug. 1985, Montreal, Vol. I, p. 263.

61. O. Ferreira, P. Dervin, M. Pernot and R. Penelle: Proc. ICOTOM 5, 1978, Aachen (Germany), Vol. I, p. 337.

62. I.L. Dillamore and W.T. Roberts: Acta. Met., 12 (1964), p. 281.

63. W.B. Hutchinson: Met. Sci., 8 (1974), p. 185.

64. P. Van Houtte: Private Communication, April, 1983.

65. T. Suzuki, K. Akai, M. Shiga and Y. Nakamura: Met. Trans. A, 16A (1985), p. 27.

APPENDIX A: FORTRAN PROGRAM 'RZERO'

```
CCC
CCC    USING A NUMERICAL METHOD (ORTHOGONALIZATION METHOD) IN ORDER
CCC    TO FIT A POLYNOMIAL TO THE Ezz(OR X) AND Eyy(OR Y) DATA PNTS
CCC    AND FIND THE SLOPE AT THE ORIGIN WHICH IS dEyy/dEzz=R
CCC
      IMPLICIT REAL*8(A-H,L-Z),INTEGER(I,J,K)
      COMMON B,DELTA,JJJ
      EXTERNAL F
      DIMENSION W(10),X(10),Y(10),A(10,10),FI(10,10),GA(10),BET(10),
     .AA(10),BB(10),C(10),B(10),XX(10),YY(10),TO(10)
      DATA W/20.D0,4.D0,5.D0,6.D0,7.D0,8.D0,9.D0,10.D0,11.D0,12.D0/
      READ(5,*)II
      DO 4 I=1,II
      READ(5,*)X(I),Y(I)
      X(I)=X(I)/1.D4
      Y(I)=Y(I)/1.D4
    4 CONTINUE
      KTRY=1
      WRITE(6,17)
   17 FORMAT('SCALE:DIF.BETWEEN TICK MARKS(>E2MAX/5.7&>E3MAX/3.7)')
      READ(9,*)DELTA
      SCALE=DELTA*1.D+4
    1 WRITE(6,2)
    2 FORMAT('DEGREE OF POLYNOMIAL')
      READ(9,*)JJ
      JJJ=JJ+1
      GA(1)=0.D0
      BET(1)=0.D0
      A(2,1)=0.D0
      DO 5 I=1,II
      GA(1)=GA(1)+W(I)
      FI(1,I)=1.D0
      A(2,1)=A(2,1)+W(I)*X(I)
      BET(1)=BET(1)+W(I)*X(I)
    5 CONTINUE
      A(2,1)=-A(2,1)/GA(1)
      A(1,1)=1.D0
      A(2,2)=1.D0
      A(1,2)=0.D0
      DO 6 I=1,II
      FI(2,I)=X(I)+A(2,1)
    6 CONTINUE
      DO 8 J=2,JJJ
      GA(J)=0.D0
      BET(J)=0.D0
      DO 7 I=1,II
      BET(J)=BET(J)+W(I)*X(I)*FI(J,I)**2
      GA(J)=GA(J)+W(I)*FI(J,I)**2
    7 CONTINUE
      IF (J.EQ.JJJ) GO TO8
      AA(J+1)=-BET(J)/GA(J)
      BB(J+1)=-GA(J)/GA(J-1)
```

```
      IF(J.EQ.JJJ) GO TO 8
      DO 70 I=1,II
      FI(J+1,I)=X(I)*FI(J,I)+AA(J+1)*FI(J,I)+BB(J+1)*FI(J-1,I)
   70 CONTINUE
    8 CONTINUE
      DO 10 J=1,JJJ
      C(J)=0.D0
      DO 9 I=1,II
      C(J)=C(J)+W(I)*Y(I)*FI(J,I)
    9 CONTINUE
      C(J)=C(J)/GA(J)
   10 CONTINUE
      DO 120 J=1,2
      DO 119 K=3,6
      A(J,K)=0.D0
  119 CONTINUE
  120 CONTINUE
      DO 12 J=3,JJJ
      DO 11 K=2,JJJ
      A(J,K)=A(J-1,K-1)+AA(J)*A(J-1,K)+BB(J)*A(J-2,K)
      IF(K.GT.J) A(J,K)=0.D0
      IF(K.EQ.J) A(J,K)=1.D0
      A(J,1)=AA(J)*A(J-1,1)+BB(J)*A(J-2,1)
   11 CONTINUE
   12 CONTINUE
      DO 25 J=1,JJJ
      B(J)=0.D0
      DO 30 K=J,JJJ
      B(J)=B(J)+C(K)*A(K,J)
   30 CONTINUE
   25 CONTINUE
      WRITE(6,99)B(1),B(2),B(3)
      WRITE(6,998)B(4),B(5),B(6)
      WRITE(6,999)B(7),B(8),B(9)
   99 FORMAT(4X,'B1=',D13.5,13X,'B2=',D13.5,13X,'B3=',D13.5)
  998 FORMAT(4X,'B4=',D13.5,13X,'B5=',D13.5,13X,'B6=',D13.5)
  999 FORMAT(4X,'B7=',D13.5,13X,'B8=',D13.5,13X,'B9=',D13.5)
      X1=0.D0
  103 X2=X1+1.D-3
      X3=X1+2.D-3
      IF(X3.GT.X(II)) GO TO 105
      F1=F(X1)
      F2=F(X2)
      IF(F2.LT.F1) GO TO 111
      F3=F(X3)
      S1=(F2-F1)/(X2-X1)
      S2=(F3-F2)/(X3-X2)
      X1=X2
      GO TO 103
  111 WRITE(6,112)X1
  112 FORMAT('CURVE DECREASING AT E3=',D12.4,':POLYNOMIAL FIT NO GOOD')
```

```
      GO TO 333
105   CONTINUE
      TEST1=F(0.D0)
      TEST2=F(3.D0)
      TEST3=F(5.D0)
      WRITE(6,888)TEST1,TEST2,TEST3
888   FORMAT(4X,'T1=F(0)=',D13.5,2X,'T2=F(3=',D13.5,2X,'T3=F(5)=',D13.5)
      WRITE(6,107)
107   FORMAT('PRINT 1 TO PLOT THE CURVE')
      READ(9,*)KPLOT
      IF(KPLOT.GT.1) GO TO 333
      WRITE(6,108)
108   FORMAT('PRINT 1 IF BOTTOM CURVE')
      READ(9,*)KPOS
      CALL PLOTON
      IF(KPOS.EQ.1) GO TO 130
      CALL PLOT(1.,5.8,-3)
      GO TO 131
130   CALL PLOT(1.,1.,-3)
131   IF(KTRY.GT.1) GO TO 201
      CALL AXS(0.,0.,12HF3 (*10**-4),-12,5.7,0.,0.,SCALE,0,0.,1.)
      CALL AXS(0.,0.,12HF2 (*10**-4),12,3.7,90.,0.,SCALE,0,0.,1.)
      CALL AXS(5.7,0.,1H ,-1,3.7,90.,0.,SCALE,0,0.,1.)
      CALL AXS(0.,3.7,1H ,1,5.7,0.,0.,SCALE,0,0.,1.)
      DO 200 I=1,II
      XX(I)=X(I)/DELTA
      YY(I)=Y(I)/DELTA
      CALL CIRCLE(XX(I),YY(I),.035)
200   CONTINUE
201   CONTINUE
      DO 74 J=1,JJJ
74    CONTINUE
      CALL FNPLOT(0.,XX(II),1,F)
      CALL ENDPLT
      KTRY=KTRY+1
333   WRITE(6,205)
205   FORMAT('PRINT 1 TO TRY ANOTHER POLYNOMIAL')
      READ(9,*)KK
      IF(KK.EQ.1) GO TO 1
      STOP
      END
      REAL FUNCTION F*8(X)
      IMPLICIT REAL*8(A-H,L-Z)
      INTEGER J
      COMMON R(10),DELTA,JJJ
      Y=0.D0
      DO 110 J=2,JJJ
      U=X*DELTA
      Y=Y+R(J)*U**(J-1)
110   CONTINUE
      YY=B(1)+Y
      F=YY/DELTA
      RETURN
      END
```

APPENDIX B: FORTRAN PROGRAM 'MOSTA'

```
CCC
CCC    INTERSECTION OF HILL'S ELLIPSOID BY VARIOUS PLANES
CCC    PLOTTING OF (SIGMA1,SIGMA2) YIELD LOCUS
CCC
       DIMENSION ORD1(500),ORD2(500),ORD3(500),ORD4(500)
       DIMENSION ABS1(500),ABS2(500),ABS3(500),ABS4(500)
       DIMENSION X(500),Y(500)
CCC
C ENTRY OF HILL'S COEFFICIENTS
CCC
1      READ(9,*)F,G,H
       WRITE(6,100)F,G,H
100    FORMAT(5X,'F=  ',E9.3,5X,'G=  ',E9.3,5X,'H=  ',E9.3/)
       READ(9,*)N
CCC
CCC    INTERSECTION BY THE PLANE X=0
CCC
       TEST=(F+G)/(F*H+F*G+G*H)
       IF(TEST.GE.0)GO TO 2
       WRITE(6,21)
21     FORMAT(/10X,'HILL COEFFICIENTS INCORRECT')
       GO TO 1
2      CALL DEGRE2(N,(F+G),(G+H),(F*G+G*H+F*H),F,ABS1,ORD1)
CCC    INTERSECTION BY THE PLANE Y=0
       TEST=(F+G)/(F*G+G*H+F*H)
       IF(TEST.GE.0)GO TO 3
       WRITE(6,21)
       GO TO 1
3      CALL DEGRE2(N,(F+G),(G+H),(F*G+G*H+F*H),G,ABS2,ORD2)
CCC    INTERSECTION BY THE PLANE Z=0
       TEST=(F+H)/(F*G+F*H+G*H)
       IF(TEST.GE.0)GO TO 4
       WRITE(6,21)
       GO TO 1
4      CALL DEGRE2(N,(F+H),(G+H),(F*G+F*H+G*H),H,ABS3,ORD3)
CCC    INTERSECTION BY THE PLANE X+Y+Z=0
       TEST=(F+G)/(F*G+G*H+F*H)/2.
       IF(TEST.GE.0)GO TO 5
       WRITE(6,21)
       GO TO 1
5      ALPHA=SQRT(TEST)
       DO 30 I=1,N
       IP=2*N+1-I
       ABS4(I)=ALPHA*(-1.+FLOAT(I-1)*2./FLOAT(N-1))
       DISC=6.*((F+G)-2.*(F*G+G*H+F*H)*ABS4(I)*ABS4(I))
       DISC=ABS(DISC)
       ORD4(I)=(1.732*(F-G)*ABS4(I)+SQRT(DISC))/(F+G)/3.
30     ORD4(IP)=(1.732*(F-G)*ABS4(I)-SQRT(DISC))/(F+G)/3.
```

```
CCC   R E S U L T S
      READ(9,*)M
      IF (M.EQ.0) GO TO 401
      WRITE(6,200)
200   FORMAT(5X,121('*')/5X,'*',2X,'ABS1',3X,'*',2X,'ORD1P',2X,'*',
     .2X,'ORD1N',2X,'*',2X,'ABS2',3X,'*',2X,'ORD2P',2X,'*',2X,
     .'ORD2N',2X,'*',2X,'ABS3',3X,'*',2X,'ORD3P',2X,'*',2X,'ORD3N',
     .2X,'*',2X,'ABS4',3X,'*',2X,'ORD4P',2X,'*',2X,'ORD4N',2X,'*'
     ./5X,121('*'))
      DO 10 I=1,N
      IP=2*N+1-I
10    WRITE(6,300)ABS1(I),ORD1(I),ORD1(IP),ABS2(I),ORD2(I),
     .ORD2(IP),ABS3(I),ORD3(I),ORD3(IP),ABS4(I),ORD4(I),ORD4(IP)
300   FORMAT(5X,'*',12(F9.3,'*'))
      WRITE(6,400)
400   FORMAT(5X,121('*'))
401   CALL SIGMA1(ABS1,ORD1,N)
      STOP
      END
      SUBROUTINE DEGRE2(N,T1,T2,T3,T4,Y,Z)
      DIMENSION Y(1),Z(1)
      ALPHA=SQRT(T1*T2/T3)
      DO 3 I=1,N
      IP=2*N+1-I
      Y(I)=ALPHA*(-1.+FLOAT(I-1)*2./FLOAT(N-1))
      DISC=T1/T2-Y(I)*Y(I)*T3/T2/T2
      DISC=ABS(DISC)
      Z(I)=((T4/T2)*Y(I)+SQRT(DISC))/(T1/T2)
3     Z(IP)=((T4/T2)*Y(I)-SQRT(DISC))/(T1/T2)
      RETURN
      END
      SUBROUTINE SIGMA1(X,Y,N)
      DIMENSION X(1),Y(1)
      CALL PLOTON
      CALL PLOT(4.5,4.5,-3)
      CALL PLOT(4.0,0.0,2)
      CALL SYMBOL(3.5,0.05,0.1,11HSIGMA1-AXIS,0.0,6)
      CALL SYMBOL(0.05,3.9,0.1,11HSIGMA2-AXIS,0.0,6)
      CALL PLOT(0.0,4.0,3)
      CALL PLOT(0.0,0.0,2)
      CALL PLOT(2*X(1),2*Y(1),3)
      DO 66 I=1,N
      X(I)=2*X(I)
      Y(I)=2*Y(I)
66    CALL PLOT(X(I),Y(I),2)
      DO 67 I=1,N
      X(I+N)=-X(I)
      Y(I+N)=-Y(I)
67    CALL PLOT(X(I+N),Y(I+N),2)
      CALL ENDPLT
      RETURN
      END
```

APPENDIX C: FORTRAN PROGRAM 'GENHILL'

```
CCC
CCC    TO FIND M KNOWING Q AND R,BY USING THE SECANT METHOD
CCC    FROM FORM 2 OF GEN.HILL PLANAR ISOTROPY CRITERION:
CCC    (S1+S2)**M+(1+2*R)*(S1-S2)**M=2*(1+R)*SU**M
CCC
       IMPLICIT REAL*8(A-H,L-Z),INTEGER(I)
       COMMON R,Q
       WRITE(6,4)
   4   FORMAT('Q=    ,R=   ,M1=   ,M2=')
   1   READ(9,*)Q,R,M1,M2
       WRITE(6,*)Q
       WRITE(6,*)R
       I=1
  10   F1=F(M1)
       F2=F(M2)
       MN=(M1*F2-M2*F1)/(F2-F1)
       FN=F(MN)
       M1=M2
       M2=MN
       IF(I.GT.10)GO TO 11
       I=I+1
       IF(DABS(FN).GT.1.D-6) GO TO 10
  11   WRITE(6,15)I,FN,MN
  15   FORMAT('ITERATE=',I2,3X,'FN=',D12.4,3X,'MN=',D12.4)
       WRITE(6,12)
  12   FORMAT('PRINT 1 TO TRY AGAIN')
       READ(9,*)A
       IF(A.EQ.1.) GO TO 1
       STOP
       END
       FUNCTION F(M)
       IMPLICIT REAL*8(A-Z)
       INTEGER I
       COMMON R,Q
       F=(1.D0-M)*DLOG(2.D0)+DLOG(1.D0+R)+(M-1.D0)*DLOG((1.D0+2.D0*R)*
      1*(1.D0/(M-1.D0))+1.D0)-DLOG(1.D0+2.D0*R)-M*DLOG(Q)
       RETURN
       END
```

APPENDIX D:FORTRAN PROGRAM 'NEW1'

```
CCC
CCC    TO CALCULATE PARAMETERS C,A,B AND N,THEN R0,R90 AND R45
CCC    FROM THE PROPOSED GENERAL PLANAR ANISOTROPY CRITERION:
CCC    2f(SIJ)=|AS11+BS22|**M+C|S11-S22|**M+2NS12**M=1.
CCC    1ST SYSTEM(DATA:S1,S2,S45,SP1)
CCC
       IMPLICIT REAL*8(A-H,J-Z),INTEGER (I)
       COMMON X1,X2,XX1,M,N,P,Q,CP,CPP
     1 WRITE(6,2)
     2 FORMAT('X1,X2,XX1,X45')
       READ(9,*)X1,X2,XX1,X45
       M=17.D-1
       C1=1.D-3
       C2=1.D-4
       N=1.D0/(M-1.D0)
       P=1.D0/M
       Q=P/N
     8 I=1
       F1=F(C1)
       F2=F(C2)
    10 CP=(C1*F2-C2*F1)/(F2-F1)
       CN=DABS(CP)
       FN=F(CN)
       IF (DABS(FN).LT.1.D-8) GO TO 11
       C1=C2
       C2=CN
       F1=F2
       F2=FN
       IF(I.GT.15) GO TO 11
       I=I+1
C      WRITE(6,*)I,FN,CP
       GO TO 10
    11 WRITE(6,14)
    14 FORMAT('F SOLUTION')
       WRITE(6,*)I,FN,CP
       AA=-CN+X1**(-M)
       BB=-CN+X2**(-M)
       IF(AA.LT.0.D0.OR.BB.LT.0.D0) GO TO 50
       AA=AA**P
       BB=BB**P
       R0=(BB*AA**(M-1.D0)-CP)/(-AA**M-BB*AA**(M-1.D0))
       R90=(AA*BB**(M-1.D0)-CP)/(-BB**M-AA*BB**(M-1.D0))
       IF(R0.LT.0.D0.OR.R90.LT.0.D0) GO TO 50
       WRITE(6,*)R0,AA
       WRITE(6,*)R90,BB
       HN=((2.D0/X45)**M-(AA+BB)**M)/2.D0
       R45=HN/(AA+BB)**M-5.D-1
       WRITE(6,*)R45,HN
       READ(9,*)II
```

```
      IF(II.EQ.1)GO TO 1
      GO TO 55
   50 CONTINUE
      I=1
      C1=C1/5.D0
      C2=C2/5.D0
      G1=G(C1)
      G2=G(C2)
   52 CPP=(C1*G2-C2*G1)/(G2-G1)
      CNN=DABS(CPP)
      GN=G(CNN)
      IF (DABS(GN).LT.1.D-8) GO TO 51
      C1=C2
      C2=CNN
      G1=G2
      G2=GN
      IF (I.GT.15) GO TO 51
      I=I+1
  CCC WRITE(6,*)I,GN,CPP
      GO TO 52
   51 WRITE(6,19)
   19 FORMAT('G SOLUTION')
      WRITE(6,*)I,GN,CPP
      AA=-CPP+X1**(-M)
      BB=-CPP+X2**(-M)
      IF(AA.LT.0.D0.OR.BB.LT.0.D0) GO TO 60
      AA=AA**P
      BB=BB**P
      R0=(BB*AA**(M-1.D0)-CPP)/(-AA**M-BB*AA**(M-1.D0))
      R90=(AA*BB**(M-1.D0)-CPP)/(-BB**M-AA*BB**(M-1.D0))
      IF(R0.LT.0.D0.OR.R90.LT.0.D0)GO TO 60
      HN=((2.D0/X45)**M-(AA+BB)**M)/2.D0
      R45=-5.D-1+HN/(AA+BB)**M
      WRITE(6,*)R0,AA
      WRITE(6,*)R90,BB
      WRITE(6,*)R45,HN
      GO TO 55
   60 CONTINUE
      I=1
      C1=C1/4.D0
      C2=C2/4.D0
      H1=H(C1)
      H2=H(C2)
   62 CPPP=(C1*H2-C2*H1)/(H2-H1)
      CNNN=DABS(CPPP)
      HN=H(CNNN)
      IF (DABS(HN).LT.1.D-8) GO TO 61
      C1=C2
      C2=CNNN
      H1=H2
      H2=HN
```

```
      IF(I.GT.15) GO TO 61
      I=I+1
      GO TO 62
   61 WRITE(6,63)
   63 FORMAT('H SOLUTION')
      WRITE(6,*)I,HN,CPPP
      AA=-CPPP+X1**(-M)
      BB=-CPPP+X2**(-M)
      AA=AA**P
      BB=BB**P
      HN=((2.D0/X45)**M-(AA+BB)**M)/2.D0
      R0=(BB*AA**(M-1.D0)-CPPP)/(-AA**M-BB*AA**(M-1.D0))
      R90=(AA*BB**(M-1.D0)-CPPP)/(-BB**M-AA*BB**(M-1.D0))
      R45=(-5.D-1)+HN/(AA+BB)**M
      WRITE(6,*)R0,AA
      WRITE(6,*)R90,BB
      WRITE(6,*)R45,HN
   55 CONTINUE
      READ(9,*)IJ
      IF(IJ.EQ.1) GO TO 1
      STOP
      END
      FUNCTION F(C)
      IMPLICIT REAL*8(A-Z)
      INTEGER I
      COMMON X1,X2,XX1,M,N,P,Q,CP,CPP
      D=DABS(-C+X1**(-M))
      E=DABS(-C+X2**(-M))
      F=(C**N+E**N)**Q-XX1*(C**P)*(D**P+E**P)
      RETURN
      END
      FUNCTION G(C)
      IMPLICIT REAL*8(A-Z)
      INTEGER I
      COMMON X1,X2,XX1,M,N,P,Q,CP,CPP
      D=DABS(-C+X1**(-M))
      E=DABS(-C+X2**(-M))
      G=((C**N+E**N)**Q-XX1*(C**P)*(D**P+E**P))/(C-CP)
      RETURN
      END
      FUNCTION H(C)
      IMPLICIT REAL*8(A-Z)
      INTEGER I
      COMMON X1,X2,XX1,M,N,P,Q,CP,CPP
      D=DABS(-C+X1**(-M))
      E=DABS(-C+X2**(-M))
      H=((C**N+E**N)**Q-XX1*(C**P)*(D**P+E**P))/(C-CP)/(C-CPP)
      RETURN
      END
```

APPENDIX E: FORTRAN PROGRAM 'NEW2'

```
CCC
CCC   TO CALCULATE PARAMETERS C,A,B AND N,THEN R0,R90 AND R45
CCC   FROM THE PROPOSED GENERAL PLANAR ANISOTROPY CRITERION:
CCC   2F(SIJ)=|AS11+BS22|**M+C|S11-S22|**M+2S12**M=1
CCC   2ND SYSTEM(DATA:S1,S2,S45,SP2)
CCC
      IMPLICIT REAL*8(A-H,J-Z),INTEGER (I)
      COMMON X1,X2,XX2,M,N,P,Q,CP,CPP
    1 WRITE(6,2)
    2 FORMAT('X1,X2,XX2,X45')
      READ(9,*)X1,X2,XX2,X45
      M=17.D-1
      C1=1.D-3
      C2=1.D-4
      N=1.DO/(M-1.DO)
      P=1.DO/M
      Q=P/N
    8 I=1
      F1=F(C1)
      F2=F(C2)
   10 CP=(C1*F2-C2*F1)/(F2-F1)
      CN=DABS(CP)
      FN=F(CN)
      IF (DABS(FN).LT.1.D-8) GO TO 11
      C1=C2
      C2=CN
      F1=F2
      F2=FN
      IF(I.GT.15) GO TO 11
      I=I+1
C     WRITE(6,*)I,FN,CP
      GO TO 10
C 11  WRITE(6,14)
C 14  FORMAT('F SOLUTION')
   11 CONTINUE
C      WRITE(6,*)I,FN,CP
      AA=-CN+X1**(-M)
      BB=-CN+X2**(-M)
      WRITE(6,13)
   13 FORMAT(2X,'*   C   *   A   *   B   *   N   * R0  * R90 * R45 *')
      IF(AA.LT.0.DO.OR.BB.LT.0.DO) GO TO 50
      AA=AA**P
      BB=BB**P
      R0=(BB*AA**(M-1.DO)-CP)/(-AA**M-BB*AA**(M-1.DO))
      R90=(AA*BB**(M-1.DO)-CP)/(-BB**M-AA*BB**(M-1.DO))
      IF(R0.LT.0.DO.OR.R90.LT.0.DO) GO TO 50
C      WRITE(6,*)R0,AA
C      WRITE(6,*)R90,BB
      HN=((2.DO/X45)**M-(AA+BB)**M)/2.DO
      R45=HN/(AA+BB)**M-5.D-1
```

```
      WRITE(6,12)CP,AA,BB,HN,R0,R90,R45
   12 FORMAT(2X,'*',4(F7.5,'*'),3(F5.3,'*'))
      READ(9,*)II
      IF(II.EQ.1)GO TO 1
      GO TO 55
   50 CONTINUE
      I=1
      C1=C1/5.DO
      C2=C2/5.DO
      G1=G(C1)
      G2=G(C2)
   52 CPP=(C1*G2-C2*G1)/(G2-G1)
      CNN=DABS(CPP)
      GN=G(CNN)
      IF (DABS(GN).LT.1.D-8) GO TO 51
      C1=C2
      C2=CNN
      G1=G2
      G2=GN
      IF (I.GT.15) GO TO 51
      I=I+1
CCC   WRITE(6,*)I,GN,CPP
      GO TO 52
C  51  WRITE(6,19)
C  19  FORMAT('G SOLUTION')
   51 CONTINUE
C      WRITE(6,*)I,GN,CPP
      AA=-CPP+X1**(-M)
      BB=-CPP+X2**(-M)
      IF(AA.LT.0.D0.OR.BB.LT.0.D0) GO TO 60
      AA=AA**P
      BB=BB**P
      R0=(BB*AA**(M-1.D0)-CPP)/(-AA**M-BB*AA**(M-1.D0))
      R90=(AA*BB**(M-1.D0)-CPP)/(-BB**M-AA*BB**(M-1.D0))
      IF(R0.LT.0.D0.OR.R90.LT.0.D0)GO TO 60
      HN=((2.D0/X45)**M-(AA+BB)**M)/2.D0
      R45=-5.D-1+HN/(AA+BB)**M
C      WRITE(6,*)R0,AA
C      WRITE(6,*)R90,BB
C      WRITE(6,*)R45,HN
      WRITE(6,12)CPP,AA,BB,HN,R0,R90,R45
      GO TO 55
   60 CONTINUE
      I=1
      C1=C1/4.DO
      C2=C2/4.DO
      H1=H(C1)
      H2=H(C2)
   62 CPPP=(C1*H2-C2*H1)/(H2-H1)
      CNNN=DABS(CPPP)
      HN=H(CNNN)
      IF (DABS(HN).LT.1.D-8) GO TO61
      C1=C2
```

```
      C2=CNNN
      H1=H2
      H2=HN
      IF(I.GT.15) GO TO 61
      I=I+1
      GO TO 62
C  61  WRITE(6,63)
C  63  FORMAT('H SOLUTION')
   61 CONTINUE
C      WRITE(6,*)I,HN,CPPP
      AA=-CPPP+X1**(-M)
      BB=-CPPP+X2**(-M)
      AA=AA**P
      BB=BB**P
      HN=((2.D0/X45)**M-(AA+BB)**M)/2.D0
      R0=(BB*AA**(M-1.D0)-CPPP)/(-AA**M-BB*AA**(M-1.D0))
      R90=(AA*BB**(M-1.D0)-CPPP)/(-BB**M-AA*BB**(M-1.D0))
      R45=(-5.D-1)+HN/(AA+BB)**M
C      WRITE(6,*)R0,AA
C      WRITE(6,*)R90,BB
C      WRITE(6,*)R45,HN
      WRITE(6,12)CPPP,AA,BB,HN,R0,R90,R45
   55 CONTINUE
      READ(9,*)IJ
      IF(IJ.EQ.1) GO TO 1
      STOP
      END
      FUNCTION F(C)
      IMPLICIT REAL*8(A-Z)
      INTEGER I
      COMMON X1,X2,XX2,M,N,P,Q,CP,CPP
      D=DABS(-C+X1**(-M))
      E=DABS(-C+X2**(-M))
      F=(C**N+D**N)**Q-XX2*(C**P)*(D**P+E**P)
      RETURN
      END
      FUNCTION G(C)
      IMPLICIT REAL*8(A-Z)
      INTEGER I
      COMMON X1,X2,XX2,M,N,P,Q,CP,CPP
      D=DABS(-C+X1**(-M))
      E=DABS(-C+X2**(-M))
      G=((C**N+D**N)**Q-XX2*(C**P)*(D**P+E**P))/(C-CP)
      RETURN
      END
      FUNCTION H(C)
      IMPLICIT REAL*8(A-Z)
      INTEGER I
      COMMON X1,X2,XX2,M,N,P,Q,CP,CPP
      D=DABS(-C+X1**(-M))
      E=DABS(-C+X2**(-M))
      H=((C**N+D**N)**Q-XX2*(C**P)*(D**P+E**P))/(C-CP)/(C-CPP)
      RETURN
      END
```

APPENDIX F: FORTRAN PROGRAM 'NEW3'

```
CCC
CCC    SAME AS NEW2 AND NEW3.3RD SYSTEM(DATA:S1,S2,S45,S3)
CCC
       IMPLICIT REAL*8(A-H,J-Z),INTEGER (I)
       COMMON X1,X2,X3,M,N,P,Q,BP
     1 WRITE(6,2)
     2 FORMAT('X1,X2,X3,X45')
       READ(9,*)X1,X2,X3,X45
       X1=1.D0/X1
       X2=1.D0/X2
       X3=1.D0/X3
       X45=1.D0/X45
       M=17.D-1
       B1=1.D-3
       B2=1.D-4
       N=1.D0/(M-1.D0)
       P=1.D0/M
       Q=P/N
     9 I=1
       F1=F(B1)
       F2=F(B2)
    10 BP=(B1*F2-B2*F1)/(F2-F1)
       BN=DABS(BP)
       FN=F(BN)
       IF (DABS(FN).LT.1.D-8) GO TO 11
       B1=B2
       B2=BN
       F1=F2
       F2=FN
       IF(I.GT.15) GO TO 11
       I=I+1
       GO TO 10
    11 WRITE(6,14)
    14 FORMAT('F SOLUTION')
       WRITE(6,*)I,FN,BP
       AA=X3-BP
       CC=X3**M-BP**M
       BB=BP
       R0=(BB*AA**(M-1.D0)-CC)/(-AA**M-BB*AA**(M-1.D0))
       R90=(AA*BB**(M-1.D0)-CC)/(-BB**M-AA*BB**(M-1.D0))
       WRITE(6,*)R0,AA
       WRITE(6,*)R90,CC
       HN=((2.D0*X45)**M-(AA+BB)**M)/2.D0
       R45=HN/(AA+BB)**M-5.D-1
       WRITE(6,*)R45,HN
       READ(9,*)II
       IF(II.EQ.1)GO TO 1
       STOP
       END
       FUNCTION F(B)
       IMPLICIT REAL*8(A-Z)
       INTEGER I
       COMMON X1,X2,X3,M,N,P,Q,BP
       F=(X3-B)**M-B**M-X1**M+X2**M
       RETURN
       END
```

APPENDIX G: FORTRAN PROGRAM 'EXPO'

```
CCC
CCC    TO FIT TO THE Rs AND Ez DATA AN EXPONENTIAL FUNCTION:
CCC    Rs=A*EXP(-BEz)+C ,AND FIND Rs AT ZERO (=A+C)
CCC
       IMPLICIT REAL*8(A-H,J-Z),INTEGER (I)
       EXTERNAL F
       COMMON W,X,Y,S,II
       DIMENSION W(10), X(10),Y(10),S(10),SS(10)
C      DATA W/20.D0,3.D0,4.D0,5.D0,6.D0,7.D0,8.D0,9.D0,10.D0,11.D0/
C      DATA S/9*0.D0/
C      DATA SS/9*0.D0/
       READ(9,*)B1,B2
       TEST=2.D0*B2
       DO 2 I=1,9
    2  SS(I)=0.D0
       READ(5,*)II
       DO 5 I=1,II
       READ(5,*)X(I),Y(I),W(I)
    5  CONTINUE
       IT=1
   15  F1=F(B1)
       F2=F(B2)
       IF (F2.EQ.F1) GO TO 25
       BN=(B1*F2-B2*F1)/(F2-F1)
       FN=F(BN)
       WRITE(6,*)IT,FN,BN
C      IF(DABS(F1+F2).LT.F2) GO TO 20
C      IF (BN.GT.TEST) BN=BN/1.D2
C      IF (BN.LT.1.D-2) BN=5*BN
       IF (DABS(FN).LT.1.D-8) GO TO 20
       B1=B2
       B2=BN
       IF(IT.GT.40) GO TO 20
       IT=IT+1
       GO TO 15
   20  CONTINUE
       GO TO 28
   25  BD=B1
       B1=B2
       B2=BD
       GO TO 5
   28  CONTINUE
C      IF (DABS(FN).GT.1.D-5) GO TO 25
       P=BN
       WRITE(6,*)IT,FN,P
       DO 30 I=1,6
       SS(1)=SS(1)+W(I)*X(I)**2*DEXP(-2*P*X(I))
       SS(2)=SS(2)+W(I)*X(I)**2*DEXP(-P*X(I))
       SS(3)=SS(3)+W(I)*Y(I)*X(I)*DEXP(-P*X(I))
       SS(4)=SS(4)+W(I)*X(I)**3*DEXP(-2*P*X(I))
       SS(5)=SS(5)+W(I)*X(I)**3*DEXP(-P*X(I))
```

```
      SS(6)=SS(6)+W(I)*Y(I)*X(I)**2*DEXP(-P*X(I))
      SS(7)=SS(7)+W(I)*X(I)**3*DEXP(-P*X(I))
      SS(8)=SS(8)+W(I)*X(I)**2
      SS(9)=SS(9)+W(I)*Y(I)*X(I)
30    CONTINUE
      A=(SS(3)*SS(8)-SS(2)*SS(9))/(SS(1)*SS(8)-SS(2)*SS(7))
      AA=(SS(6)*SS(8)-SS(5)*SS(9))/(SS(4)*SS(8)-SS(5)*SS(7))
      C=SS(9)/SS(8)-A*SS(7)/SS(8)
      CC=SS(9)/SS(8)-AA*SS(7)/SS(8)
      WRITE(6,*)A,C
      WRITE(6,*)AA,CC
      STOP
      END
      FUNCTION F(B)
      IMPLICIT REAL*8(A-H,J-Z),INTEGER (I)
      COMMON W(10),X(10),Y(10),S(9),II
      DO 4 I=1,9
4     S(I)=0.0
      DO 10 I=1,6
      S(1)=S(1)+W(I)*X(I)**2*DEXP(-2*B*X(I))
      S(2)=S(2)+W(I)*X(I)**2*DEXP(-B*X(I))
      S(3)=S(3)+W(I)*Y(I)*X(I)*DEXP(-B*X(I))
      S(4)=S(4)+W(I)*X(I)**3*DEXP(-2*B*X(I))
      S(5)=S(5)+W(I)*X(I)**3*DEXP(-B*X(I))
      S(6)=S(6)+W(I)*Y(I)*X(I)**2*DEXP(-B*X(I))
      S(7)=S(7)+W(I)*X(I)**2*DEXP(-B*X(I))
      S(8)=S(8)+W(I)*X(I)**2
      S(9)=S(9)+W(I)*Y(I)*X(I)
10    CONTINUE
      F=S(1)*S(8)**2*S(6)-S(1)*S(8)*S(5)*S(9)-S(2)*S(7)*S(6)*S(8)
     .-S(4)*S(3)*S(8)**2+S(4)*S(8)*S(2)*S(9)+S(5)*S(7)*S(3)*S(8)
      RETURN
      END
```